UNIVERSITÀ DEGLI STUDI FIRENZE

DOTTORATO DI RICERCA IN
SCIENZE BIOMEDICHE

CICLO XXIX

COORDINATORE Prof. Dello Sbarba Persio

Study of the conformational changes occurring in human transthyretin that are necessary for amyloid fibril formation in disease and for its role as a detoxifier

Settore Scientifico Disciplinare BIO/10

Dottorando

Dott. Ghadami Seyyed Abolghasem

Tutore

Prof. Chiti Fabrizio

Coordinatore

Prof. Dello Sbarba Persio

Anni 2013/2016

Department for their great support, and thanks for all children and their parents who shared in this thesis.

Dedication

To my parents.
The reason of what I become today.
Thanks for your great support and continuous care.

To my brothers and sisters.
I am really grateful to both of you.
You have been my inspiration, and my soul mates.

Table of Contents

Summary

Transthyretin (TTR) is an extracellular protein able to deposit into well-defined protein aggregates called amyloid, in pathological conditions known as senile systemic amyloidosis, familial amyloid polyneuropathy, familial amyloid cardiomyopathy and leptomeningeal amyloidosis. At least three distinct partially folded states have been described for TTR, including the widely studied amyloidogenic state at mildly acidic pH. In this study, I have used fluorescence resonance energy transfer (FRET) experiments in a monomeric variant of TTR (M-TTR) and in its W41F and W79F mutants, taking advantage of the presence of a unique, solvent-exposed, cysteine residue at position 10, that I have labelled with a coumarin derivative (DACM, acceptor), and of the two natural tryptophan residues at positions 41 and 79 (donors). Trp41 is located in an ideal position as it is one of the residues of β-strand C, whose degree of unfolding is debated. I found that the amyloidogenic state at low pH has the same FRET efficiency as the folded state at neutral pH in both M-TTR and W79F-M-TTR, indicating an unmodified Cys10-Trp41 distance. The partially folded state populated at low denaturant concentrations also has a similar FRET efficiency, but other spectroscopic probes indicate that it is distinct from the amyloidogenic state at acidic pH. By contrast, the off-pathway state accumulating transiently during refolding has a higher FRET efficiency, indicating nonnative interactions that reduce the Cys10-Trp41 spatial distance, revealing a third distinct conformational state. Overall, these results clarify a negligible degree of unfolding of β-strand C in the formation of the amyloidogenic state and establish the concept that TTR is a highly plastic protein able to populate at least three distinct conformational states.

TTR is also a protein able to inhibit amyloid sibril formation of Aβ, the peptide associate with alzheimer diseases, and to suppres the toxcicity of performed oligomers of Aβ. Pervious analyses of the *in vitro* interaction between human TTR and Aβ, have shown that TTR binds to all forms of Aβ: monomers, oligomers and fibrils. The binding occurs with higher affinity for Aβ oligomers, aggregates and fibrils with respect to Aβ monomers. Previous data do not offer any insight into the mechanism by which TTR inhibits Aβ amyloid fibril formation, oligomer toxicity and on the TTR form responsible for such an effect. In this thesis, the interaction between different variants of TTR (WT-TTR, M-TTR and W79F M-TTR) and the Aβ peptide in both the process of aggregation, as well as on pre-formed toxic

oligomers called amyloid-derived diffusible ligands (ADDLs), was studied by FRET technique. The time course of amyloid fibril formation was studied under conditions close to physiological and starting from a monomeric state of the $A\beta_{40}$ peptide, in the presence of WT-TTR, M-TTR and W97F M-TTR at different concentrations. This study showed inhibition of aggregation of $A\beta_{40}$ by transthyretin molecules. I also studied the conformational change of all three TTR variants following the interaction with $A\beta_{40}$ during aggregation at a molar ratio of 1:3 (TTR:$A\beta_{40}$). In particular, the FRET *E* of TTRs during aggregation of $A\beta_{40}$ was monitored and the results showed a change in FRET *E* of all TTR molecules as $A\beta_{40}$ aggregation proceeds, indicating a conformational conversion upon $A\beta_{40}$/TTR interaction. The far-UV CD spectra of WT-TTR, M-TTR and W79F M-TTR in the absence and presence of $A\beta_{40}$ undergoing aggregation were compared, showing that there are no changes in the secondary structure of TTRs after binding to $A\beta_{40}$ while it converts from monomers to oligomers. The fluorescence spectra recorded for both M-TTR and DACM-M-TTR in the presence of $A\beta_{42}$ ADDLs decreased in intensity with time, indicating a progressive interaction with the ADDLs. The FRET *E* value of M-TTR measured during incubation with $A\beta_{42}$ ADDLs was found to decrease progressively, indicating that a conformational change occurs for M-TTR following the interaction with $A\beta_{42}$ ADDLs. This analysis was repeated for the W79F mutant of M-TTR leading to very similar results. This confirms that a conformational change occurs also for W79F M-TTR following the interaction with $A\beta_{42}$ ADDLs and indicates an increased spatial distance between the DACM moiety attached to Cys10 and the two tryptophan residues, particularly Trp41.

Chapter 1
Introduction

1.1. Transthyretin

1.1.1. Discovery

Human transthyretin (TTR) is a protein firstly observed in the cerebrospinal fluid (CSF) (Kabat and Levine 1942) and then in the serum (Florence et al. 1942). TTR is a 55 kDa homotetrameric protein first identified using the Tiselius moving boundary electrophoresis method (Kabat et al. 1942) and later by immuno-electrophoretic analysis of concentrated CSF (Gavrilesco et al. 1955). It was initially named "prealbumin" -because of its greater electrophoretic mobility than that of albumin- it was later renamed "thyroxine-binding prealbumin" to reflect its new found role as a transporter of the thyroid hormone L-thyroxine (Ingbar 1963; Oppenheimer 1968; Robbins and Rall 1960).

However, about a decade later this name change. It was suggested by Goodman and colleagues that "thyroxine-binding prealbumin" was relatively unimportant as a carrier of L-thyroxine in the blood (Kanai et al. 1968; Raz and Goodman 1969; Raz et al. 1970). The main physiological function of the protein, they proposed, was connected with the transport of retinol (vitamin A). Goodman, who was primarily interested in retinol-binding protein (RBP), to which prealbumin complexes *in vivo*, and vitamin A metabolism, attempted to change the name prealbumin to transretin. In 1969, Goodman and colleagues were the first to show that "thyroxine-binding prealbumin" strongly interacts with RBP, the serum protein responsible for the transport of vitamin A.

Another researcher, Jacob Robbins, who made important contributions to the knowledge base concerning this protein, felt that the thyroxine-binding and transport properties of prealbumin needed to be emphasized in the name (Ferguson et al. 1975). With several compelling pieces of evidence highlighting this additional function of "thyroxine-binding prealbumin", the name TTR was put forth by the Nomenclature Committee of the International Union of Biochemistry (1981) to reflect the molecule's dual function as a transporter of thyroxine and RBP (Goodman 1985).

1.1.2. Gene Structure

The human TTR cDNA sequence was reported in 1984 by two groups, those of Shuji Mita (Mita et al. 1984) and Yoshiyuki Sakaki (Sakaki et al. 1984) and in 1985 by

Wallace and coworkers (Wallace et al. 1985). The complete structure of the TTR gene was reported in 1985 by Tsuzuki and coworkers (Tsuzuki et al. 1985) and Sakaki's group (Sasaki et al. 1985). Using cloned human TTR cDNA as a probe, Southern blot hybridization of human genomic DNA revealed that the TTR gene consists of a unique single-copy DNA, localized in the long arm of chromosome 18 (Chr 18) (Tsuzuki et al. 1985) in the q11.2-q12.1 region (Sparkes et al. 1987) (Figure 1.1). The nucleotide sequence of the entire human TTR gene, including 581 base pairs of the 5′- and 95 base pairs of the 3′-flanking sequences was determined (Tsuzuki et al. 1985). The gene has four exons of 95, 131, 136 and 253 base pairs (bp) and three introns of 934, 2090 and 3308 bp (Figure 1.1) (Sasaki et al. 1985) and spans 7.6 kb.

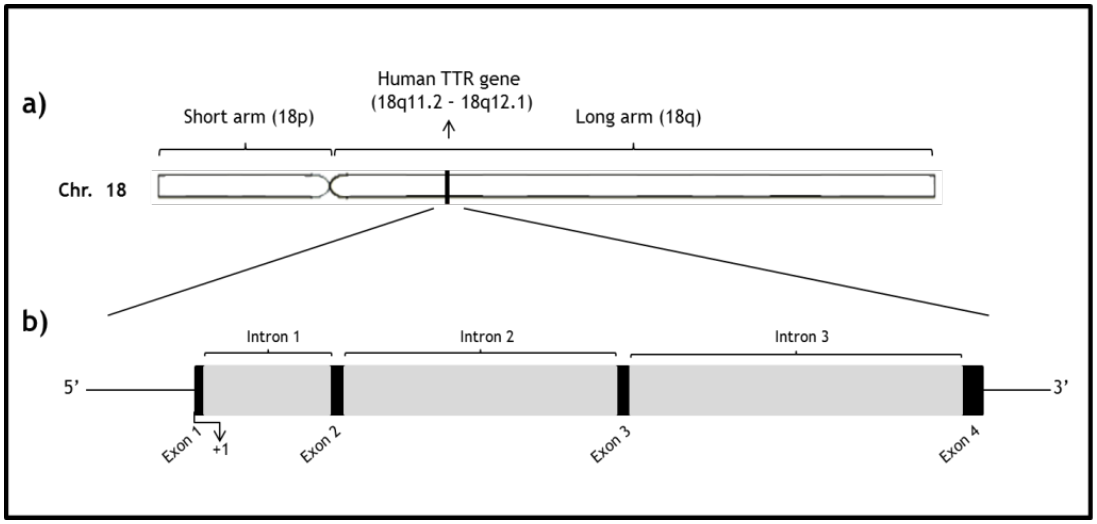

Figure 1.1. The human transthyretin (TTR) gene localization and structure: (A) Locus of TTR on chromosome 18. (B) Structure of TTR gene. Black boxes represent the exons 1, 2, 3 and 4 and the grey boxes represent the introns 1, 2 and 3.

The first exon codes for a 5'- region containing an 18 amino acids of signal peptide and the first three amino acid residues of the mature protein, exons 2, 3 and 4 encode the 4-47, 48-92 and 93-127 aa residues of the mature TTR, respectively (Sakaki and Sasaki 1985; Tsuzuki et al. 1985).

As in most eukaryotic genes, the consensus TATA and CAAT sequences are found: a TATA box sequence at position -30 to -24 bp, a CAAT box sequence from -101 to -96 bp, a GC-rich region (of approximately 20 bp), Alu sequences and several hormone responsive consensus sequences. For instance, in its proximal promoter, two overlapping sequences homologous to glucocorticoid responsive elements (GREs) were present at positions -224 and -212 bp. In the 3'-untranslated region, downstream the coding sequence, a polyadenylation signal (AATAAA) was identified at 123 bp

(Sakaki et al. 1984; Tsuzuki et al. 1985; Wakasugi et al. 1985). Unexpectedly, two independent open reading frames (ORFs), provided with respective regulatory sequences in their 5'- and 3'- flanking regions, were found within the gene, one in the first intron and the other in the third intron (Soares et al. 2003). It is not known whether these open reading frames are expressed in vivo. Tsuzuki et al. identified 300 (Tsuzuki et al. 1985) bp sequences, which were strikingly homologous to the human Alu-type repeat elements, and were shown by Sakaki and colleagues (Sasaki et al. 1985) to have opposite polarity. The single-copy TTR gene has been assigned to the long arm (q) of chromosome 18 (Wallace et al. 1986). The laboratories of both Simon and Niikawa further assigned the gene to the region 18q11.2–q12.1 (Jinno et al. 1986; Sparkes et al. 1987) Figure 1.1.

Phylogenetically, TTR gene is highly conserved. Both mouse and rat TTR genes are composed by 4 exons and 3 introns, as in human, and, the DNA sequence of the coding region of the mouse TTR gene exhibits 90 and 82% homology with the rat and the human genes, respectively. Moreover, the highest homology between mouse, rat and human TTR was observed in the promoter region, around -190 bp to the cap site (Costa et al. 1986a; Fung et al. 1988).

1.1.3. Expression and Regulation

Although plasma TTR is synthesized in the liver (Borek et al. 1981; Felding and Fex 1982), several extrahepatic sites of TTR synthesis have been described. The choroid plexus (CP) of the cerebral ventricles synthesizes (Dickson et al. 1985; Herbert et al. 1986; Soprano et al. 1985) and secretes (Dickson et al. 1986) large quantities of TTR into the cerebrospinal fluid. In the fetus, the visceral yolk sac endoderm synthesizes and secretes both TTR and RBP from the early gastrula stage (Soprano et al. 1986; Soprano et al. 1988). In addition, TTR mRNA has been detected in the pancreas (Jacobsson et al. 1989) and stomach (Soprano et al. 1985) at considerably lower levels. The physiologic role of TTR in most extrahepatic locations is unknown; in the central nervous system, however, TTR is responsible for thyroxine delivery to the brain (Dickson et al. 1987; Schreiber et al. 1990).

The liver performs essential functions in the body by uniquely expressing hepatocyte-specific genes encoding plasma proteins, enzymes involved in gluconeogenesis, glycogen storage, glucose metabolism, cholesterol homeostasis, and synthesis of bile salts (Jungermann and Katz 1989). Functional analysis of numerous hepatocyte-specific promoter and enhancer regions reveals that they are

composed of multiple cis-acting DNA sequences that bind different families of hepatocyte nuclear factors (HNFs). Previous studies carried out on mice showed that TTR gene is controlled by two major regulatory regions located in the 5' flanking region: a promoter proximal sequence at -50 to -150 bp and a distal enhancer sequence at -1.86 to -1.96 kb. These regulatory sequences are conserved in humans. In both regions, several putative regulatory sites were identified: DNA binding sites for liver-specific nuclear factors, as the hepatocyte nuclear factors 1, 3 and 4 (HNF-1, HNF-3 AND HNF-4) and CCAAT/enhancer binding proteins (C/EBP) families (Costa et al. 1986b; Costa et al. 1990). In human TTR gene, these regulatory regions were proved to be sufficient to regulate its hepatic expression (Costa et al. 1986b; Yan et al. 1990). Concerning TTR expression in choroid plexus (CP) less is known, and the few studies performed suggest that TTR is differentially regulated between liver and CP, thus involving different transcription factors (Nagata et al. 1995; Yan et al. 1990). In fact, while a shorter sequence (<1 kb) upstream the mRNA cap site is sufficient to drive TTR expression in the liver, in CP, the presence of a further upstream sequence (>3 kb) is required (Nagata et al. 1995; Yan et al. 1990). Studies performed in transgenic mice showed that the 600 bp sequence upstream of the TTR gene is enough for the TTR expression in liver and yolk sac (Yan et al. 1990) whereas sequences of approximately 6 kb upstream the coding sequence are necessary for the total tissue specific synthesis and quantitatively normal expression (Nagata et al. 1995).

Transcription of the TTR gene results in an approximately 700 bp mRNA containing a 5' untranslated region of 26-27 nucleotides, a coding region of 441 nucleotides, a 3' untranslated region of 145-148 nucleotides and a poly(A) tail (Mita et al. 1984; Soprano et al. 1985). TTR is synthesized as a precursor with a larger molecular weight, the pre-TTR, which includes a signal peptide at the N-terminal region that is cleaved upon TTR translocation to the endoplasmic reticulum (Soprano et al. 1985).

TTR is mainly synthesized by hepatocytes in the liver (Dickson et al. 1985) and secreted to the peripheral circulation, where its concentration ranges from 20 to 40 mg/dL (Vatassery et al. 1991). TTR plasma concentrations varies with age: newborns have about a half of that in healthy adults (Vahlquist et al. 1975) and declines after age 50 (Ingenbleek and De Visscher 1979). TTR is also synthesized by choroid plexus epithelial cells (CPECs) in the CNS (Soprano et al. 1985) and secreted unidirectionally into the CSF (Aleshire et al. 1983; Herbert et al. 1986), where its

concentration ranges from 2 to 4 mg/dL, and represents approximately 20 to 25 % of the total protein content in the CSF (Weisner and Roethig 1983). It was previously reported that 1 g of CP contained about 25 times larger amounts of TTR mRNA than 1 g of liver (Dickson et al. 1985), showing the very active synthesis of TTR in this tissue.

Liver and CP are responsible for up to 90 % of the total TTR amount. Nevertheless, despite some controversy, various authors also described small amounts of TTR in the pancreas islets of Langerhans, heart, muscles, stomach, spleen (Soprano et al. 1985), human placenta, human scalp skin and hair follicles (Adly 2010), retinal pigment epithelium in the eye (Cavallaro et al. 1990) and meninges, in various animal models. Studies showed that in the course of human embryonic development, TTR is firstly detectable in the fetal blood since the 8th week of gestation (Jacobsson 1989) in the tela choroidea, the precursor of CP and, later, in the liver (Harms et al. 1991) and pancreas (Jacobsson 1989). Furthermore, others observed TTR mRNA in endodermal cells of the visceral yolk sac, tela choroidea and hepatocytes since the 10th day of gestation (Murakami et al. 1987).

In evolutionary terms, TTR synthesis occurs in fish (Santos and Power 1999), reptiles, birds and mammalian ancestors (Richardson et al. 1994). In the first, TTR is mainly produced in liver, while in reptiles it is mostly synthesized by CP (Achen et al. 1993) and, in birds and mammals, it occurs in both tissues (Harms et al. 1991), suggesting that TTR has a common fish ancestor (Santos and Power 1999) or its expression occurred first in CP and later in liver (Schreiber et al. 1990). TTR has been implicated in acute stressful conditions and is involved in stages of stress response (Ingenbleek and De Visscher 1979). It is well demonstrated that regulation of TTR expression in liver is different from CP. Studies showed that in liver, TTR levels are decreased, to a minimum of 25%, during chronic inflammation or malnutrition conditions due to the release of cytokines, which bind to hepatocyte receptors that express transcriptional factors potentially involved in the inhibition of TTR transcription (Dickson et al. 1985). Regarding the regulation of TTR expression in CP, less is known and further studies are required. In fact, previous studies showed that: during an acute phase response, rat CP TTR levels are not changed, nicotine increased mRNA TTR levels time- and dose-dependently in rat CP, TTR expression and secretion is increased after administration of leaf extracts of Gingko biloba (Watanabe et al. 2001), various sex steroid hormones (SSHs) as 17β-estradiol (E2), 5α-dihydrotestosterone (DHT) and progesterone (P) are up-regulated TTR expression

in murine CP (Quintela et al. 2008; Quintela et al. 2009; Quintela et al. 2011). Aged rats exhibited increased TTR mRNA levels in CP, after a short-term consumption of omega-3-rich fish oil (Puskas et al. 2003). TTR expression is decreased in neonatal CNS of rats subjected to a maternal separation induced stress (Kohda et al. 2006).

1.1.4. Protein Structure

X-ray crystallography and diffraction studies determined the three dimensional structure of TTR and revealed a 55 kDa tetramer, composed of four identical subunits assembled around a central channel (Blake et al. 1971). Much of the information on the structure of TTR was obtained from crystallographic studies performed by Haupt and Heide (Haupt and Heide 1966), who were first to crystallize the human form of the protein. A schematic drawing of the dimer of TTR is shown in Figure 1.2A while a drawing of the whole tetrameric molecule is presented in Figure 1.2B using PDB entries of 1F41, ribbon tracing of the dimer of TTR (Figure 1.2A) was produced by Pymol package from the same coordinates as in Figure 1.2B (taken from Blake, 1971). Each monomer contains 127 amino acids brought together in a β-sandwich structure organized in two extensive β-sheets, each composed of 4 β-strands, namely DAGH and CBEF (Figure 1.2A). The strands are 7-8 residues long, except the strand D that has only 3 residues. With the exceptions for strands A and G, strands interact in an anti-parallel fashion arranged in a topology analogous to the classical Greek key barrel. Each monomer exhibits a single α-helix segment of 9 residues located at the end of β-strand E (75-83 residues), which connects to the F strand (Blake et al. 1971). The strands DAGH mold the channel surface and the strands CBEF define the external surface of the monomer in the tetrameric structure. The monomer-monomer interactions consist of antiparallel hydrogen bonding between strands F and H of one monomer and F' and H' of another monomer, resulting in a dimer (Figure 1.2). The interactions that bring dimers together to form the tetramer, however, primarily involve hydrophobic interactions at interfaces involving all four monomers (Figure 1.2). These loops interactions are involved in stabilizing the AB to CD quaternary interface and in defining the outer boundary of the hormone-binding sites (HBS) (Blake et al. 1971; Foss et al. 2005). The four monomers that constitute the TTR tetramer form a cylindrical open, large, central and hydrophobic channel - the HBS – where the binding sites for T4, and other hormones and small molecules, are located (Blake et al. 1974; Blake et al. 1971). This channel is about 8 Å in diameter and 50 Å long is formed. This central channel contains two identical binding sites for the L-

thyroxine hormone, while the outer surface of the molecule houses four binding sites for the vitamin A specific carrier, retinol- binding protein (Blake et al. 1974; Blake et al. 1971; Monaco et al. 1995). The quaternary structure of TTR has a globular protein shape whose overall size is 70 Å x 55 Å x 50 Å (Blake et al. 1974; Blake et al. 1971).

1.1.5. Physiological Functions

TTR plays many functions. As a serum and CSF protein, TTR functions primarily as a transport protein. Synthesized mainly by the liver, serum TTR is known to transport about 20% of the hormone L-thyroxine in the bloodstream (Blake et al. 1974; Hagen and Elliott 1973). Thyroxine-binding globulin, the major L-thyroxine carrier in the blood, accounts for 70% of L-thyroxine's transport while serum albumin accounts for the remaining 10%. However, TTR is thought to be the main transporter of L-thyroxine in the CSF (Schreiber et al. 1990). In the central nervous system, TTR is synthesized *de novo* by the choroid plexus, a secretory structure located in the ventricles of the brain (Herbert et al. 1986). There, it acts as the primary transport protein for L-thyroxine, transporting up to 80% of the hormone in CSF (Hagen and Elliott 1973).

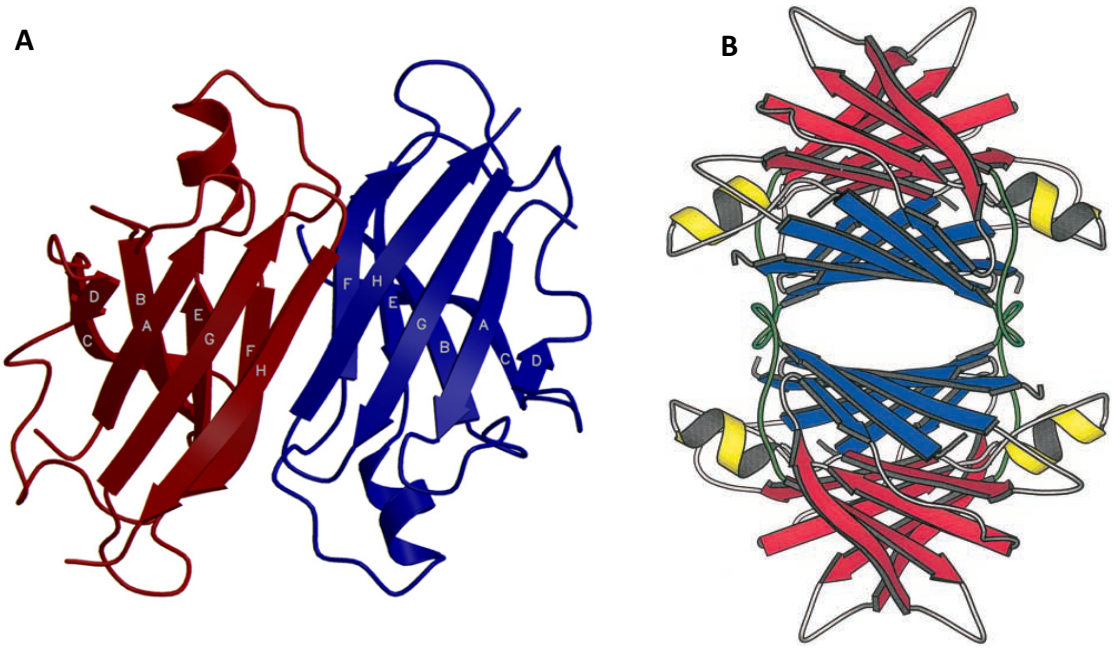

Figure 1.2. (A) A schematic drawing of the dimer moiety of TTR. Each monomer is comprised of two four-stranded β-sheets denoted CBEF and DAGH (the dimer interface lies between β-strands HH' and FF'; the prime symbol refers to a strand from another monomer within the dimer). The arrows represent β-strands, which are labelled according to their order in the primary amino acid sequence of the protein (Taken from Blake, 1971). (B) Representation of wild-type (wt) ribbon TTR structure.

TTR also aids in the transport of vitamin A through its interaction with RBP, forming the TTR-RBP-retinol complex (Kanai et al. 1968; Peterson et al. 1998). The association of TTR with RBP has been shown to be essential to the delivery of vitamin A to target cells (Bellovino et al. 1996). With a molecular weight of 21,000, RBP would be rapidly eliminated from the plasma by glomerular filtration in the kidneys if it were not in complex with TTR. Hence, the transport and distribution of L-thyroxine and retinol, via interaction with RBP, in CSF and plasma, respectively, are the first main functions attributed to TTR (Hagen and Elliott 1973; Monaco et al. 1995; Raz and Goodman 1969; Schreiber et al. 1990).

Presently, it is well known that TTR actions largely exceed those initially proposed and increasing evidences link TTR to a number of neuropathological conditions as AD, nerve biology and repair and proteolytic activity (Saraiva et al. 1988). In fact, several *in vitro* and *in vivo* studies showed that TTR is also implicated in regulation of neuropeptide Y (NPY) processing by its cleavage (Liz et al. 2009), depression and exploratory activity by modulation of the noradrenergic system, enhancement of nerve regeneration (Liz et al. 2009) through megalin-mediated internalization (Fleming et al. 2007), maintenance of normal cognitive processes during aging by acting on retinoid signaling pathway (Brouillette and Quirion 2008), and Aβ fibrils sequestration through the formation of stable complexes with Aβ peptide, preventing its deposition (Costa et al. 2008; Li et al. 2011; Schwarzman et al. 1994; Stein and Johnson 2002). TTR also cleaves Aβ aggregates or bind to them protecting against their toxicity (Cascella et al. 2013; Costa et al. 2008).

Although TTR is primarily known as a transport protein for L-thyroxine and retinol-binding protein, recent in vitro studies have shown that small molecules of a diverse variety of scaffolds-stilbenes, benzodiazepines, and phenoazines—are able to bind TTR in the L-thyroxine binding pocket (Adamski-Werner et al. 2004; Buxbaum and Reixach 2009; Johnson et al. 2009). The promiscuous binding of TTR to such aromatic compounds has led to the hypothesis that circulating TTR in the plasma (0.2-0.3 mg/mL) may play a role in the removal of potentially toxic substances or by-products of metabolism (Buxbaum and Reixach 2009). This hypothesis, however, is yet to be confirmed.

1.1.5.1. Transport of Thyroxine

Thyroid hormones including T4 and T3 (THs), are lipophilic hormones synthesized by the thyroid gland and secreted into the bloodstream. They play several main

functions. THs are essential in the normal growth, development and function of the central nervous system (CNS) (Thompson et al. 1996), participating in the maintenance of the brain homeostasis (Hulbert 2000). In mammals, most of the THs produced is T4, but T3, which is derived from the deiodination of T4 in the thyroid gland or in the periphery, constitutes the biologically active form (Yamauchi et al. 1999). In humans, the THs are secreted into the peripheral circulation but only a residual percentage of the hormone circulate in a free form (Bartalena 1990). In fact, in humans, more than 99% of THs circulate bound to one of the three major plasma TH carrier proteins: thyroxine-binding globulin (TBG), TTR and albumin and, in rodents, bound to TTR and albumin. In rodents and humans, from the three THs distributor proteins mentioned, only TTR is also produced in the brain turning it into the major T4 carrier in the CSF, transporting about 80% of its total amount (McCammon et al. 2002). In mammals, TTR also binds T3 but with lower affinity than T4. Human TTR has an intermediate affinity for T4 and T3 (7 x 107 M-1 and 1.4 x 107 M-1, respectively), while TBG has the highest and albumin the lowest affinity for these hormones (Loun and Hage 1992).

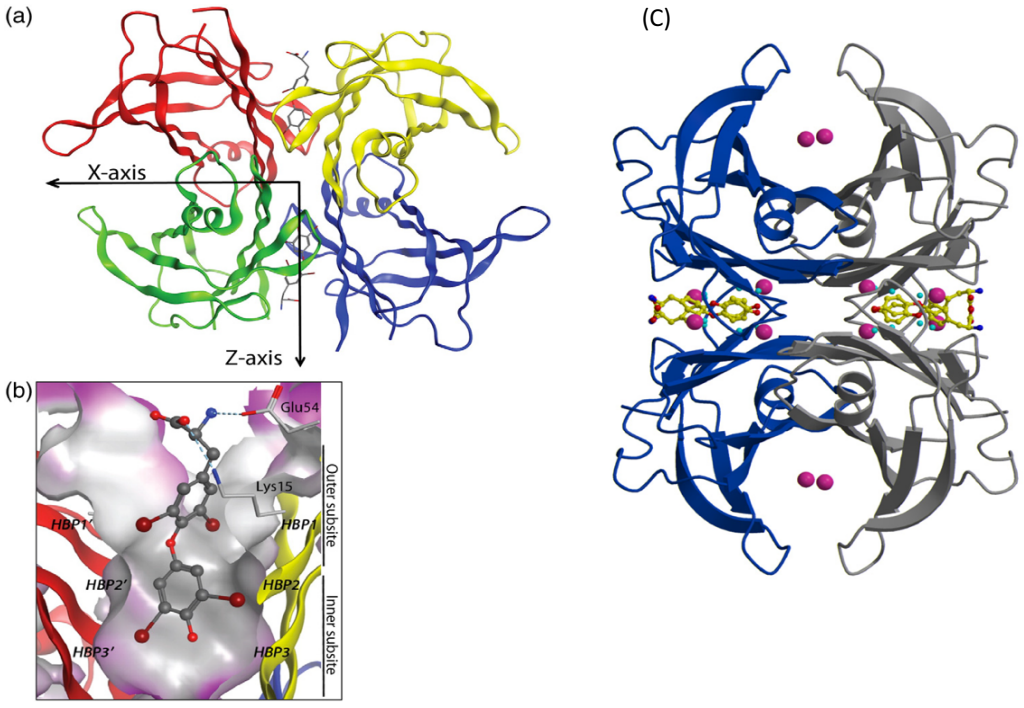

Figure 1.3. Structure of TTR (Protein Data Bank code: 2ROX). (A) Ribbon diagram depiction of TTR with the crystallographic 2-fold axis (z-axis) bisecting the T4 binding channel comprising the weaker of TTR's two dimer–dimer interfaces. (B) Close-up view of one thyroid hormone binding site with T4 (ball-andstick representation) bound, showing the iodide substituents occupying symmetry-related HBPs. Primed amino acids refer to those comprising symmetry-related subunits. Hydrogen bonds are shown as lightblue broken lines. This figure was adapted from Connelly et al. (C) Binding sites of the halide atoms. The free halides are depicted in pink and included are also the positions of thyroxine in ball-and-stick (iodines from thyroxine are in cyan).

TTR has two binding sites for T4 located in the central hydrophobic channel in the TTR tetrameric structure (Blake et al. 1974). Although these two potential binding sites to T4, each located between two of the 4 monomers, under physiological conditions only one binding site is occupied by T4, due to negative cooperativity (Blake et al. 1974). It has, however, been shown *in vitro* that with an excess of thyroxine (4:1, T4: TTR), TTR with two bound thyroxine molecules was the major complex and with an increased excess (5:1) only the fully saturated complex was observed (McCammon et al. 2002). The T4 binding channel has three main regions: a hydrophobic region formed by the hydroxyl group of Ser_{112}, Ser_{115}, Ser_{117} and Thr_{119} residues at the tetramer center, a hydrophobic portion formed by the methyl groups of Leu_{17}, Thr_{106}, Ala_{108} and Val_{121} and a charged residues group of Lys_{15}, Glu_{54} and His_{56} near the binding channel entrance that form hydrogen bond contacts, which hold T4 in the binding channel (Figure 1.3) (Klabunde et al. 2000; Wojtczak et al. 1996).

Due to T4-TTR binding, the last has emerged as a potential mediator of the T4 transport from the blood to tissues, especially into the brain (Dickson et al. 1987), through the Blood-cerebrospinal fluid barrier (BCSFB), where TTR is the major THs binding protein found (Hagen and Elliott 1973). However, the role of TTR in the delivery of THs to target tissues has been controversial (Palha et al. 2002) and, currently, the more accepted hypothesis is the free hormone hypothesis, which postulates that the free hormone concentration in blood is crucial for its biological activity, rather than the protein-bounded hormone concentration (Mendel et al. 1989). Free THs can enter cells via TH transporters located in plasma membrane or by passive diffusion and, the identified membrane bound TH transporters may assist their uptake in specific tissues (Sousa et al. 2005). A subsequent study corroborated this hypothesis: in TTR-null mice it was showed that TTR is not crucial for THs entry into the brain or other tissues (Palha et al. 1997), suggesting the presence of an alternative mechanism for T4 metabolism in the absence of TTR and a consequent redundant role of TTR in TH homeostasis, only acting as a storage molecule for THs in plasma and CSF (Palha 2002; Sousa et al. 2005).

1.1.5.2. Transport of the Complex Retinol – RBP

The TTR tetramer transports retinol in the bloodstream, through the formation of a TTR-RBP-retinol complex (Soprano et al. 1986). The RBP is a 21 kDa (183 amino acids) molecule. The retinol molecule is bound to the highly hydrophobic core of

RBP (Kanai et al. 1968). It is synthesized and secreted primarily by hepatocytes and constitutes the exclusive retinol transporter in blood (Soprano et al. 1986). The RBP secretion is stimulated upon its association with retinol, which alters the conformation of the protein. X-ray crystallography showed the conformational three dimensional structure of TTR-RBP-retinol complex and, although TTR has theoretically four binding sites for RBP, under physiological conditions, only one molecule binds to TTR tetramer, Figure 1.4 as shown in (Kopelman et al. 1976). However, *in vitro*, TTR is able to bind to two RBP molecules, each establishing molecular interactions with one of the dimers, blocking the another binding site presented in the other monomer (Figure 1.4) (Monaco et al. 1995). Interactions between RBP and TTR are mediated by residues at the entrance of the ligand binding pocket and span across the two TTR dimers. Both RBP- and T4- binding sites are independent from each other (Monaco et al. 1995).

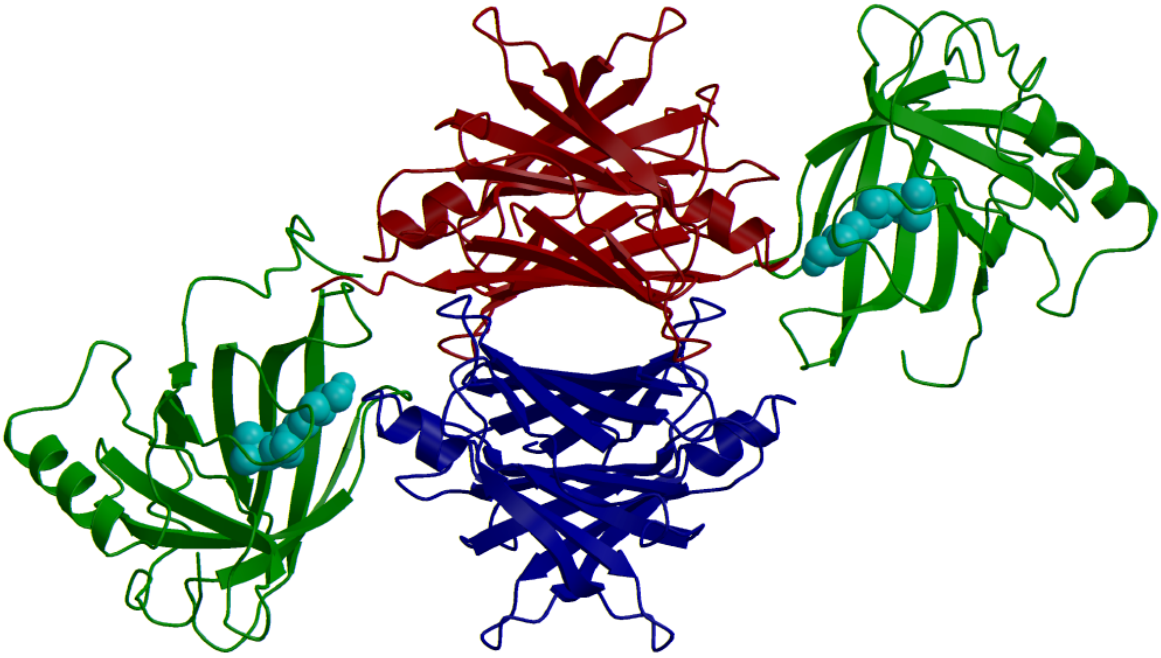

Figure 1.4: Ribbon representation of the quaternary structure of the *in vitro* complex TTR-Retinol-binding protein (RBP) - retinol complex. TTR tetramer is represented in red and blue. The retinol (vitamin A) is represented in light blue and the RBP molecules are in green. The center of the TTR channel, the HBS, which bind T4 and other small molecules, is represented empty in the figure (center). Adapted from Monaco et al. 1995.

RBP circulates in the bloodstream bound to TTR only when it is complexed with retinol, as a 1:1 molar protein complex (Goodman 1985), which facilitates its release and protects its glomerular filtration and catabolism (Raz et al. 1970). In turn, RBP constitutes the main mechanism by which cells acquire retinol because RBP protects retinol from oxidation and prevents the retinol plasma insolubility (Soprano et al.

1988). TTR also binds to retinoic acid but with less affinity than retinol (Smith et al. 1994). Retinol is an essential micronutrient in several functions, namely vision, development, reproduction and cellular differentiation (Raz et al. 1970). After retinol is delivered to tissues, the affinity of (Raz and Goodman 1969) RBP to TTR becomes reduced and, once in cells, retinol can be stored or metabolized . In plasma, both RBP and retinol prevent TTR misfolding, through stabilization of its tetrameric structure and the formation of the TTR-RBP-retinol complex may also function as a reservoir of RBP-retinol. Actually, TTR-null mice show a significant increase in the renal filtration of the retinol-RBP complex and a consequent decrease in plasma RBP and retinol levels (Episkopou et al. 1993). However, the total retinol levels in the tissues of these animals remains similar to those observed in wild-type (wt) animals, suggesting alternative mechanisms to compensate the loss of retinol delivery to tissues mediated by RBP (Raz and Goodman 1969).

The retinol uptake by cells is controversial and various mechanisms have been proposed: retinol can enter the cells by simple diffusion (Fex and Johannesson 1988); also, there could exist unidentified specific membrane receptors that interact with the complex resulting in its endocytosis (Gjoen et al. 1987); and, a third mechanism, also involving a receptor, but adding a role for cellular RBP as an acceptor of retinol inside cells, suggesting that apo-RBP remains outside the cell (Sivaprasadarao and Findlay 1994). The second and the third proposed mechanisms are the most accepted ones and, the controversy is whether RBP is internalized via, or not, during the retinol transfer by endocytosis. Until now, the role of TTR in this process is not yet clarified.

TTR is highly homologous to previously isolated TTRs despite the fact that its amino acid sequence shares only 40–55% identity with the sequence of TTR from other vertebrates (Raz and Goodman 1969). It must be emphasized, however, that the amino acids involved in the formation of the central channel in which T3 and T4 bind, are 90% homologous to human TTR and that the amino acids involved in the binding to RBP4 in higher vertebrates are also highly conserved (Figure 1.5A) (Raz and Goodman 1969). The three-dimensional structure was generated based on the known X-ray structures from human, rat, and chicken TTRs and on the sea bream TTR amino acid sequence (Power et al. 2000). According to this model, the overall topology of sea bream TTR has been conserved and the predicted monomer-monomer and dimer-dimer interfaces and tetrameric structures are similar to those determined by X-ray crystallography of human, rat, and chicken TTRs.

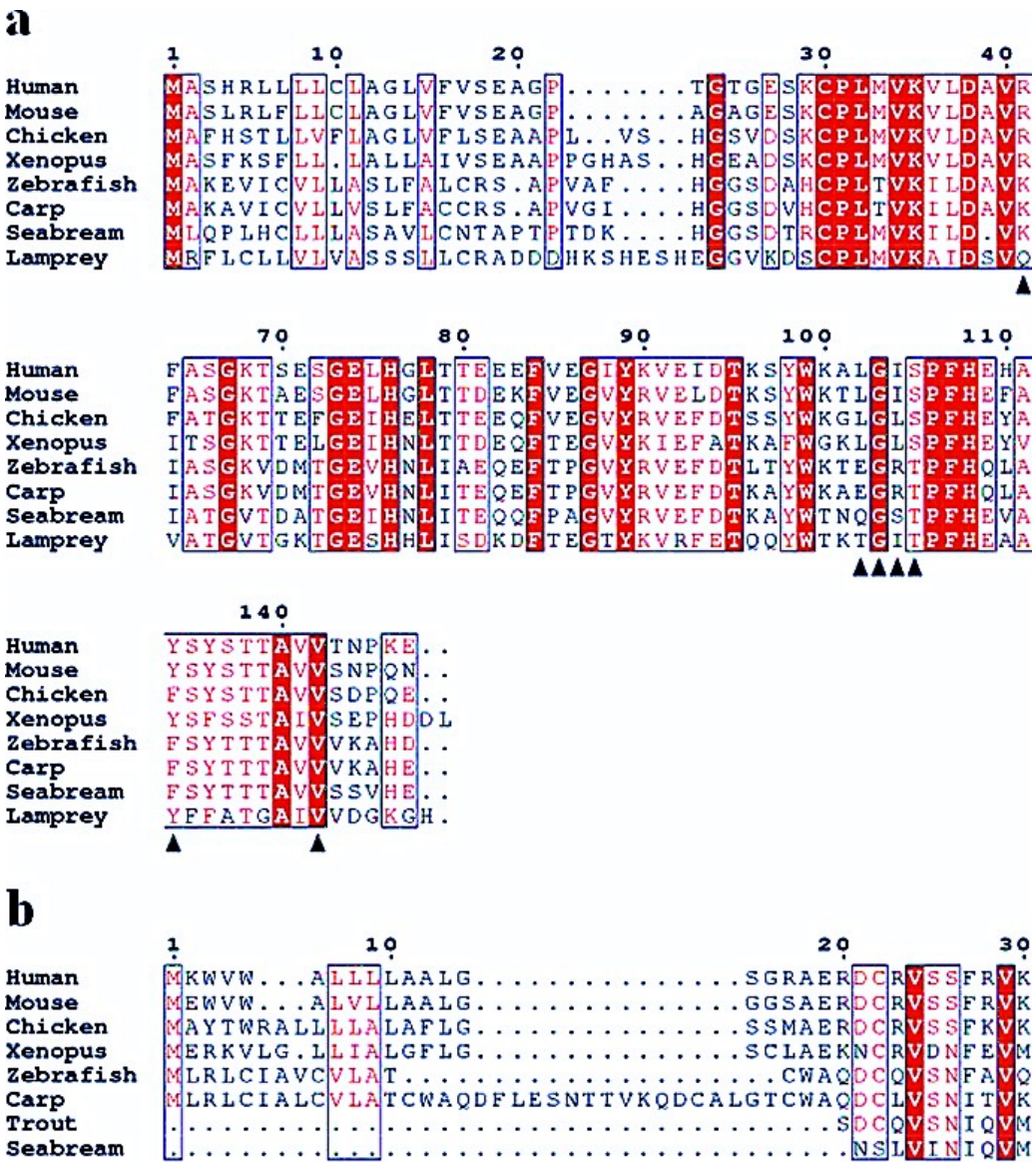

Figure 1.5. Sequence alignment of (A) TTR and (B) RBP from different vertebrates. The residues identical in all the sequences presented are shaded in red. The residues identical or chemically similar in at least six sequences are denoted by red characters. The amino acid residues in the human RBP and TTR involved in forming the RBP-TTR complex interactions are indicated by arrowheads. Sequence alignments were constructed with CLUSTAL W (Thompson et al. 1996) and annotated with Espript (Gouet et al. 1999).

1.1.5.3. Other Functions

As mentioned, TTR has been described as an important molecule that participates in several mechanisms. Beyond those already discussed, TTR plays numerous actions mainly related with various neuropathological conditions, such as AD, nerve biology and repair and anti-apoptotic and proteolytic activities (Murakami et al. 2010).

Previous studies showed that TTR has anti-apoptotic pancreatic activity as it protects β cells from apolipoprotein C-III-induced apoptosis (Jacobsson et al. 1989). Also, the anti-apoptotic activity of TTR was only observed in the tetrameric structure and it was postulated that the TTR monomer conversion must be involved in β cells

destruction in diabetes type 1 patients (Refai et al. 2005). These authors concluded that TTR is a functional component in pancreatic β cell stimulus-secretion coupling (Refai et al. 2005).

Approximately 1-2% of the plasma TTR circulates bound to high density lipoproteins (HDL) via its interaction with apolipoprotein A-I (apoA-I), which forms the TTR-apoA-I complex (Sousa et al. 2005). Liz and coworkers showed that TTR is able to cleave the C-terminus of free and lipidated apoA-I, promoting a decrease in the capacity of HDL to promote cholesterol efflux and to bind to their receptor and an increase in apoA-I amyloidogenic potential. Furthermore, authors demonstrated that the TTR proteotylic activity is slightly compromised when it is complexed with T4 and, it is lost when bound to RBP (Liz et al. 2004; Liz et al. 2007).

Neuropeptide Y (NPY) is involved in several brain mechanisms and TTR is also implicated in its regulation (Nunes et al. 2006). Liz and colleagues, showed that the NPY cleavage between Arg33 and Arg35 aa residues induced neuronal regeneration (Liz et al. 2009).

Finally, it is well known that TTR acts in Aβ metabolism as it forms stable complexes with Aβ, inhibiting its aggregation/fibril formation and clearance (Costa et al. 2008; Li et al. 2013; Schwarzman et al. 1994). Morever, TTR had also been described as exerting proteolytic actions in Aβ peptide, as it was showed that TTR cleaves the Aβ fibrils, generating smaller Aβ peptides, less toxic than the full length ones (Costa et al. 2008). This issue is further discussed in the following section (1.3 Alzheimer's Disease).

1.2. Transthyretin and its role in Disease

1.2.1. Disease associated with amyloid formation by TTR

The conversion of TTR from a uniquely folded, functional protein to highly stable, fibrillar aggregates called amyloid has been implicated in a number of disorders. TTR is one of the few proteins associated with systemic amyloidosis, a group of disorders resulting from the extracellular deposition of well-defined protein aggregates characterized by a fibrillar morphology, cross-β structure and peculiar tinctorial properties in the presence of specific dyes such as Congo red or thioflavin S (Liu et al. 2014; Westermark et al. 2007). These include senile systemic amyloidosis (SSA), a late onset disease in which wild-type TTR deposits primarily in the heart, and the

familial amyloid polyneuropathies and cardiomyopathies (FAP and FAC), wherein point mutations in the gene encoding TTR result in the deposition of protein aggregates in the peripheral nerves and heart, respectively, and the rare central nervous system selective amyloidosis (CNSA). The CNSA-associated mutants target the central nervous system (Table 1.1). Amyloid deposition of wild-type TTR occurs in the heart of 10-25% of humans older than 80 years, resulting in SSA, often leading to congestive heart failure (Lie and Hammond 1988; Tanskanen et al. 2008). Amyloid deposition by TTR is accelerated by the presence of any of the approximately 100 different amyloidogenic mutations of TTR responsible for early-onset TTR amyloidosis with autosomal dominant inheritance, such as FAP, FAC and leptomeningeal amyloidosis (Connors et al. 2003; Garzuly et al. 1996). TTR-related FAP and FAC usually have an earlier age of onset than that of SSA, occurring as early as the second decade of life. This early age of disease onset is presumably due to the decreased stability of variant TTR with respect to the wild-type protein (Table 1.1).

Table 1.1. TTR in relation to disease onset

Disease	Mutation	Clinical Classification	Age of onset (years)	Affected Population
Senile Systemic Amyloidosis (SSA)	Wild-Type	Cardiomyopathy	>60	10-25% of population over 80 years of age
Familial Amyloid Cardiomyopathy (FAC)	Various Mutations such as V122I, L111M, V20I	Cardiomyopathy	>65 >60	3-4% African Americans (~1.3 Million) 5% West Africans, High penetrance Geographic clusters
Familial Amyloid Polyneuropathy (FAP)	Various Mutations such as V30M and non V30M	Peripheral neuropathy ± cardiomyopathy	15–80	Worldwide
Central Nervous System Selective Amyloidosis (CNSA)	Highly destabilized mutant TTR (e.g., A25T or D18G TTR)	CNS amyloidosis	<50	Rarest TTR amyloid group

Table was derived from (Johnson et al. 2010).

Today, over 100 mutations in the gene encoding TTR have been implicated in the autosomal dominant disorders named FAP and FAC (Benson 1989; Damas and Saraiva 2000; Saraiva 2001). A list of all TTR mutations associated with such disorders is reported in a database named "*Mutations of Hereditary Amyloidosis*" [http://www.amyloidosismutations.com/mut-attr.php]. As shown in Figure 1.6, these amyloid causing mutations are distributed throughout the entire molecule of TTR. It

is important to note that many of the mutations associated with TTR amyloid formation are conservative, resulting in little or no perturbation to the overall structure of the protein (Hornberg et al. 2000; Steinrauf et al. 1991; Terry et al. 1993). Most of the mutations, however, have been shown to influence the thermodynamic stability of TTR, a property which correlates well with disease severity (Bonifacio et al. 1996; Hammarstrom et al. 2002; Jiang et al. 2002; Jiang et al. 2001a; Mccutchen et al. 1993; Quintas et al. 1997; Sekijima et al. 2005). For instance, mutations known to severely destabilize the native fold of TTR, such as the L55P mutation, often display an aggressive pathology with disease onset occurring as early as the second decade of life (Hou et al. 2007).

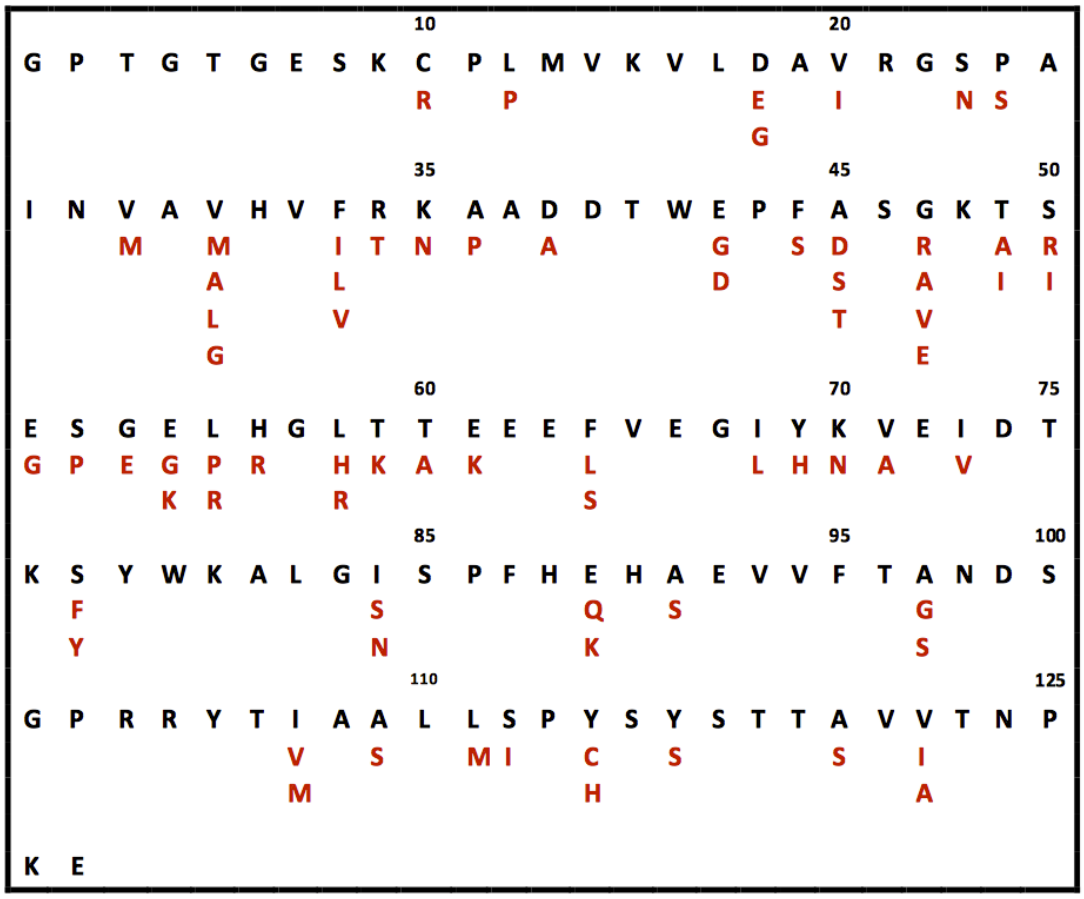

Figure 1.6. Amino acid sequence of human TTR. Amyloid causing mutations are highlighted in red and positioned underneath primary sequence of TTR. (Adapted from Hou, Aguilar et al., 2007)

Strikingly, not all TTR mutations lead to pathology. Non-amyloidogenic mutations, such as the T119M mutation, have been identified and shown to stabilize the native fold of TTR. These mutations have also been shown to have a protective effect against the development of disease in heterozygotic individuals with different

mutations in both alleles of the TTR gene (Hammarstrom et al. 2001; Hammarstrom et al. 2003; Shnyrov et al. 2000).

1.2.2. Structural Features of amyloid fibrils

The presence of fibrillar protein aggregates is a hallmark of all amyloid diseases (amyloidoses), including the TTR disorders mentioned in the previous section. It is important to note that while there are many chemically distinct proteins known to form amyloid *in vivo*, all amyloid fibrils, possess the structural features and properties discussed herein, irrespective of the protein from which they are derived.

Much of the structural information available about amyloid fibrils come from imaging techniques, such as electron and atomic force microscopy, and X-ray fiber diffraction patterns of isolated fibrils. Under an electron microscope, amyloid deposits typically appear as uniform, unbranched, fibrillar structures-about 100 Å in diameter- of variable length (Cohen and Calkins 1959) (Figure 1.7A). X-ray fiber diffraction patterns of isolated fibrils reveal what appears to be a unique cross-β structure. This conformation consists of β-sheets that run parallel to the long axis of the fibril while their constituent strands run perpendicular to the fibril axis (Eanes and Glenner 1968; Jaroniec et al. 2002; Pras et al. 1968). A schematic of this is shown Figure 1.7B.

It is important to note that amyloid fibrils formed *in vitro* are morphologically indistinguishable from those formed *in vivo*. Overall, the term "amyloid" is generally used to refer to insoluble, highly ordered fibrillar aggregates with specific tinctorial or dye-binding properties.

Although amyloid fibril formation has been implicated in the aetiology of the TTR amyloidoses, it is currently unclear whether the accumulation of fibrils in specific organs and tissues or the process of fibril formation is responsible for disease pathology and progression. With this topic widely discussed and debated in the field, the remainder of the introduction will focus on the mechanism of amyloid fibril formation by TTR.

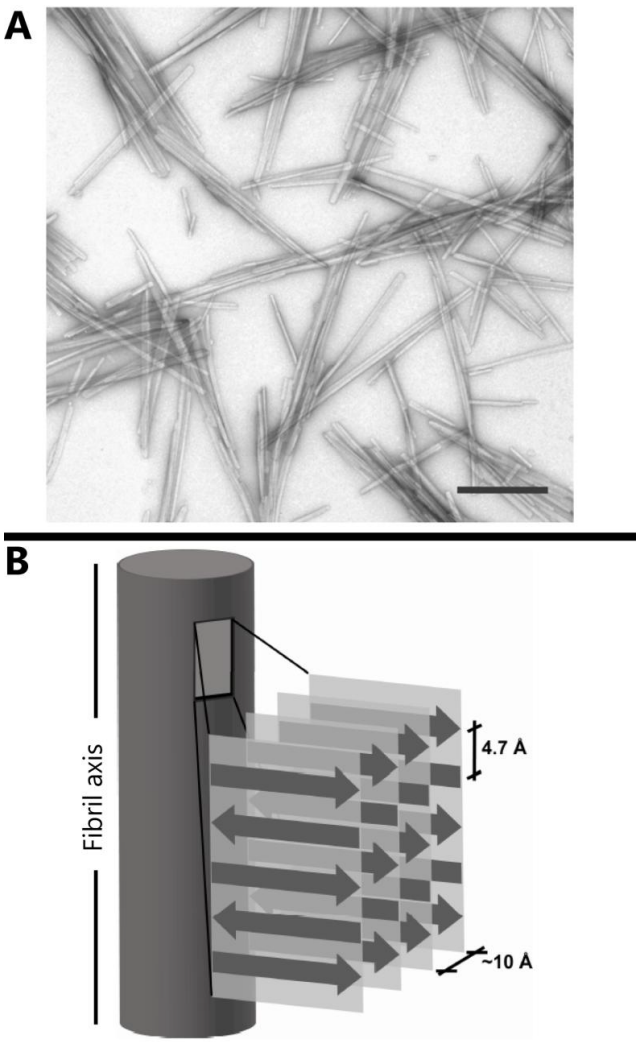

Figure 1.7. Structural features of the amyloid fibril. (A) Electron micrograph of TTR amyloid fibrils formed with residues 105-115 in vitro (scale bar: 200 nm). (B) Schematic of the cross-β structure of amyloid fibrils. The structural repeat of 4.7 Å along the fibril axis corresponds to the spacing between adjacent β-strands while the 10 Å spacing perpendicular to the fibril axis corresponds to the separation of the β-sheets (Taken from Jaroniec et al., 2002).

1.2.3. Mechanism of Amyloid Formation

The precise mechanism by which TTR undergoes amyloid fibril formation *in vivo* is currently unknown. While it is not yet clear how and where TTR forms amyloid in humans, biophysical studies reveal that tetramer dissociation is the rate-limiting step for amyloidogenesis and that the natively folded monomer must first undergo partial denaturation to become competent for misassembly through a nonnucleated thermodynamically favorable process (Figure 1.8) (Colon and Kelly 1992; Hammarstrom et al. 2002; Hammarstrom et al. 2001; Hammarstrom et al. 2003; Jiang et al. 2001b; Lai et al. 1996; Liu et al. 2000; Sekijima et al. 2005). This occurs very inefficiently under physiological conditions but is accelerated under acidic conditions because the tetramer to natively folded monomer to partially denatured monomer

equilibria are shifted toward the latter, facilitating amyloidogenesis. (Colon and Kelly 1992; Hammarstrom et al. 2002; Hammarstrom et al. 2001; Hammarstrom et al. 2003; Jiang et al. 2001b; Lai et al. 1996; Liu et al. 2014; Liu et al. 2000; Sekijima et al. 2005)

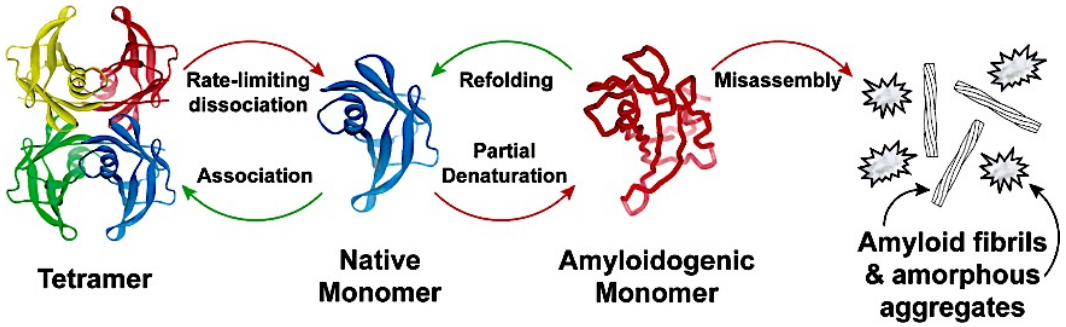

Figure 1.8. Schematic of the TTR amyloidogenesis pathway based on biophysical studies with insight from pathological studies. Rate-limiting tetramer dissociation affords natively folded monomers that can either reassociate or partially unfold. At sufficient concentration, the misfolded monomers can assemble via a downhill polymerization to afford a variety of aggregate morphologies including amorphous aggregates and amyloid fibrils. The small soluble TTR oligomers formed early in this pathway are reported to be cytotoxic (Reixach et al. 2004; Sousa et al. 2001).

The most compelling evidence for the unit responsible for TTR fibrillogenesis came from the work of Kelly and colleagues, who reported that acidic conditions mimicking the lysosomal environment induce the dissociation of TTR into a monomeric, partially unfolded amyloid competent intermediate which self assembles into fibrils *in vitro* (Colon and Kelly 1992; Kelly 1998; Kelly et al. 1997; Lai et al. 1996; Peterson et al. 1998). Studies conducted by other groups using serum-range concentrations of TTR at nearly physiological pH and microscopy studies coupled with mass per length measurements also confirmed that TTR fibrillogenesis likely results from the self-assembly of a monomeric unit (Gouet et al. 1999). Over time, the emergence of additional studies on the mechanism of TTR fibril formation, including those conducted by Liu and collegues (Liu et al. 2000), led to the realization that the building block for TTR amyloid fibril formation is the monomeric subunit of the protein, albeit with an altered tertiary structure.

Therefore, the concept emerged that a strategy for ameliorating the amyloidoses caused by the misfolding and misassembly of a protein like TTR, which normally adopt folded, non-amyloidogenic 3-D structures, focuses on preventing the conformational excursions from the native state or partial denaturation that renders them amyloidogenic (Figure 1.9) (Hammarstrom et al. 2003; Johnson et al. 2009; Kelly 1998; Kelly et al. 1997; Miroy et al. 1996). Stabilizing the properly folded,

non-amyloidogenic conformations of these proteins is considered to be the most conservative approach for treating these maladies, because it is still unclear which misfolded or misassembled TTR conformation, leads to proteotoxicity (Lacor et al. 2004; Lambert et al. 1998; Reixach et al. 2004; Sousa et al. 2001). There is mounting evidence that stopping the process of amyloidogenesis without necessarily clearing the deposited amyloid fibrils is sufficient to stop the degeneration of post-mitotic tissue and disease progression (Coelho 2007; Rydh et al. 1998). In the case of TTR amyloidogenesis, the tetramer must first dissociate and then the natively folded monomer must undergo partial denaturation in order for the TTR subunits to become aggregation competent (Hammarstrom et al. 2002; Hammarstrom et al. 2001; Hammarstrom et al. 2003; Jiang et al. 2001a; Johnson et al. 2012; Kelly et al. 1997; Lai et al. 1996).

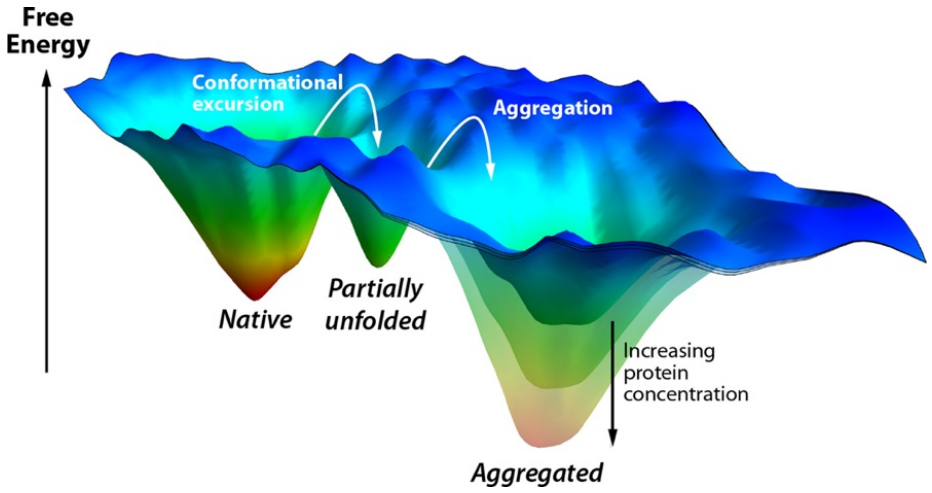

Figure 1.9. Folding free energy landscape of an amyloidogenic protein that normally forms a well folded 3D structure, but can also aggregate as a consequence of a conformational change, e.g., TTR or lysozyme. Three energy wells are shown: the native state, a partially unfolded amyloidogenic intermediate, and an aggregated state. Conformational excursions convert the native state to the partially unfolded state, which can then aggregate. The stability of the aggregated state depends on the protein concentration. At low protein concentrations, it would be less stable than the native state, and therefore not substantially populated. As the protein concentration increases, it becomes increasingly stable, and will eventually become the most stable state.

Several mechanisms have been proposed to explain the aggregation of amyloidogenic proteins (Ferrone 1999; Powers and Powers 2006). In the most widely accepted mechanism, multiple chains of the amyloidogenic protein assemble into an oligomeric nucleus in the rate-limiting step, before the rate of amyloid fibril formation becomes substantial. This scenario is referred to as a nucleated polymerization (Figure 1.10, top) (Ferrone 1999). For other proteins, e.g. Aβ whose aggregation appears to cause Alzheimer's disease, rapid oligomerization of the amyloidogenic protein into spherical or amorphous micelle-like assemblies is

observed and these undergo slow conversion into amyloid fibrils in a process associated with a high activation barrier. The latter mechanism is referred to as a nucleated conformational conversion and appears to govern Aβ aggregation, at least in vitro (Figure 1.10, middle panel) (Lee et al. 2012). TTR aggregation proceeds by yet a third mechanism, referred to as a downhill polymerization reaction (Hurshman et al. 2004). After rate-limiting tetramer dissociation, and monomer misfolding, the partially denatured TTR monomers aggregate very efficiently because the misassembled dimer is more stable than the dimer and the misassembled trimer is more stable than the disassembled dimer, etc. TTR aggregation does not require nucleus formation, is not amenable to seeding, and is limited only by the relatively low activation barriers of the bimolecular association of misfolded TTR monomers and oligomers, thus the downhill polymerization designation (Figure 1.10, bottom panel) (Hurshman et al. 2004).

After monomeric TTR undergoes partial denaturation, it spontaneously misassembles into a variety of aggregate morphologies, including amyloid fibrils and more structurally diverse aggregates exhibiting varying extents of cross-β-sheet structure (Figure 1.8) (Hurshman et al. 2004; Lashuel et al. 1999). Because TTR aggregation is very efficient once the misfolded monomer state is reached, it seems unwise to try to block TTR aggregation after the rate-limiting tetramer dissociation. The tetramer–monomer–unfolded monomer equilibria (Figure 1.8) are strongly thermodynamically linked (Hurshman Babbes et al. 2008). Thus, destabilization of either the tetramer or the monomer (and perhaps even the dimer in some mutants) can enhance TTR amyloidogenicity (Hammarstrom et al. 2003; Hurshman et al. 2004; Hurshman Babbes et al. 2008; Jiang et al. 2001a; Kelly et al. 1997; Lashuel et al. 1999; Mccutchen et al. 1993; Sekijima et al. 2005). Generally, the disease-associated TTR mutations characterized to date either decrease the tetrameric quaternary structural stability, or accelerate tetramer dissociation, or decrease the monomer's tertiary structure stability, or cause a combination of these effects (Hammarstrom et al. 2003; Hurshman et al. 2004; Hurshman Babbes et al. 2008; Jiang et al. 2001a; Kelly et al. 1997; Lashuel et al. 1999; Mccutchen et al. 1993; Sekijima et al. 2005).

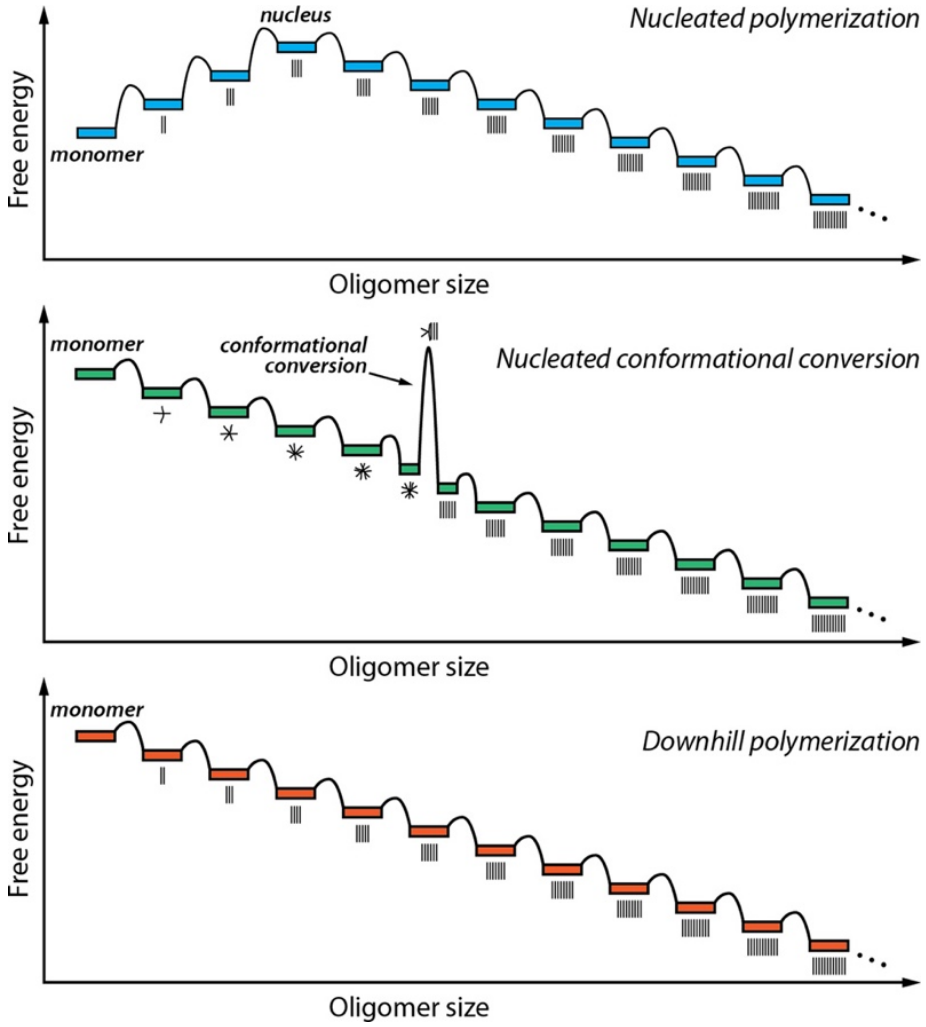

Figure 1.10. Energy diagrams associated with three distinct mechanisms of protein aggregation. In a nucleated polymerization (top), the initial association events are unfavorable until a critical size is reached. The oligomer of this size is referred to as the nucleus. Subsequent steps are favorable, making further growth favorable for oligomers larger than the nucleus. In a nucleated conformational conversion (middle), facile initial association steps form amorphous oligomers. Oligomers of a certain size can undergo a rate-limiting conversion step, in which they change from an amorphous structure to a cross-β-sheet fibrillar state. Subsequent steps are favorable, as in the nucleated polymerization. In a downhill polymerization (bottom), the mechanism by which TTR aggregates, all of the association steps are favorable after formation of the amyloidogenic intermediate, and there is no kinetic barrier to oligomerization. The aggregates shown are ordered, but they need not be; TTR forms a collection of aggregate structures.

1.2.4. Structure of the amyloidogenic state

Considerable effort has been expended to determine the structure of the monomeric amyloidogenic state of TTR populated at weakly acidic pH values. Early studies performed by Kelly and coworkers illustrated that the monomeric, amyloid competent intermediate formed in the fibrillogenesis pathway of TTR consists of six β-strands, instead of the eight normally observed in the native monomer (Kelly et al. 1997; Lai et al. 1996). Local conformational changes involving the C and D strands of the monomeric subunit were thought to occur immediately following TTR tetramer dissociation, leading to the exposure of key hydrophobic residues normally buried in

the native form of the protein (Kelly et al. 1997; Lai et al. 1996). In fact, biophysical and limited proteolysis experiments have led to the conclusion that upon acidification tetrameric TTR dissociates into monomers with the subsequent unfolding of the β-strand C, the β-strand D and the connecting CD loop (Kelly et al. 1997; Lai et al. 1996).

In another report, it was proposed, on the basis of hydrogen/deuterium exchange experiments coupled to NMR, that the β-sheet CBEF is the most destabilized upon acidification of TTR at pH 4.5 (Liu et al. 2000). Significant advances have been reached with a double mutant of TTR carrying two single mutations (F87M/L110M) designed to destabilise the molecular interface between the subunits that compose the tetramer (Jiang et al. 2001b). This double mutant, generally referred to as M-TTR, was shown to be stable as a monomer at neutral pH and has proved a unique tool for characterizing, at the molecular level, the transition from the folded non-amyloidogenic monomer populated at neutral pH to the amyloidogenic state populated at low pH (Jiang et al. 2001b). Solution NMR studies have shown that M-TTR is folded at neutral pH, with many of the resonances of the β-sheet DAGH exhibiting line broadening, particularly the β-strand H, indicative of structural fluctuations (Lim et al. 2013). By contrast, the β-sheet CBEF is not just folded, but also substantially packed. Upon acidification to pH values promoting amyloid fibril formation, line broadening extends to the β-strand D, the D-E loop, the E-F helix, and the residues of the A-B loop forming interactions with the helix, whereas most residues of the β-sheet CBEF maintain sharp, non-broadened resonances (Lim et al. 2013). These observations have been confirmed later on tetrameric TTR at mildly low pH (Lim et al. 2016b).

Hence, it is not yet clear if the partial unfolding of the monomeric folded unit of TTR to produce the amyloidogenic state involves the β-strands C and D and the interconnecting loop (Kelly et al. 1997; Lai et al. 1996), the CBEF β-sheet (Liu et al. 2000) or only the peripheral portion of the DAGH β-sheet (Lim et al. 2013). A scheme of the proposed amyloidogenic states of TTR is presented in Figure 1.11.

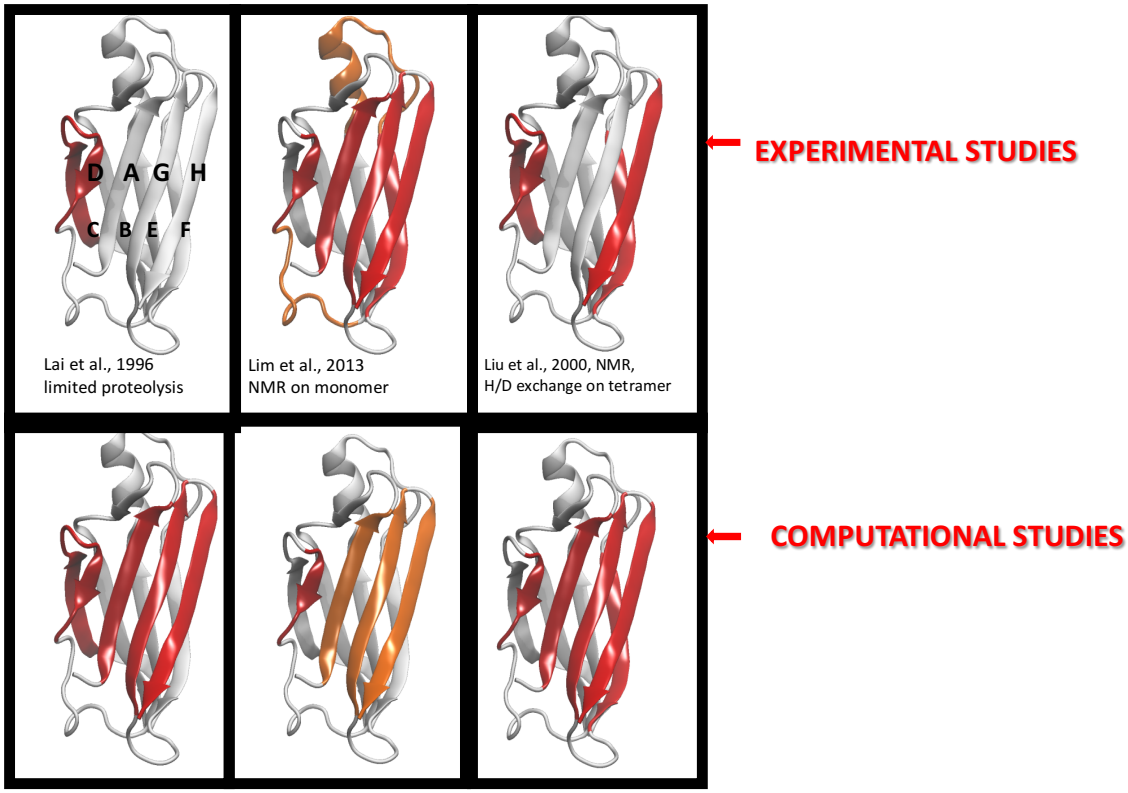

Figure 1.11. Structural rearrangements in the TTR monomer thought to give rise to the amyloidogenic intermediate. The red colour indicates the unfolding segments and the orange colour shows the destabilize protein segment.

In an independent study, the folding process of M-TTR was characterized kinetically and at equilibrium using a number of biophysical probes, leading to the identification of a molten globule state populated at equilibrium at low urea concentrations and to an off-pathway partially folded state populated transiently during the folding process of M-TTR (Conti et al. 2014). The correspondence between any of such conformational states and the amyloidogenic state of M-TTR populated at weakly acidic pH has not yet been established.

1.2.5. The possible role of proteolytic cleavage in amyloid fibril formation

In addition to full-length M-TTR, the TTR fragment encompassing residues 49-123 and generated by proteolytic cleavage of the peptide bond Lys48–Thr49, was proposed to be the main fragment present in *ex vivo* TTR amyloid fibrils, regardless of the presence, nature or position of the amyloidogenic mutation (Bergstrom et al. 2005; Ihse et al. 2013; Thylen et al. 1993). The protease responsible for such a

cleavage has not yet been identified, but the highly specific cleavage suggests that it could be a trypsin-like serine protease. Meanwhile Westermark and collaborators have elegantly characterized the constituents of TTR amyloid fibrils extracted from cardiac amyloid deposits and adipose tissue, identifying two clearly, distinct categories (Bergstrom et al. 2005; Ihse et al. 2013; Westermark et al. 1996). Type A fibrils contain a high proportion of truncated species that are not found in type B fibrils, which are composed almost entirely of full-length TTR. The possible pathogenic role of proteolytic cleavage is suggested further by the clinical course in patients with hereditary TTR amyloidosis who undergo liver transplantation to replace their variant TTR production with wild-type TTR. Individuals with type A fibrils in their cardiac deposits have a notably poorer outcome, often with rapidly progressive cardiac involvement (Gustafsson et al. 2012; Marcoux et al. 2015).

It was recently shown that limited proteolysis of the highly destabilized S52P variant of TTR generates the 49–127 fragment that, if released under physiological fluid agitation, rapidly self-aggregates into very stable aggregates together with the full-length protein (Mangione et al. 2014). This behavior has also been found in other variants (Marcoux et al. 2015). It is not yet clear if the proteolytic cleavage occurs before or after the fibrils are deposited, but the molecular mechanism of this remarkable phenomenon and whether it underlies amyloid fibrillogenesis by other amyloidogenic TTR variants, including the wild-type protein, are fundamental to understanding the pathogenesis of this amyloid disease (Mangione et al. 2014).

1.2.6. Transgenic Animals

Multiple attempts have been made to generate transgenic murine models of TTR amyloidosis (Kohno et al. 1997; Tagoe et al. 2007; Teng et al. 2001; Yamamura et al. 1987). Successful models use the human TTR gene regulated by its own promoter with tissue specific expression. They require integration of multiple copies of the gene and production of large amounts of the human protein in the mouse. Transgenic animals expressing low concentrations of amyloid-prone mutant human TTR, including the very aggressive L55P variant (L55P TTR) do not develop amyloid deposits. Silencing the murine gene by targeted disruption in the presence of the human L55P TTR gene resulted in tissue deposition (Sousa et al. 2002; Tagoe et al. 2007). These observations suggest that incorporation of endogenous murine TTR subunits into heterotetramers otherwise composed of transgene-encoded human TTR increases the kinetic stability of such heterotetramers, thereby preventing

dissociation, aggregation, and deposition. However, at present, none of the murine transgenic models of TTR amyloidosis exhibits ideal characteristics. While some of the variations reflect general differences between humans and mice, the details of which are not fully understood, some others are a consequence of particular features of murine molecules and their interaction with transgene products (Reixach et al. 2008). Additionally, animal models only represent an experimental surrogate and results obtained from mouse experiments do not necessarily recapitulate the human situation.

Despite these limitations transgenic animals have proven particularly useful in the assessment of small molecules in pre-clinical studies, particularly when a promising drug requires validation at the animal model level before undergoing clinical trials (Almeida and Saraiva 2012; Teixeira et al. 2016). Similarly, animal models expressing human TTR have been very useful in the validation of methods based on RNA silencing in ameliorating the symptoms and histopathology of TTR amyloidosis (Butler et al. 2016; Goncalves et al. 2016).

1.3. Alzheimer's Disease

1.3.1. Discovery the disease and the amyloid hypothesis

In 1906, at the 37th meeting of the Society of Southwest German Psychiatrists in Tübingen, Alois Alzheimer presented the case of his patient Auguste Deter. In this single case, he described the main clinical and neuropathological characteristics of a disease that was later named after him: memory disturbance, cognitive impairment, neuron loss, miliary bodies (plaques) and dense bundles of fibrils (tangles) (Alzheimer 1907). Today, it is known that Alzheimer's disease (AD) is the most common neurodegenerative disease, with nearly 30 million cases worldwide (data from Alzheimer's Association, 2012). AD is a neurodegenerative disorder widely abundant in elderly people. Pathological hallmarks of AD include intracellular neurofibrillary tangles consisting of insoluble deposits of hyper-phosphorylated microtubule-associated tau protein and extracellular amyloid plaques deposition, mainly composed by neurotoxic Aβ peptides (Maccioni et al. 2001).

Despite the many pathological characteristics of AD, the most consensual hypothesis that explains the disease process is the amyloid hypothesis. It states that

the gradual accumulation and aggregation of the hydrophobic Aβ peptides can directly and indirectly, through the generation of a complex cascade of molecular events, result in progressive synaptic and neuritic injury, which, subsequently, leads to hyperphosphorylation of tau and formation of neurofibrillary tangles (Hardy and Higgins 1992). Indeed, Aβ accumulation, oligomerization and deposition within the brain are the main hallmarks in the pathogenesis of AD and imbalances between its production and clearance results in AD progression. Aβ is found in the extracellular fluids of the brain, including the CSF, and in the interstitial fluids surrounding neurons and glial cells in brain lobes (Vigo-Pelfrey et al. 1993).

1.3.2. Amyloid-beta metabolism

The Aβ peptides (~4kDa) are proteolytic cleavage products of the sequential processing of the amyloid precursor protein (APP) by β- and γ-secretases. The amyloid precursor protein (APP) is a highly conserved transmembrane, type-1, integral glycoprotein that is ubiquitously expressed and around 110-135 kDa in size (Selkoe et al. 1988). APP is composed of three domains: a large hydrophilic N-terminal extracellular domain, a single hydrophobic transmembrane domain and a small C-terminal cytoplasmic domain (Kang et al. 1987). It is ubiquitously expressed in neuronal and non-neuronal cells. The APP gene is located on chromosome 21 (Goate et al. 1991; Korenberg et al. 1989). Through alternative splicing 8 isoforms of APP are generated. Among these, APP695, APP751 and APP770 are the three major isoforms containing 695, 751, and 770 amino acids, respectively (Sandbrink et al. 1996). APP695 is mainly expressed in the CNS, particularly in neurons, while APP751 and APP751 are also widely expressed in other tissues (O'Brien and Wong 2001). The highest levels of APP695 expression in the brain could be detected in the cerebellum, cortex and hippocampus (Sola et al. 1993). APP is synthesized in the endoplasmic reticulum and it is transported through the Golgi apparatus to the trans-Golgi-network (TGN) and TGN-derived vesicles to the cell surface to be cleaved or endocytosed and, either back into the TGN (Caporaso et al. 1994) or degraded by lysosomes, where α-, β- and γ-secretases act (Nunes et al. 2006).

The cleavage of APP involves a variety of secretases (α-, β- and γ-secretases) and can occur in two different pathways: a non-amyloidogenic pathway, which prevents the formation of Aβ peptides (α- and γ-secretase cleavages), and an amyloidogenic pathway, which generates Aβ peptides (β- and γ-secretase cleavages). The amyloidogenic pathway comprises an initial cleavage by β-secretase that

generates a larger extracellular soluble APP-beta (sAPPβ) and a membrane anchored C-terminal end (C99). Then, γ-secretase acts on C99 in the Aβ domain generating Aβ peptide and the APP intracellular domain (AICD). The γ-secretase cleavage site within the C99 is variable and produces a variety of Aβ peptides whose sizes range from 39 to 43 amino acids (Figure 1.12). Even though, there are two major Aβ species, $A\beta_{1\text{-}40}$ and $A\beta_{1\text{-}42}$. The predominant form is the $A\beta_{1\text{-}40}$, whose levels are ten times higher comparing to $A\beta_{1\text{-}42}$ (Lorenzo and Yankner 1994). However, $A\beta_{1\text{-}42}$ is more prone to aggregate and to form amyloid fibrils (Jarrett and Lansbury 1993), is significantly more neurotoxic and is the major specie accumulated in senile plaques (Tsuzuki et al. 2000). The Aβ peptides are mainly produced by plasma membranes and released to the extracellular space where they can deposit as senile amyloid plaques (LaFerla et al. 2007). They can also be deposited as diffuse deposits as an intermediate step in the formation of compact amyloid plaques. It is clear that APP cleavage takes a central position in AD pathogenesis, as alterations in its processing result in increased Aβ peptide generation, which is deposited as amyloid plaques in AD brains (Li et al. 2011). Indeed, aberrant and/or cumulative Aβ production, have been postulated to be the main etiological basis of AD.

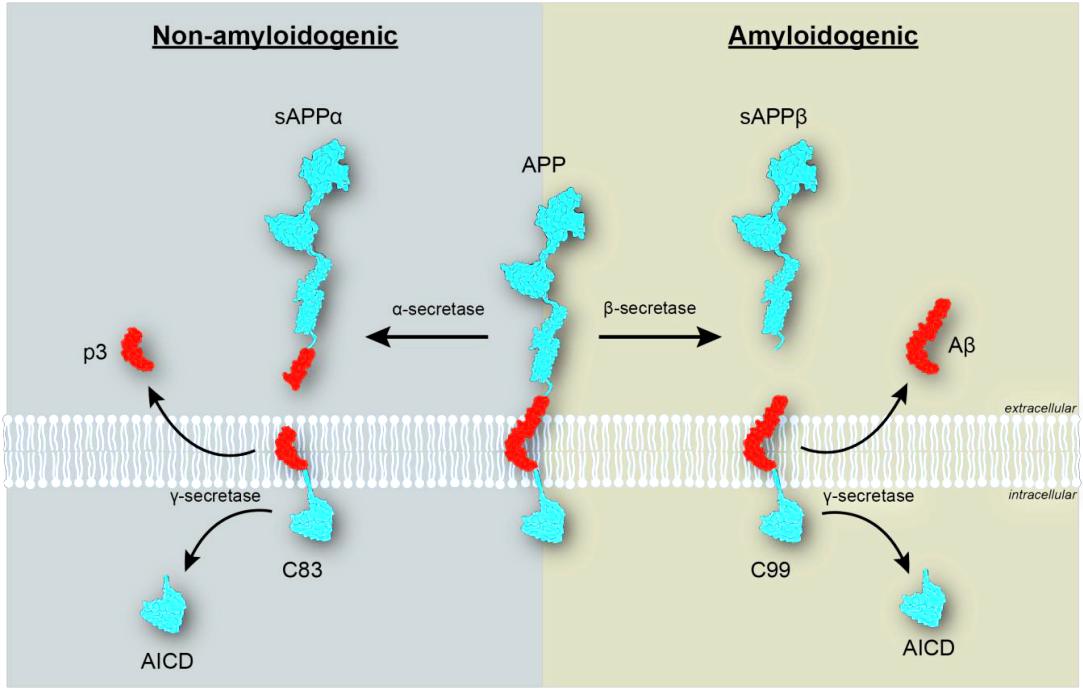

Figure 1.12. APP processing. Schematic diagram showing non-amyloidogenic and amyloidogenic APP processing. In the non-amyloidogenic processing APP is sequentially cleaved by α-secretase and γ-secretase (left) releasing the p3 fragment. In the amyloidogenic processing the Aβ peptide is released via β-secretase and γ-secretase (right).

1.3.3. Role of TTR as an Aβ detoxifier

The clearance of Aβ in the human CNS takes place in the extracellular space and is controlled by the brain Aβ degradation and its efflux from the CNS to the peripheral circulation through the blood-brain barrier or BCSFB (Zlokovic 2004). This process is mediated by various proteins. In fact, some reports recognized several extracellular proteins, present in CSF, as Aβ carriers: α-1-antichymotrypsin (Aksenova et al. 1996), apolipoprotein E (ApoE) (Strittmatter et al. 1993) and apolipoprotein J (ApoJ) and TTR (Schwarzman et al. 1994). The sequestration hypothesis for the Aβ clearance emerged. It suggests that normally produced Aβ is sequestrated by certain extracellular proteins, thereby preventing amyloid formation and Aβ toxicity (Schwarzman et al. 1994).

Several proteins are involved in Aβ production, degradation and clearance (Santos et al. 2012). Among them, TTR has been described as a protective molecule in Aβ metabolism (Schwarzman et al. 1994) because it binds to Aβ, forming stable complexes (Mazur-Kolecka et al. 1997) and preventing its aggregation/amyloid formation (Schwarzman et al. 1994). In fact, the non-mutated form of TTR was identified as the major Aβ binding protein in the CSF that could decrease the aggregation state of the peptide and its toxicity (Carro et al. 2002; Schwarzman et al. 1994). Morever, other authors observed that TTR expression is induced in response to an overproduction of Aβ peptides (Stein and Johnson 2002) and an inverse correlation exists between TTR levels and senile plaques abundance (Elovaara et al. 1986; Merched et al. 1998; Serot et al. 1997), raising the possibility of an inadequate physiological sequestration of Aβ in the CSF/extracellular fluid (Serot et al. 1997). Moreover, lack of amyloid plaques in young AD mouse models is associated with increased levels of TTR, whereas neutralization of TTR is associated with increased Aβ levels, tau phosphorylation, neuronal loss and apoptosis in the hippocampus (Stein and Johnson 2002). Even though, it remains unknown whether the decreased levels of TTR in the CSF are restricted to AD and are a primary or a later event in the disease onset/progression (Chiang et al. 2009).

An *in vitro* protein-protein interaction study, between TTR and Aβ aggregates indicated that TTR is protective due to its capacity to bind toxic or pretoxic Aβ aggregates, both intra and extracellularly. Using APP23 transgenic mice models of AD carrying the human TTR (hTTR) gene, authors showed that hTTR overexpression was ameliorative whereas silencing of the endogenous mouse TTR gene accelerated the development of AD phenotype (Buxbaum et al. 2008). Others

observed that Aβ levels and deposition were higher in the brains of an AD model of transgenic mice crossed to carriers of a TTR hemizygous deletion (ceAPPswe/PS1ΔE9/TTR+/- mice) compared to age-matched controls (ceAPPswe/PS1ΔE9/TTR+/+ mice) (Choi et al. 2007), without altering APP processing. Likewise, transgenic mice harboring APPswe/PS1ΔE9 transgenes that lead to development of AD, maintained in an enriched environment, resulted in increased TTR expression and notable declines in cerebral Aβ levels and amyloid deposits, compared to mice held in standard housing conditions (Lazarov et al. 2005). In Caenorhabditis elegans expressing human Aβ42, TTR diminished the neurodegeneration prompted by the Aβ toxic peptides (Link 1995). Despite such finding, a recent study in Tg2576 mice concluded that the absence of TTR inhibited Aβ deposition (Wati et al. 2009). Besides some controversy, TTR is generally considered as a neuroprotective molecule in AD (Fleming et al. 2009).

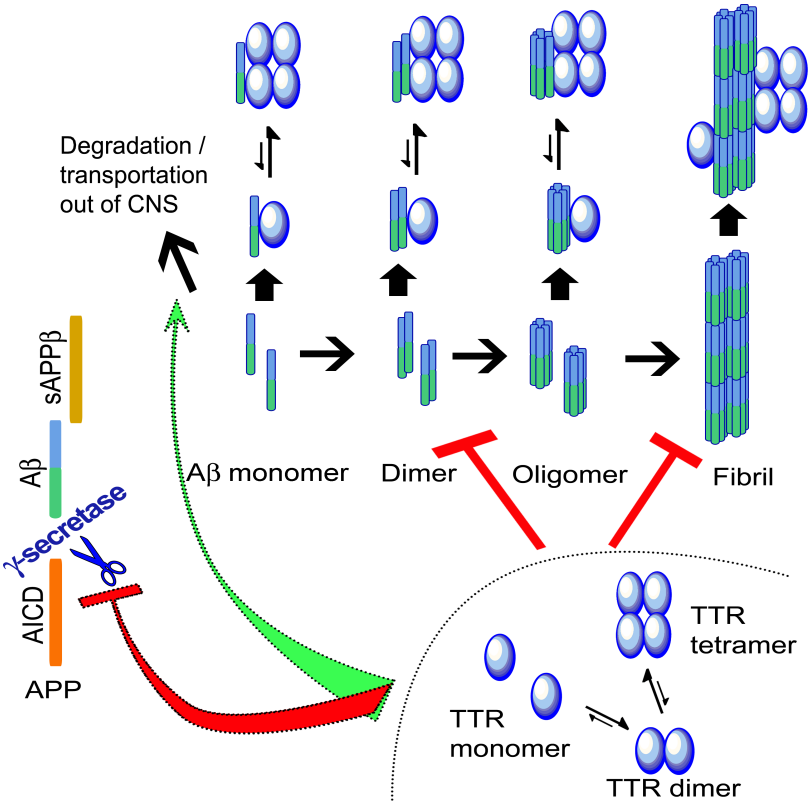

Figure 1.13. Proposed mechanisms of TTR inhibition of Aβ toxicity. TTR inhibition of Aβ aggregation (fibril formation) was reported by many groups (Schwarzman et al. 1994; Buxbaum et al. 2008; Li et al. 2011; Costa et al. 2008; Giunta et al. 2005; Liu et al. 2006) and current evidence suggested that the binding is mediated by association of monomeric TTR to Aβ. It is also possible that TTR facilitates Aβ degradation directly (Costa et al. 2008) or indirectly, transports of Aβ from CNS into serum (plasma sink hypothesis) (Schwarzman et al. 1994; Schwarzman et al. 2004). TTR may also inhibit Aβ production by inhibition of g-secretase cleavage (Li et al. 2011).

Costa and coworkers showed that TTR decreased the rate of aggregation without affecting the fraction of Aβ in the aggregate pool and promoted removal of

deposited/insoluble Aβ in amyloid plaques (Costa et al. 2008). The nature of TTR-Aβ binding was confirmed by various authors and it is now well established that it occurs on Aβ monomers, oligomers and fibrils. Analyses of the *in vitro* interaction between human TTR and Aβ, using predominantly solid phase assay systems, have shown that TTR binds to all forms of Aβ: monomers, oligomers and fibrils (Buxbaum et al. 2008; Costa et al. 2008; Du and Murphy 2010; Liu and Murphy 2006). The binding depends on the quaternary structure of TTR, with monomeric TTR binding Aβ with higher affinity than tetrameric TTR (Buxbaum et al. 2008; Costa et al. 2008; Du et al. 2012; Du and Murphy 2010; Liu and Murphy 2006). Moreover, the binding occurs with higher affinity for Aβ oligomers, aggregates and fibrils with respect to Aβ monomers (Buxbaum et al. 2008; Costa et al. 2008; Du et al. 2012; Du and Murphy 2010; Liu and Murphy 2006). In addition to inhibiting Aβ fibril formation, TTR was also shown to bind to preformed Aβ oligomers and fibrils and reduce their toxicity to murine primary neurons and human neuroblastoma SH-SY5Y cells (Cascella et al. 2013; Li et al. 2011). It was then shown that low concentrations of TTR tetramers are able to inhibit Aβ aggregation in vitro through the biding of monomeric Aβ to the thyroxine binding pocket of the TTR tetramer, ano observation obtained with NMR and epitope mapping (Li et al. 2013). In the same study it was found that M-TTR did not bind Aβ monomers, while its was able to bind Aβ oligomers and inhibit fibril formation (Li et al. 2013). This suggested that inhibition of fibrillogenesis is mediated by TTR tetramer binding to Aβ monomers and M-TTR binding of Aβ oligomers. However, the precise mechanisms by which the TTR-Aβ interaction occurs and how TTR alters Aβ aggregation and clearance are not completely understood.

It is important to note that, although nearly consistent global data regarding the role of TTR in Aβ degradation and clearance, some of the contradictory results could be promoted by variables that were not considered or evaluated, as the gender or the animal model. Accordingly, a study performed in APPswe/PS1A246E transgenic mice crossed with TTR-null mice, showed a gender-associated modulation of brain Aβ levels and brain sex steroid hormones (SSHs) by TTR, thus suggesting that decreased levels of brain SSHs in female mice with reduced TTR expression may underlie their AD-like neuropathology (Oliveira et al. 2011). More recently, similar results were obtained by Ribeiro and colleagues (2012) where they found decreased plasma TTR levels in mild-cognitive impairment and AD patients, gender-dependent (Ribeiro et al. 2012).

Despite intensive research about the TTR-Aβ binding and on the role of TTR (both tetramer and monomer TTR) in Aβ aggregation, degradation and clearance, further studies are required to disclose the mechanisms that mediate the expression of TTR, particularly in choroid plexus and to unravel the whole functions of TTR in Aβ metabolism, aggregation and clearance.

1.4. Aim of thesis

As described in section 1.2, transthyretin (TTR) is a homotetrameric protein and is one of the few human proteins associated with systemic amyloidosis. In spite of its link to human pathology, an anti-amyloidogenic effect that prevents fibril formation of the amyloid β (Aβ) peptide associated with Alzheimer's disease (AD) and that inhibits Aβ oligomer toxicity has been proposed for TTR. As described in section 1.3, previous data do not offer any insight into the mechanism by which TTR inhibits Aβ fibril formation and oligomer toxicity and on the TTR form responsible for such an effect. Furthermore, the key structural events inducing TTR to adopt an amyloidogenic conformation are not yet clear.

In this thesis, I tried to address both aspects. I labeled various form of TTR (WT-TTR, M-TTR, W79F-M-TTR, W41F-M-TTR) with a coumarin derivative, which generates the FRET phenomenon with the endogenous tryptophan residues present in native TTR. In this FRET strategy, the tryptophan residues act as FRET donors and the coumarin derivative as the FRET acceptor. The ability of TTR to form soluble oligomers and insoluble fibrils, on the one hand, on to act as a molecular detoxifier, on the other hand, are based on the structural plasticity of the protein and thus on subtle conformational changes in the soluble state of TTR. FRET is an ideal technique to detect such subtle structural changes and is thus a very promising approach to address these two issues. In addition, the key structural events at the basis of TTR self-aggregation and TTR-oligomer interaction were monitored with a number of techniques. These include X-ray crystallography, optical absorption spectroscopy, far-UV circular dichroism spectroscopy, intrinsic and extrinsic fluorescence spectroscopy, stopped-flow devices, turbidimetry, dynamic and static light scattering, atomic force microscopy, and other biophysical and biochemical techniques.

Chapter 2
Materials and methods

2.1 Protein expression, purification and mutagenesis of TTRs

The pMMHa plasmid containing the WT-TTR or M-TTR gene was transformed into competent BL21 DE3 Epicurian Gold cells (Strategene, Amsterdam, Netherlands). M-TTR was previously obtained by introducing two mutations at the dimer-dimer interface (F87M and L110M) in the Hu-TTR plasmid DNA by site-directed mutagenesis (Jiang et al. 2001). Moreover, two mutant proteins named W79F-M-TTR and W41F-M-TTR were produced by site-directed mutagenesis starting from the DNA plasmid of M-TTR. Mutations in the gene coding for M-TTR were generated using the QuickChange site-directed mutagenesis kit (Agilent Technologies, Santa Clara, CA, USA). The DNA sequences of the wild-type and mutated genes were checked with DNA sequencing.

Both the WT and mutant proteins were isolated and purified from recombinant sources following previously described procedures (Reixach et al. 2008). In brief, the initial culture of *Escherichia coli* cells containing the plasmid was grown until cell growth was visible before inoculating 15 ml of such culture into 1.5 L of LB media with 100 μg/ml of ampicillin in 2.8-liter Fernbach flasks. Cells were grown at 37°C with vigorous shaking until an OD_{600} of 1.0–1.2 was reached; they were then induced with 1 mM isopropyl β-D-thiogalactoside (IPTG) and grown overnight at 37°C with vigorous shaking, except for W41F M-TTR which was incubated overnight at 25 °C. Cells were then harvested by centrifugation at 8,200 rpm (21,0000 g) for 10 min at 4 °C using a Beckman JA-10 rotor kept in the cold room; then the cells were resuspended in 400 ml (100 ml per liter of culture) of TBS (20 mM Tris, 0.5 M NaCl, pH 7.5 1 mM PMSF and 1 mM EDTA), then sonicated in the cold room, or ice bath (3x3 min with 3 s pulses, 100 amplitude resting, 1 min between cycles). Pellet cell debris was collected by centrifugatrion at 9,000 rpm (12,000 g) for 15 min (Beckman JA-10 rotor), the resuspended ammonium sulfate pellet was desalted by dialysis against 25 mM Tris, pH 8.0 at 4 °C. To increase purity and remove soluble aggregates, the resulting solution was chromatographed on a ionic exchange, HR-Q column (23 ml) using buffers A (25 mM Tris, pH 8.0, 1 mM EDTA) and buffer B (25 mM Tris, pH 8.0, 1 M NaCl, 1 mM EDTA) with the gradient program starting from 0% buffer B, going to 20% buffer B in 1CV; going to 35% buffer B in 9CV; keeping 35% buffer B for 1/2CV and then going to 100% buffer B in 2CV. The samples were collected at 21% buffer B till 35% buffer B. Pool fractions containing

TTRs were concentrated down to ~20 ml using an ultrafilter and a 10 KDa MWCO membrane. These TTR variants were further purified by gel filtration by employing a Superdex 75 gel filtration column (Amersham Pharmacia, Piscataway, NJ). The purification yield of WT-TTR, M-TTR and W79F-M-TTR was usually ~10−30 mg/L of LB culture. By contrast, the purification yield of W41F-M-TTR was low, usually ~5−15 mg/L of LB culture. Purified proteins were stored at −20 °C in 20 mM phosphate buffer, pH 7.4. The molecular masses of the purified variants were checked with MALDI mass spectrometry. Protein purity was found by SDS-PAGE to be >95% in all cases.

2.2 Purification of $A\beta_{40}$ monomer

The recombinant $A\beta_{40}$ peptide was expressed in the *Escherichia coli* BL21Gold (DE3) strain (Stratagene, Amsterdam, Netherlands) and purified as described previously with slight modifications (Walsh et al. 2009). Solutions of monomeric peptides were prepared by dissolving the lyophilized $A\beta_{40}$ peptide in 6 M GuHCl. Monomeric forms were purified from potential oligomeric species and salt using a Superdex 75 10/300 GL column (GE Healthcare, Uppsala, Sweden) at a flowrate of 0.5 mL/min, and eluted in 20 mM sodium phosphate buffer, pH 7.4, 25 °C supplemented with 150 mM NaCl. The center of the absorbance peak was collected and the peptide concentration was determined from the absorbance of the resulting solution using $\varepsilon_{280} = 1490\ mol^{-1}\ cm^{-1}$.

2.3 Labeling of TTRs with DACM

Each protein variant was diluted to 0.2 mM in 20 mM phosphate buffer at pH 7.4, 25 °C. Aliquots of DACM dissolved in pure DMSO were added to a tenfold molar excess of dye. The sample was wrapped with aluminium foil and incubated under shaking for 1 h at 37 °C. The reaction was quenched with 5 µl of TFA. The unbound dye was removed by extensive dialysis, using membranes with a 3.0 kDa molecular weight cut off, and the sample was then centrifuged to remove any precipitate. DACM concentration of the resulting labelled protein sample was determined using $\varepsilon_{381} = 27{,}000\ M^{-1}\ cm^{-1}$. Protein concentration was measured at 280 nm using $\varepsilon_{280} = 18450\ M^{-1}\ cm^{-1}$ for M-TTR, $\varepsilon_{280} = 77600\ M^{-1}\ cm^{-1}$ for wt TTR, $\varepsilon_{280} = 12950\ M^{-1}$

cm^{-1} for W79F and W41F M-TTR, after subtraction of the contribution of an equimolar concentration of DACM-GSH.

2.4 Dynamic Light Scattering (DLS) Measurements

All TTR samples were prepared at a final protein concentration of 15 μM in 20 mM phosphate buffer, pH 7.4, 25 °C or 20 mM acetate buffer, pH 4.4, 25 °C. $A\beta_{40}$ samples were prepared at various peptide concentrations in 20 mM phosphate buffer pH 7.4, 25 °C, 150 mM NaCl. Before the measurements, the protein samples were filtered with Anotop filters having a cutoff of 20 nm (Whatman, Little Chalfont, UK). DLS measurements were performed using a Zetasizer Nano S device from Malvern Instruments (Malvern, Worcestershire, U.K.) thermostated with a Peltier system. Low-volume 10 × 4 mm disposable cells were used. The values of refractive index and viscosity set on the instrument were determined using the software provided with the instrument, based on the information of buffer and temperature provided by the user. The hydrodynamic radius was deduced from translational diffusion coefficients using the Stokes-Einstein equation. Diffusion coefficients were inferred from the analysis of the decay of the scattered intensity autocorrelation function. All such calculations were performed by the instrument automatically. The presented size distributions were the average of three consecutive measurements.

2.5 X-ray Crystallography

DACM-WT-TTR and DACM-M-TTR were concentrated and buffer-exchanged at 4 °C with Amicon Ultra-4 Centrifugal Filter Unit with Ultracel-3 membrane, Ultracel® - 3K (Merck Millipore, Billerica, MA, USA) down to a final concentration of 12 mg/ml, in 100 mM KCl, 20 mM Sodium Phosphate, pH 7.4. Both were crystallized by sitting drops technique at 20 °C: DACM-WT-TTR crystallized in 0.2 M $CaCl_2$, 0.1 M HEPES sodium, pH 7.5, 28% v/v polyethylene glycol 400; DACM-M-TTR crystallized in 0.2 M $CaCl_2$, 0.1 M sodium acetate, pH 4.6, 20% v/v 2-propanol. Both were cryoprotected adding glycerol to the crystallization solution (final concentration 30% v/v) and flash-frozen in liquid nitrogen. Diffraction data for DACM-WT-TTR and DACM-M-TTR were collected at the European Synchrotron Radiation Facility (ESRF, Grenoble, France) at the ID23-1 and at the ID23-2 beam line to the resolution of 1.42 Å and 1.7 Å, respectively.

To assess if DACM was damaged during the X-ray data-collection, crystal absorption spectra were collected before and after the diffraction experiment at ID29S (ESRF): both spectra display the maximum absorption at 384 nm typical of DACM and their intensities are comparable ruling out major radiation damage (data not shown).

The diffraction data were integrated and processed using MOSFLM (Leslie 1992), POINTLESS and SCALA (Collaborative Computational Project 1994; Evans 2006; McNicholas et al. 2011). The crystal structure of DACM-WT-TTR was determined using BALBES (Long et al. 2008) while that of DACM-M-TTR was determined by MOLREP (Vagin and Teplyakov 1997) using the structure of M-TTR (pdb code: 1GKO) as a search model. Refinement was performed using Refmac5 and Phenix Refine (Adams et al. 2010; Murshudov et al. 1997). Manual model building, visual inspection, addition of water molecules were carried out with Coot (Emsley and Cowtan 2004). Images of all TTR structures were generated by CCP4mg (McNicholas et al. 2011).

2.6 Molecular Dynamics (MD) Simulations

M-TTR was modelled with the Amber99sb force field (Hornak et al. 2006), while DACM was modelled with the GAFF force field (Wang et al. 2004). Starting from the X-ray crystallographic structure of DACM-M-TTR, the system was solvated with 5171 TIP3P water molecules in a volume of 1750 $Å^3$. A MD simulation was carried out with Gromacs 4.5.5 for 20 ns at the temperature of 300 K, maintained by a Nosè-Hoover thermostat.

2.7 Fluorescence spectroscopy

Fluorescence emission spectra (excitation 290 nm) were recorded using a PerkinElmer LS 55 spectrofluorimeter (Waltham, MA, USA) equipped with a thermostated cell holder attached to a Haake F8 water bath (Karlsruhe, Germany). For typical FRET measurements protein samples were diluted to a concentration of 3 μM in 0.5 ml, in 20 mM sodium phosphate buffer, 0.0-7.8 M urea, pH 7.4, 25 °C, unless stated otherwise. A 4 x 10 mm quartz cuvette was used. For FRET measurements during TTR aggregation protein samples were diluted to a

concentration of 1, 3, 7, 14, 28 μM in 0.7 ml under the conditions reported in the "Turbidimetry" section (section 2.10). A 2 x 10 mm quartz cuvette was used.

FRET of TTRs during aggregation of $A\beta_{40}$ was monitored by collecting fluorescence emission spectra of the sample fractions taken during the incubation of $A\beta_{40}$ with TTRs at molar ratio 1:3 (TTR: $A\beta_{40}$). TTRs (monomer) and $A\beta_{40}$ concentrations were 3 and 9 μM, respectively, in 20 mM sodium phosphate buffer, pH 7.4, 25 °C. A 2 x 10 mm quartz cuvette was used.

$A\beta_{42}$-derived diffusible ligands (ADDLs) solutions were prepared by incubating $A\beta_{42}$ for 24 hr using Lambert and coworkers' protocol (Lambert et al. 1998). The time dependent changes of FRET of TTRs interacting with ADDLs was determined by collecting fluorescence emission spectra of TTRs at o, 20, 40 and 60 min in the presence and absence of ADDLs. A 2 x 10 mm quartz cuvette was used.

2.8 Equilibrium urea unfolding

28-34 samples of TTRs were prepared containing 3 μM protein in 20 mM phosphate buffer, pH 7.4, with urea concentrations ranging from 0 to 7.8 M and were incubated for 1 hr at 25 °C. Fluorescence spectra were acquired at 25 °C from 300 to 550 nm (excitation 290 nm) using the spectrofluorimeter, water bath and cuvette described above. Plots of fluorescence at a given wavelength (either 348 nm or 462 nm) *versus* urea concentration were analyzed with the two-state unfolding model provided by Santoro and Bolen (Jiang et al. 2001b; Santoro and Bolen 1988) to obtain quantitative measurements of the free energy change upon denaturation in the absence of denaturant ($\Delta G_{H_2O}^{U-F}$), the dependence of the free energy change upon denaturation on urea concentration (m value) and the concentration of middle denaturation (C_m).

2.9 Stopped-Flow measurements

Unfolding and refolding reactions of TTRs were followed using a Bio-Logic (Claix, France) SFM-3 stopped-flow device equipped with an FC-08 cuvette, coupled to a fluorescence detection system and thermostated with a Haake F8 water bath (Karlsruhe, Germany). Excitation wavelength was 290 nm. Band-pass filters cutting emission below 385 nm and 320 nm were used to monitor DACM and tryptophan fluorescence, respectively. All the experiments were performed in 20 mM phosphate buffer at pH 7.4 and 25 °C, at final protein concentrations of 1.5−2.9 μM. For the

unfolding experiments, native proteins in 0.5 M urea were diluted into solutions containing urea at final concentrations ranging from 3.0 to 6.5 M. Refolding reactions were initiated by 10- to 20-fold dilutions of the protein denatured with 5 M urea into solutions containing low urea at final concentrations ranging from 0.25 to 3.5 M. The dead time was generally 10.4 ms. Folding/unfolding kinetic traces were analysed as previously described (Conti et al. 2014). In another set of experiments, the equilibrium signal measured at the end of unfolding kinetics was plotted *versus* urea concentration to linearly extrapolate the fluorescence of the labelled or unlabelled unfolded protein under native conditions (0.5 M and 2.1 M urea).

2.10 Turbidimetry

15 μM M-TTR and 15 μM DACM-M-TTR were incubated in 20 mM acetate buffer, pH 4.4, 37 °C, in the presence of 0, 30, 60, 90 or 137 mM NaCl. 15 μM W79F-M-TTR and 15 μM DACM-W79F-M-TTR were incubated in 20 mM acetate buffer, pH 5.6, 37 °C, in the presence of 0, 30, 60, 90 or 137 mM NaCl**.** The time dependent development of turbidity at 450 nm was followed at 37 °C using a Jasco V-630 spectrophotometer (Tokyo, Japan), thermostated within ± 0.1 °C by a Haake F8 water bath (Karlsruhe, Germany) and using a 10 mm path length cell. All turbidity values were blank subtracted.

2.11 Far-UV CD spectroscopy

Far-UV CD spectra of samples of containing 16 μM M-TTR, W41F M-TTR and W79F M-TTR in 20 mM sodium phosphate buffer, pH 7.4, 25 °C were collected from 185 to 250 nm using a J-810 Spectropolarimeter from Jasco (Tokyo, Japan) equipped with a thermostated cell holder attached to a Thermo Haake C25P water bath (Karlsruhe, Germany). All spectra were blank subtracted and converted to mean residue ellipticity per residue [Θ]. A 0.1 cm path length cuvette (Hellma, Müllheim, Germany) was used.

Additionally, the far-UV CD spectra of WT-TTR, M-TTR and W79F-M-TTR in the absence and presence of $A\beta_{40}$ following a co-incubation of 30 min were compared in 20 mM sodium phosphate buffer, pH 7.4, 25 °C using the same instrument and cell. Total protein concentrations of 0.1 mg/ml were used when recording the CD

spectra of either individual proteins or protein mixtures (TTR- $A\beta_{40}$). In the case of protein mixtures, mean residue ellipticity values [Θ] were calculated as:

$$[\Theta]_{mix} = \Theta / [(c_1 n_1)/m_1) + (c_2 n_2 /m_2)] \quad (1)$$

where l is the path length and has a value of 0.1 cm, n_1 and n_2 are the numbers of residues of TTR and $A\beta_{40}$, respectively, m_1 and m_2 are the molecular masses in daltons of TTR and $A\beta_{40}$, respectively, c_1 and c_2 are the protein concentrations of TTR and $A\beta_{40}$, respectively, expressed in mg/ml for each of the two proteins in the mixture. The theoretical average ellipticity values per residue ($[\Theta]_{avg}$), assuming that neither unstructured-to structured transitions nor secondary structure rearrangements occur, were calculated as follows:

$$[\Theta]_{avg} = ([\Theta]_1 n_1 + [\Theta]_2 n_2 R)/(n_1 + n_2 R) \quad (2)$$

where $[\Theta]_1$ and $[\Theta]_2$ correspond to the measured mean residue ellipticity values, n_1 and n_2 to the number of residues of TTR and $A\beta_{40}$, respectively, and R to the excess molar ratio of protein.

2.12 ThT Fluorescence

The obtained $A\beta_{40}$ sample was diluted with 20 mM phosphate buffer, 150 mM NaCl at pH 7.4, 25 °C to the desired peptide concentration ranging from 5 μM to 20 μM and supplemented with a small volume of 1 mM Thioflavin T (ThT) solution to a final ThT concentration of 20 μM. In another set of experiments, the obtained $A\beta_{40}$ sample and one TTR sample (either WT-TTR, M-TTR or W79F M-TTR) were diluted to a final $A\beta_{40}$ concentration of 10 μM and to various protein concentrations, ranging from 0.0001 μM to 10 μM, in 20 mM phosphate buffer, 150 mM NaCl, pH 7.4, 25 °C and supplemented with a small volume of 1 mM Thioflavin T (ThT) solution to a final ThT concentration of 20 μM. All samples were prepared in low binding eppendorf tubes on ice using careful pipetting to avoid introduction of air bubbles. Each sample was then pipetted into multiple wells of a 96-well half-area, low-binding, clear bottom and PEG coating plate (Corning 3881), 80 mL per well. ThT fluorescence was measured using plate reader (Fluostar Omega, Fluostar Optima, or Fluostar Galaxy; BMG Labtech).

2.13 AFM imaging

$A\beta_{40}$ samples were removed from the aggregation reaction and were directly deposited onto freshly cleaved mica surfaces and allowed to dry for 30 min. Samples were then washed with Milli-Q water and then dried with nitrogen. AFM images were acquired using a VEECO Dimension 3100 atomic force microscope (Bruker, USA) and a JPK Nanowizard software. The instrument was operated in tapping mode in air using n-type silicon cantilevers with resonant frequencies between 65 and 130 kHz.

2.14 Seeding experiments

For the seeded experiments, preformed fibrils were prepared prior to the experiment, just as above incubating 20 μM $A\beta_{40}$ samples in 20 mM sodium phosphate buffer, pH 7.4 with 150 mM NaCl and 20 μM ThT. The ThT fluorescence was monitored to verify the formation of fibrils. Samples were then collected from the wells into low-binding tubes. Under the considered conditions, the monomer concentration is negligible at equilibrium. The final concentration of fibrils, in monomer equivalents, was considered equal to the initial concentration of monomer. Fibrils were then added to freshly prepared $A\beta_{40}$ monomer samples in order to reach either 5% or 35% final concentration of seeds. Each sample was then pipetted into multiple wells of a 96-well half-area, low-binding, clear bottom and PEG coating plate (Corning 3881), 80 mL per well and incubated under the same conditions described above.

2.15 Cell cultures

Human SH-SY5Y neuroblastoma cells (ATCC Microbiology, Manassas, VA) were cultured in DMEM, F-12 Ham with 25 mM HEPES and $NaHCO_3$ (1:1) and supplemented with 10% FBS, 1.0 mM glutamine and antibiotics. Cell cultures were maintained in a 5.0% CO_2 humidified atmosphere at 37 °C and grown until they reached 80% confluence for a maximum of 20 passages.

2.16 MTT reduction assay

The effect of protein oligomers on cell viability was assessed using SH-SY5Y cells in 96-well plates, and using the 3-(4,5-dimethylthiazol-2-yl)-2,5-diphenyltetrazolium bro-mide (MTT) assay as described (Pensalfini et al. 2011). Preformed oligomers of

M-TTR preincubated for different length of time and at different concentrations of NaCl from 0 to 137 mM were incubated, and their toxicity tested.

2.17 Statistical analysis

Light scattering data was expressed as mean ± standard error of the mean (SEM). Data of MTT reduction were expressed as mean ± standard deviation (SD) or standard error of the mean (SEM). Comparisons between different groups were performed using ANOVA followed by Bonferroni's post-comparison test. A p-value lower than 0.05 was considered statistically significant.

Chapter 3
Results

3.1 Study of the conformational changes of TTRs using FRET

3.1.1 Purification and Labeling of M-TTR

I first purified M-TTR and labelled it with N-(7-Dimethylamino-4-Methylcoumarin-3-yl)Maleimide (DACM), as described in the *Methods* section. The samples containing the purified unlabelled and labelled proteins were analysed with MALDI mass spectrometry (Figure 3.1). A single peak at 13895±10 and 14193±10 Da were detected for unlabelled and labelled M-TTR respectively, in agreement with the expected molecular weights of the two protein samples, i.e. 13894.7 Da and 14193.0, respectively. In the mass spectrum of DACM-M-TTR I could not detect peaks corresponding to the molecular weights of M-TTR with double or triple DACM labelling, excluding the presence of M-TTR labelled with two or more DACM moieties. I could not detect any peak corresponding to unlabelled M-TTR, indicating that no detectable unlabelled protein remained at the end of the labeling reaction.

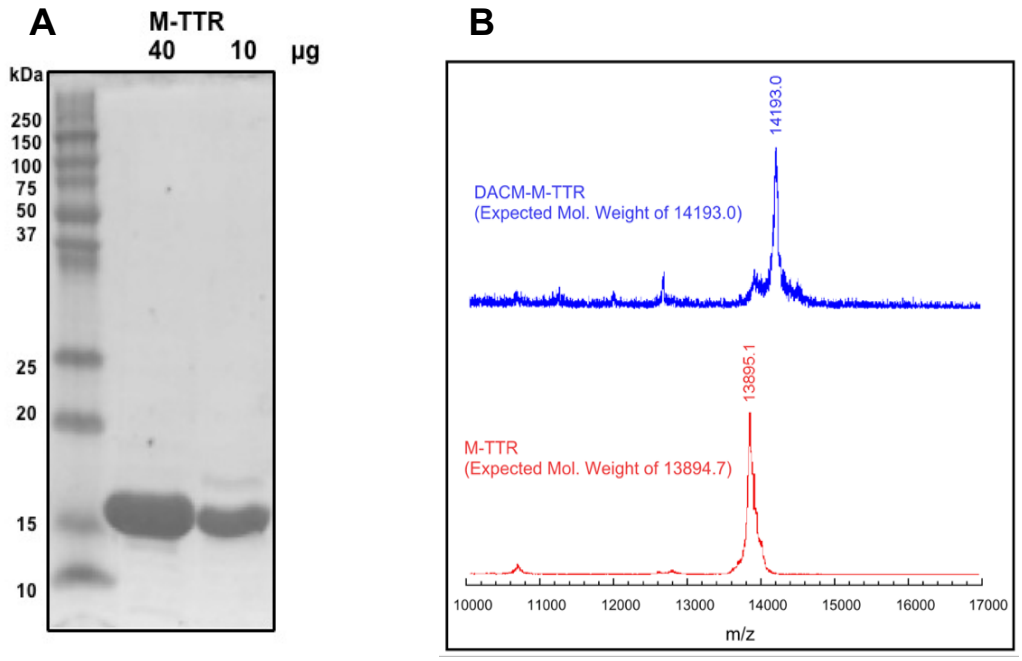

Figure 3.1. M-TTR purification and Labelling. (A) SDS-PAGE of M-TTR after purification. An aliquot of the protein after purification (40 µg, left) and following a 4-fold dilution (10 µg, right) were loaded. (B) MALDI mass spectrometry analysis of M-TTR (blue) and DACM-M-TTR (black). The expected molecular weights for human M-TTR and DACM-M-TTR are 13894.7 and 14193.0, respectively.

As an evidence that unlabelled and labelled M-TTR are monomeric, I assessed the size distributions of M-TTR, DACM-M-TTR and wild-type tetrameric

TTR (WT-TTR) by means of dynamic light scattering (DLS) at pH 7.4, 25 °C (Figure 3.2). An apparent hydrodynamic diameter of 4.20±0.11 nm was observed for M-TTR, which is consistent with the hydrodynamic diameter of monomeric folded M-TTR, as reported previously (Conti et al. 2014; Jiang et al. 2001b; Pires et al. 2012). An apparent hydrodynamic diameter of 5.03±0.10 nm was observed for DACM-M-TTR. This diameter is higher than that of unlabelled M-TTR, possibly due to the presence of the covalently attached and solvent exposed DACM moiety. A diameter of 5.03±0.10 nm is, however, significantly lower than that measured for wild-type tetrameric TTR (6.17±0.02 nm) and of that expected for labelled dimeric M-TTR (> 5.23 nm) and labelled tetrameric M-TTR (> 6.66 nm). Overall, the DLS results indicate that both M-TTR and DACM-M-TTR are monomeric.

Next, in order to gauge the labelling degree of DACM-M-TTR, I acquired optical absorption spectra of DACM-M-TTR and of DACM covalently attached to glutathione (DACM-GSH) at pH 7.4, 25 °C and at the same probe concentration (Figure 3.2B). The concentration of DACM bound to M-TTR was determined by measuring the optical absorption at 381 nm (A_{381}), using a molar extinction coefficient (ε_{381}) of 27,000 cm^{-1} M^{-1} (Figure 1C, blue spectrum). Protein optical absorption in the DACM-M-TTR sample was then reconstructed by subtracting the spectrum of DACM-GSH (Figure 1C, green spectrum) from that of DACM-M-TTR sample (Figure 1C, blue spectrum). In the resulting difference spectrum (Figure 1C, red spectrum), protein concentration was measured at 280 nm (A_{280}), using a molar extinction coefficient (ε_{280}) of 18,450 cm^{-1} M^{-1} (an ε_{280} value of 12,950 cm^{-1} M^{-1} was used for the W79F mutant described below). Labelling degree *d* was then calculated using:

$$d(\%) = 100 \cdot (A_{381} \,/\, \varepsilon_{381}) \,/\, (A_{280} \,/\, \varepsilon_{280}) \qquad (1)$$

The spectroscopic investigation described below was carried out with samples having $d \geq 95\%$.

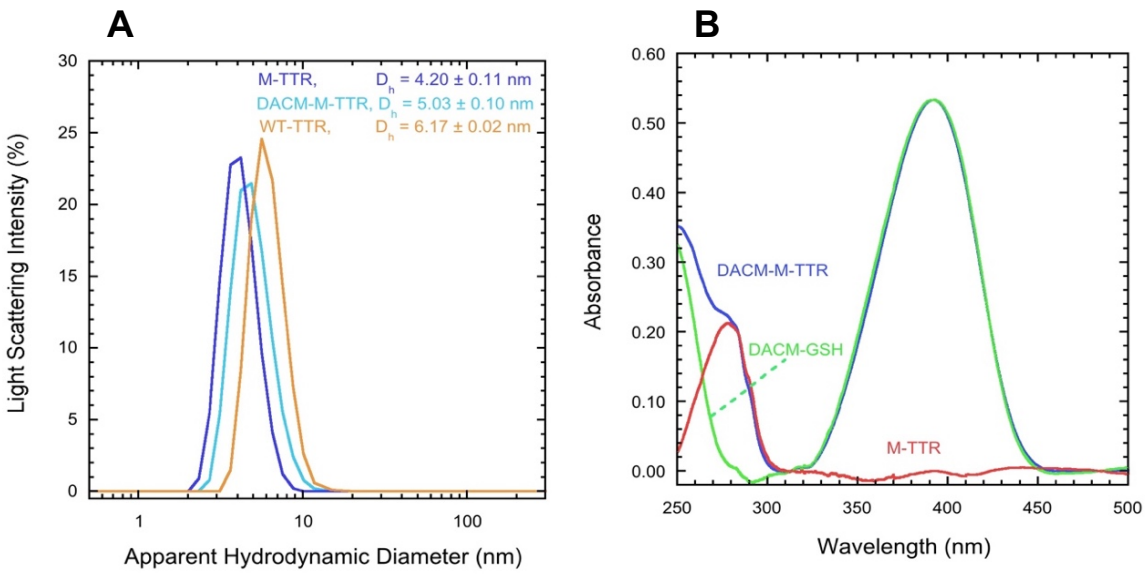

Figure 3.2. Size distributions and optical absorption spectra of labeled and unlabeled M-TTR, (A) Size distributions of M-TTR, DACM-M-TTR and WT-TTR samples obtained with DLS at pH 7.4, 25 °C. (B) Optical absorption spectra of DACM-M-TTR (blue) and DACM-GSH (green) at pH 7.4, 25 °C and at the same probe concentration. The difference spectrum obtained by subtracting the latter from the former is also shown (red).

The fluorescence spectrum of M-TTR at pH 7.4, 25 °C (excitation at 290 nm) is dominated by a major large band at 330-350 nm (Figure 3.3A, red spectrum), resulting largely from Trp41 as the fluorescence of Trp79 is largely quenched (Lai et al. 1996). The fluorescence spectrum of an equimolar quantity of DACM-GSH, acquired under the same conditions (excitation at 290 nm), is very low in intensity and negligible (Figure 3.3B, green spectrum). By contrast, the fluorescence spectrum of an equimolar quantity of DACM-M-TTR under the same conditions (excitation at 290 nm) is characterized by a significant decrease of tryptophan fluorescence intensity, relative to the spectrum of M-TTR, and a substantial enhancement of the DACM emission intensity, relative to the spectrum of DACM-GSH, indicating that FRET is occurring. FRET is largely due to the energy transfer from Trp41 to DACM, both because the fluorescence of Trp79 is quenched and because Trp79 is more distant from DACM compared to Trp41. Importantly, the fluorescence intensity of the tryptophan band is not completely cancelled, leading to a FRET efficiency value (*E*) intermediate between 0 (no FRET) and 1 (full FRET), making it possible to monitor changes of the distance between donor (Trp41) and acceptor (DACM) by FRET measurements. The FRET process occurs whenever the fluorescence emission spectrum of a fluorophore, called the donor, overlaps with the optical absorption

spectrum of another molecule, called the acceptor (Lakowicz 2006). Such an overlap between the fluorescence emission spectrum of tryptophan and the optical absorption spectrum of DACM is illustrated in Figure 3.3B.

Overall, these data indicate that DACM-M-TTR is monomeric, singly labelled with an efficiency close to 100% and with donor/acceptor distance ideal for FRET measurements.

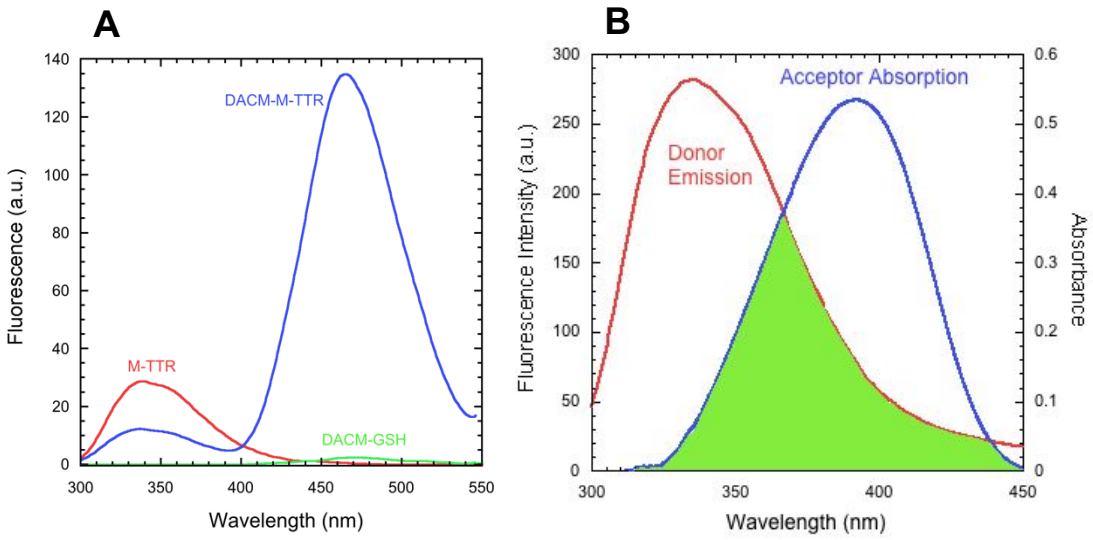

Figure 3.3. Fluorescence spectra and FRET phenomenon of M-TTR. (A) Fluorescence spectra of M-TTR (red), DACM-M-TTR (blue) and DACM-GSH (green) at pH 7.4, 25 °C (excitation 290 nm). (B) The fluorescence emission spectrum of a fluorophore (red), called the donor, overlaps with the optical absorption spectrum of another molecule, called the acceptor (blue).

3.1.2 X-Ray crystal structures of DACM-M-TTR and DACM-WT-TTR

In order to determine if DACM labeling on Cys10 affects M-TTR structure, the X-ray crystal structures of DACM-WT-TTR and DACM-M-TTR were determined at high resolution by our collaborates, Stefano Ricagno and Benedetta Maria Sala at the university of Milan, and compared with that of WT-TTR and M-TTR previously deposited in the Protein Data Bank. Data collection and refinement statistics are reported in Table 3.1. In both structures, from Cys10 to Asn124 all polypeptide chains are well traceable into the electron density map and, in the case of DACM-M-TTR, the F87M/L110M mutations are clearly detectable (Figure 3.4). As observed in most of the previous TTR structures, the first nine residues are flexible and not present in the electron density. In both DACM-WT-TTR and DACM-M-TTR, the presence of some extra density around Cys10 suggests the presence of DACM. The quality of such density is too poor to allow the building of DACM in the model, suggesting a high degree of conformational flexibility of the DACM moiety (Figure 3.5).

Table 3.1. Data collection and refinement statistics for DACM-WT-TTR and DACM-M-TTR

Crystal[a]	**DACM-WT-TTR**	**DACM-M-TTR**
Space group	P $2_12_12_1$	P $2_12_12_1$
Unit cell constants (Å)	a = 43.68, b = 64.49, c = 85.27 α, β, γ = 90°C	a = 64.44, b = 83.76, c = 86.53 α, β, γ = 90°C
Resolution (Å)	22.35 – 1.42 (1.50 – 1.42)	22.04 – 1.70 (1.79 – 1.70)
R_{merge} (%)[b]	9.7 (73.0)	11.1 (77.2)
I/σI	8.1 (2.1)	8.1 (1.9)
Completeness (%)	99.1 (99.2)	99.5 (99.8)
Multiplicity	5.0 (5.0)	4.1 (4.3)
Molecules per asymmetric unit	2	4
Refinement		
R_{work} (%)[c]	16.0	15.0
R_{free} (%)	21.7	22.3
Ramachandran plot, *n* (residues)		
Most favoured region	200	421
Allowed region	3	8
Outliers	0	2
RMSD[d]	0.31Å 114/114 Cα	0.60Å 115/115 Cα

[a] Values given in parenthesis refer to the high-resolution shell.
[b] $R_{merge} = \Sigma_{hkl} \Sigma_j I_{hkl,j} - \langle I_{hkl} \rangle / \Sigma_{hkl} \Sigma_j I_{hkl,j}$ where I is the observed intensity and <I> is the average intensity.
[c] $R_{work} = \Sigma_{hkl} F_o - F_c / \Sigma_{hkl} F_o$ for all data except 5–10%, which were used for the R_{free} calculation.
[d] RMSD values calculated from the structural superposition of the DACM-WT-TTR and DACM-M-TTR structures with the non-labeled WT-TTR (pdb code: 1BMZ) and M-TTR (pdb code: 1GKO).

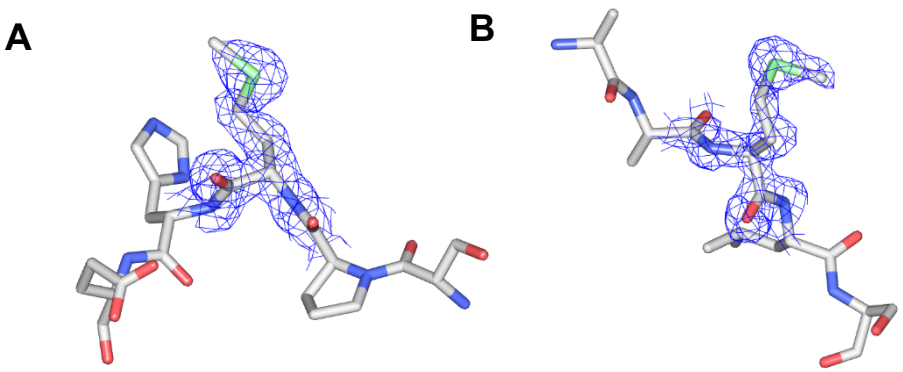

Figure 3.4. Zoomed-view of the mutated amino acids Met87 and Met110 of DACM-M-TTR structure.

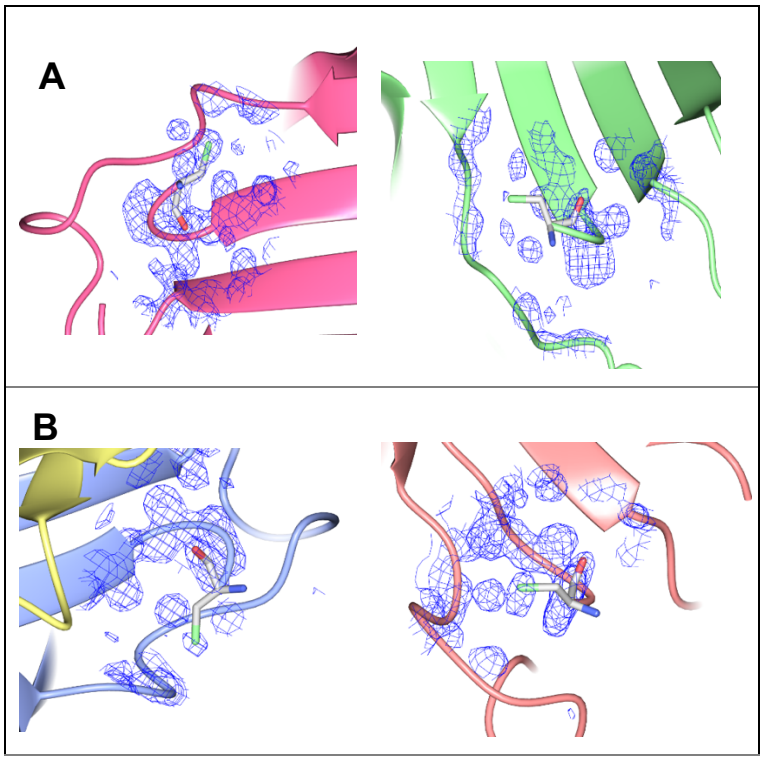

Figure 3.5. Zoomed-view of the region around the labelled Cys10 residue. (a) Cys10 of chain A and B of DACM-wt-TTR structure. (b) Cys10 of chain A and B of DACM-M-TTR structure.

DACM-WT-TTR and DACM-M-TTR crystallised in $P2_122_1$ and $P2_12_12_1$ space group, respectively: DACM-WT-TTR has two molecules in the asymmetric unit (AU), whereas the AU of the DACM-M-TTR structure contains four molecules, as already observed in the M-TTR structure (Jiang et al. 2001b). Superimposition of the DACM-labelled variants with the corresponding non-labeled variants shows that the structures of the DACM-WT-TTR and DACM-M-TTR are perfectly superimposable onto those of WT-TTR and M-TTR, respectively, indicating that DACM labeling does not interfere with the TTR native fold (Figure 3.6 A, B and Table 3.1).

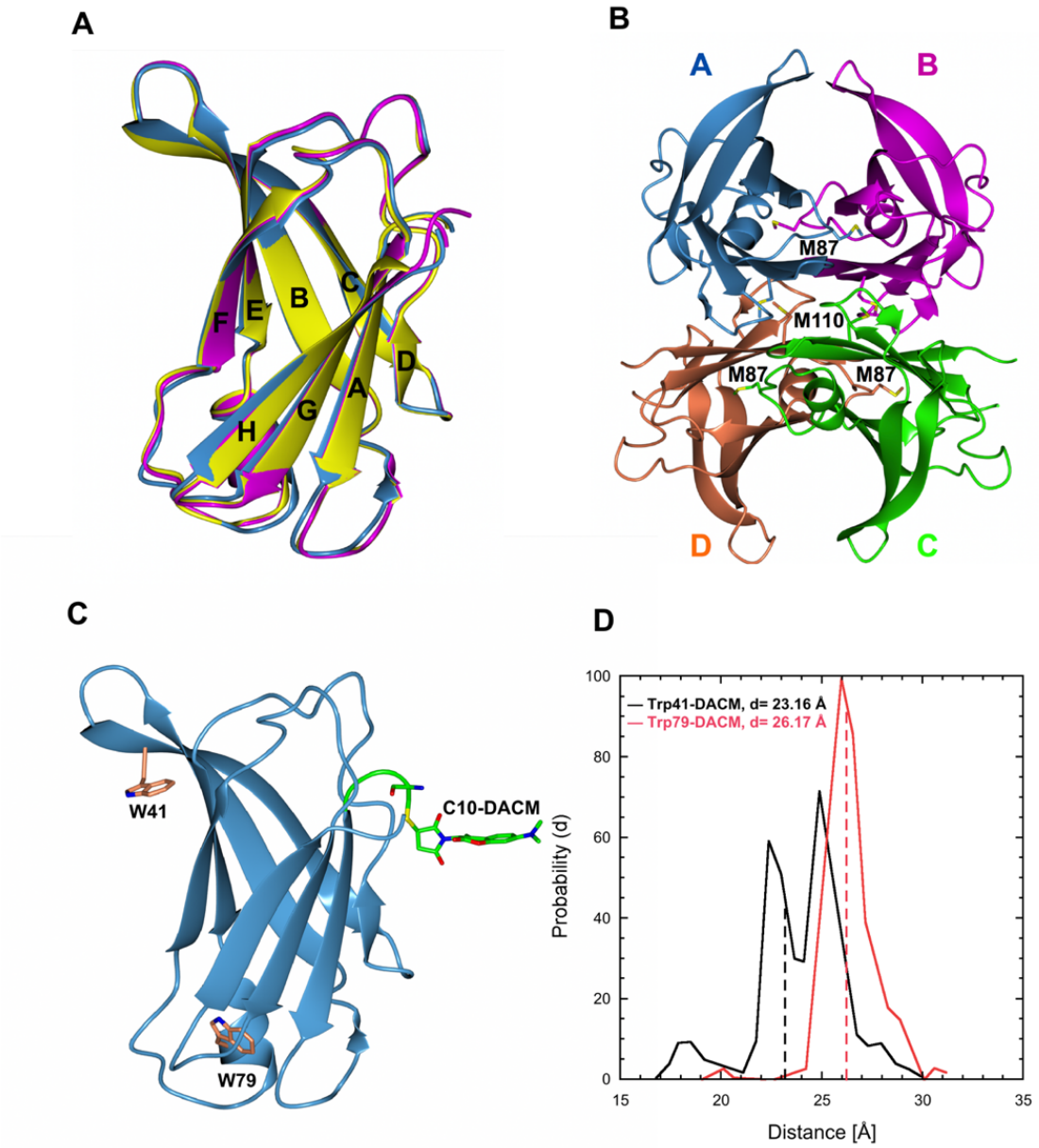

Figure 3.6. X-ray crystal structures of DACM-M-TTR and DACM-WT-TTR. (A) Superposition of the structures of DACM-M-TTR (blue), DACM-WT-TTR (magenta) and WT-TTR (yellow, pdb code: 1BMZ). (B) Tetrameric structure of DACM-M-TTR. The residues Met87 and Met110, that destabilize the tetrameric structure in solution, are shown as sticks. (C) MD simulations of DACM-M-TTR: Trp41, Trp79 and the three most populated conformations of Cys10-DACM are shown as sticks. (D) Distributions of the spatial distances between the centers of mass of Trp41 and DACM (black) and those of Trp79 and DACM (red), calculated using MD simulations starting from the crystal structure of DACM-M-TTR. The dashed lines indicate the spatial distances assuming a single average conformer for the DACM moiety.

As mentioned above, DACM was not traceable in the electron density, due to its high mobility. Thus, MD simulations of the solvated DACM-M-TTR were performed, as described in the Materials and Methods, to provide the correct distribution of the DACM conformers, weighted according to Boltzmann statistics. The DACM moiety was not found to be randomly distributed in space during the simulation, but it has certain conformations more populated than others (Figure

3.6C). The mean Trp41-DACM and Trp79-DACM spatial distances, calculated over the centers of mass, were found to be 23.16 Å and 26.17 Å, respectively (Figure 3.6D).

3.1.3 Determination of FRET efficiency for various conformational states

3.1.3.1 FRET efficiency of native M-TTR and Förster distance of the Trp/DACM pair

I first determined the FRET efficiency of DACM-M-TTR under conditions in which the protein is folded, at pH 7.4, 25 °C. To this aim I mixed different volumes of samples containing M-TTR and DACM-M-TTR, each at the same concentration of 3 μM, to achieve different percentages of labelled M-TTR, from 0 to 100%. Fluorescence emission spectra were obtained for all the resulting samples using an excitation wavelength of 290 nm (Figure 3.7A). The emission spectrum of unlabeled M-TTR (0% DACM-M-TTR) showed an intense peak at 330-350 nm, resulting from tryptophan fluorescence emission, and no emission at 465 nm due to the absence of the DACM moiety (Figure 3.7A, red spectrum). By contrast, the emission spectrum of labeled M-TTR (100% DACM-M-TTR) shows a low intensity peak at 330-350 nm and an intense peak at 465 nm, due to the energy transfer from the excited tryptophan residues to the DACM group, which fluoresces at 465 nm (Figure 3.7A, blue spectrum). The samples presenting intermediate degrees of labelling have an intermediate behaviour, with the donor and acceptor peaks decreasing and increasing in intensity with labelling degree, respectively (Figure 3.7A, red to blue spectra).

The FRET efficiency can be calculated using (Lakowicz 2006):

$$E = 1 - \frac{F_{DA}}{F_D} \qquad (2)$$

where E is the FRET efficiency, F_{DA} and F_D are the fluorescence emission values of the donor in the presence and absence of acceptor, respectively, i.e. the tryptophan emission values at 348 nm measured for the samples containing 100% and 0% DACM-M-TTR, respectively. This led to E = 0.70±0.02. In order to achieve more accurate measurements of F_{DA}, F_D and E I plotted the tryptophan fluorescence emission at 348 nm *versus* the percentage of DACM-M-TTR and analyzed the

resulting plot with a procedure of best fitting using a linear equation (Figure 3.7B). This provided more accurate values of F_{DA} and F_D and a value of $E = 0.72 \pm 0.02$.

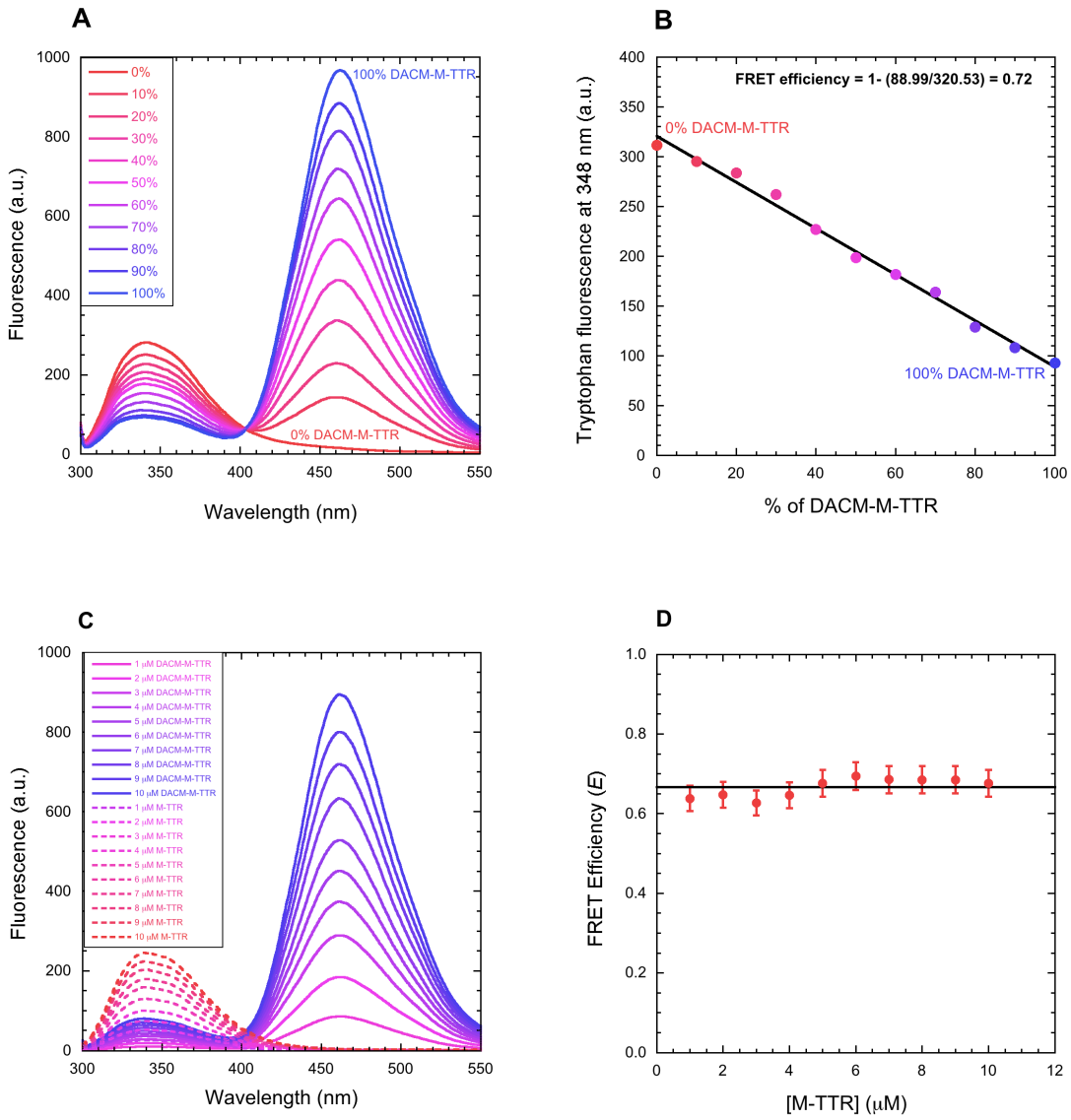

Figure 3.7. FRET of native M-TTR. (A) Fluorescence spectra of mixtures of M-TTR and DACM-M-TTR at the indicated percentages of the latter, at 3 μM total protein concentration, pH 7.4, 25 °C. (B) Tryptophan fluorescence emission at 348 nm *versus* the percentage of DACM-M-TTR. The straight line represents the best fit of the data points to a linear function. (C) Fluorescence spectra of M-TTR (dashed lines) and DACM-M-TTR (continuous lines) at various protein concentrations ranging from 1 to 10 μM, pH 7.4, 25 °C (excitation 290 nm). (D) Plot of *E versus* M-TTR concentration. The straight line represents the average value.

I then measured the fluorescence spectra of M-TTR and DACM-M-TTR at various protein concentrations ranging from 1 to 10 μM (Figure 3.7C) and measured the E values at each of these concentrations (Figure 3.7D). E was found to be independent of protein concentration, indicating that M-TTR and DACM-M-TTR remain largely monomeric under this range of protein concentration. In addition, the value of E remains lower than that measured for tetrameric DACM-WT-TTR (data

not shown), corroborating the absence of protein tetramerisation under the conditions studied here.

In order to determine the distance between Trp41 (donor) and DACM (acceptor) in the folded monomer using the *E* value, we first determined experimentally the Förster distance using:

$$R_0^6 = 8.79\times10^{-5}\left(\kappa^2\, n^{-4}\, Q_D\, J(\lambda)\right) \quad (3)$$

where R_0 is the Förster distance (in Å), κ^2 is the orientation factor describing the relative orientation of the transition dipole moments of the donor and the acceptor, *n* is the refractive index of the aqueous solution, Q_D is the quantum yield of an isolated donor, and $J(\lambda)$ is the integral expressing the degree of spectral overlap between donor emission and acceptor absorption (units of $nm^4\ M^{-1}\ cm^{-1}$) (Lakowicz 2006; Nazarov et al. 2006). A k^2 value of 0.87 was used as a good approximation of a donor-acceptor orientation factor of a folded protein (Visser et al. 2008), whereas *n*, Q_D and $J(\lambda)$ were determined experimentally (Table 2). This allowed the R_0 parameter to be determined for folded M-TTR as 24.9±1.4 Å (Table 2). We then used these R_0 and *E* values determined experimentally for folded M-TTR to determine the donor-acceptor distance (*R*) using the equation (Lakowicz 2006):

$$R^6 = R_0^6\,(1/E - 1) \quad (4)$$

where *R* is the distance between the centers of mass of Trp41 and DACM (in Å). This led to a value of *R* of 21.3±1.6 Å, in good agreement with that determined from X-ray crystallography (*R* = 23.2±2.0 Å). All such values are reported in Table 3.2.

Table 3.2. FRET parameters of M-TTR [a]

Conformational state	R (Å)	E	R_0 (Å)	Q_D	n	$J(\lambda)$ ($nm^4\ M^{-1}\ cm^{-1}$)	κ^2
Native	21.3 (±1.6)	0.72 (±0.02)	24.9 (±1.4)	0.050 (±0.008)	1.332 (±0.001)	$1.96\ 10^{14}$ ($\pm 0.20\ 10^{14}$)	0.87 (±0.2)
Unfolded	30.8 (±1.7)	0.29 (±0.01)	26.5 (±1.4)	0.070 (±0.004)	1.384 (±0.002)	$3.09\ 10^{14}$ ($\pm 0.15\ 10^{14}$)	0.67 (±0.2)
Equilibrium Partially-Folded	24.0 (±1.6)	0.63 (±0.02)	26.2 (±1.3)	0.054 (±0.003)	1.358 (±0.001)	$2.66\ 10^{14}$ ($\pm 0.13\ 10^{14}$)	0.87 (±0.2)
Amyloidogenic Partially-Folded	21.1 (±1.2)	0.73 (±0.02)	24.9 (±1.4)	0.049 (±0.003)	1.332 (±0.001)	$2.03\ 10^{14}$ ($\pm 0.10\ 10^{14}$)	0.87 (±0.2)

[a] E values were determined experimentally from the fluorescence spectra of DACM-M-TTR and M-TTR, respectively. Q_D was determined experimentally using free tryptophan as a reference. n was determined experimentally using a 2WAJ ABBE bench refractometer from Optika Microscopes (Bergamo, Italy). $J(\lambda)$ was determined experimentally as the integral expressing the degree of spectral overlap between donor emission and acceptor absorption. κ^2 was assumed to be 0.87±0.2 for folded proteins and 2/3 (0.67±0.2) for unfolded proteins. R_0 values were determined using equation 3. R values were determined from E and R_0 values using equation 4.

3.1.3.2 FRET efficiency of urea-induced unfolded and molten globule states of M-TTR

Next, I acquired fluorescence spectra of M-TTR and DACM-M-TTR (excitation 290 nm) at urea concentrations ranging from 0 to 7 M at pH 7.4, 25 °C (Figure 3.8A,B). The corresponding urea denaturation curves (spectroscopic signal *versus* urea concentration at equilibrium) were obtained using tryptophan fluorescence at 362 nm as a spectroscopic probe for both the labelled and unlabeled proteins (Figure 3.8C). The analysis yielded values of conformational stability in the absence of denaturant ($\Delta G_{H_2O}^{U-F}$) of 20.4±1.5 and 11.1±1.5 kJ mol^{-1}, dependencies of $\Delta G_{H_2O}^{U-F}$ on urea concentration (m value) of 6.9±0.5 and 4.3 ±0.5 kJ mol^{-1} M^{-1} and midpoint of denaturation (C_m) of 3.0±0.1 and 2.6±0.1 M for M-TTR and DACM-M-TTR, respectively. The values obtained for M-TTR are in reasonable agreement with those obtained previously conducted under slightly different conditions (Conti et al. 2014). The urea denaturation curve of DACM-M-TTR was also obtained using DACM fluorescence at 462 nm as a spectroscopic probe (Figure 3.8D). This led to values of

12.4 ±1.3 kJ mol^{-1}, 4.9±0.4 kJ mol^{-1} M^{-1} and 2.5±0.1 M for $\Delta G_{H_2O}^{U-F}$, m and C_m, respectively, in agreement with those obtained using tryptophan fluorescence as a spectroscopic probe. This analysis indicates that the conformational stability of DACM-M-TTR is significantly lower than that of M-TTR, indicating that the labeling has an effect on protein conformational stability, as it is often observed for mutations.

In principle one can obtain a urea denaturation curve by plotting the FRET efficiency (*E*) *versus* urea concentration. However, such a curve suffers from different conformational stabilities of labelled and unlabelled M-TTR which makes it difficult to compare fluorescence spectra for the two proteins at the same urea concentration and determine *E* at each urea concentration. In spite of these difficulties, it is possible to determine the *E* values at low (< 1.2 M) and high (> 4.8 M) urea concentrations when the major conformational transition has not yet and has completely occurred, respectively, for both labelled and unlabeled proteins. The FRET *E* values at 5.0 and 6.0 M urea, when DACM-M-TTR is unfolded, are remarkably lower than those determined at 0.0 and 1.0 M urea, indicating a significantly higher distance between the DACM moiety attached to Cys10 and the two tryptophan residues (Figure 3.8E). The DACM fluorescence at 462 nm also decreases from 0.0-1.0 M to 5.0-6.0 M urea (Figure 3.8D), confirming that the spatial distance between DACM and the two tryptophan residues increases upon unfolding and gives us the opportunity to observe the movement of DACM from tryptophan in the transition area which the FRET *E* could not be calculated.

Importantly, the FRET *E* value at 1.0 M urea is similar, within experimental error, to that determined at 0.0 M urea (Figure 3.8E). The DACM fluorescence also does not change significantly (Figure 3.8D). This indicates that the equilibrium molten globule state previously detected at low urea concentrations and having a transition at 0.0-2.4 M urea (Conti et al. 2014) has an unmodified distance between the DACM moiety and Trp41.

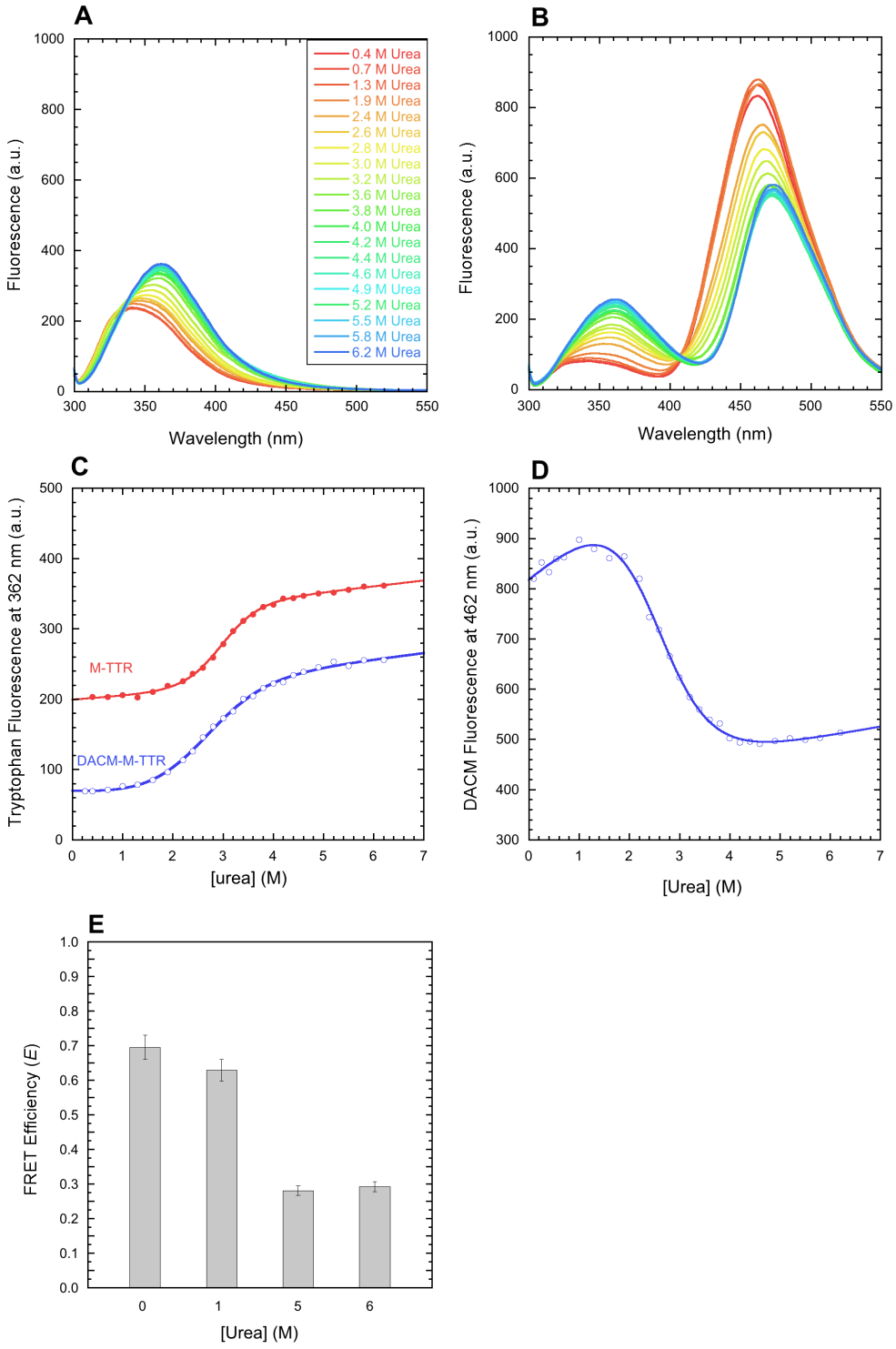

Figure 3.8. FRET of urea-unfolded and molten globule states of M-TTR. (A,B) Fluorescence spectra of M-TTR (A) and DACM-M-TTR (B) at urea concentrations ranging from 0 to 7 M at pH 7.4, 25 °C (excitation 290 nm). (C) Urea denaturation curves (spectroscopic signal *versus* urea concentration) using tryptophan fluorescence at 362 nm as a spectroscopic probe for both M-TTR and DACM-M-TTR. (D) Urea denaturation curve of DACM-M-TTR, using DACM fluorescence at 462 nm as a spectroscopic probe. (E) FRET efficiency (*E*) values at the indicated urea concentrations, pH 7.4, 25 °C.

3.1.3.3 FRET efficiency of the transiently populated partially folded state of M-TTR

I monitored the folding and unfolding processes of M-TTR and DACM-M-TTR in real time by diluting the urea-unfolded proteins into solutions containing low urea concentrations (folding) and by diluting the folded protein into solutions containing high urea concentrations (unfolding) using a stopped-flow device coupled to a fluorescence detection system (Figure 3.9A,B). The analysis of the resulting kinetic traces of folding and unfolding with a procedure of best fit using exponential functions allowed the rate constants for the major folding/unfolding transition (k) to be determined at the various urea concentrations (see *Materials and methods* for further details). These values were used to build the plot of ln(k) versus urea concentration, generally referred to as Chevron plot, for both the labelled and unlabelled proteins (Figure 3.9C). The C_m values obtained from the analysis of these plots, calculated as the urea concentration at which extrapolated refolding and unfolding rate constants are equal (3.2±0.2 M and 2.2±0.2 M for M-TTR and DACM-M-TTR, respectively), were in good agreement with those determined from equilibrium experiments (3.0±0.1 M and 2.5±0.1 M, respectively). The downward curvature in the folding branch of the M-TTR plot results from a rapidly formed, off-pathway, partially folded species that forms rapidly and accumulates during the folding process (Conti et al. 2014). Such a curvature was also observed for DACM-M-TTR (Figure 3.9C). The extrapolated unfolding rate constants in the absence of denaturant were 1.82±0.18 s^{-1} (Conti et al. 2014) and 6.73±0.70 s^{-1} for M-TTR and DACM-M-TTR, respectively. Given the conformational stabilities obtained by equilibrium experiments, the folding rate constants under the same conditions would be ~7100 s^{-1} (Conti et al. 2014) and ~890 s^{-1}, respectively, on the assumption they were two-state folders. By contrast, the refolding rate constants extrapolated by experimental data were orders of magnitude lower than the calculated values, i.e. 81±8 s^{-1} (Conti et al. 2014) and 53±5 s^{-1} for M-TTR and DACM-M-TTR, respectively. This corroborates the hypothesis that a partially folded species accumulates for both M-TTR and DACM-M-TTR.

To determine the FRET efficiency of such a partially folded state, I inspected the kinetic trace for folding in the presence of 0.5 M urea, using a band-pass filter that cuts the signal below 385 nm to monitor the fluorescence of the DACM moiety and exclude that of the tryptophan indole groups (Figure 3.9D). Such a kinetic trace involved a decrease in DACM fluorescence, complete in ~50 ms in 0.5 M urea, as

DACM-M-TTR underwent refolding (Figure 3.9D). The signal of the unfolded protein extrapolated down to 0.5 M urea by linear extrapolation from measurements at high urea concentrations, where the protein is 100% unfolded, was remarkably lower (Figure 3.9D). This analysis revealed that the transient partially folded state of M-TTR has a FRET efficiency higher not just than the unfolded state, but also than the fully folded state. As a control, the kinetic trace for folding in the presence of 2.1 M urea, where the partially folded state cannot be detected, did not show such a burst-phase increase of DACM fluorescence (data not shown).

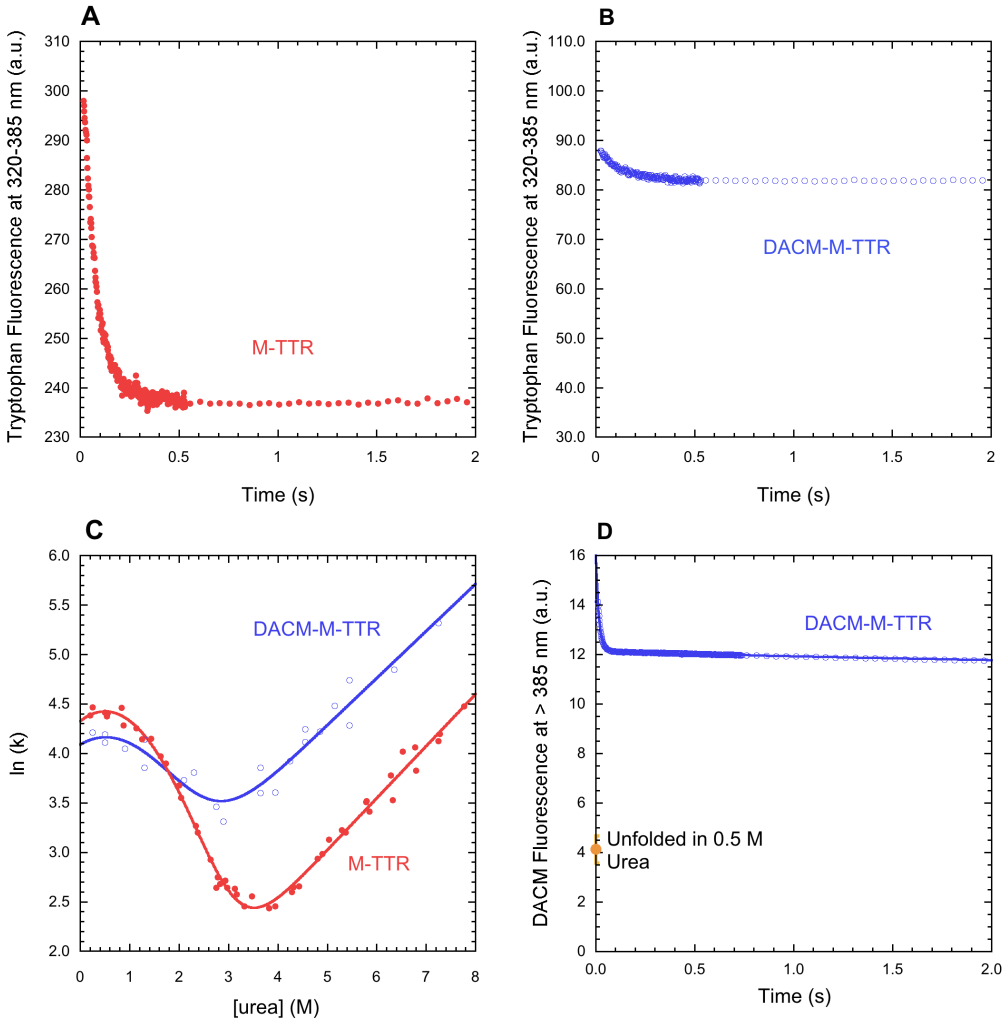

Figure 3.9. FRET during M-TTR refolding. (A,B) Refolding time course of M-TTR (red ●) and DACM-M-TTR (blue ○) monitored by tryptophan fluorescence (excitation 290 nm, emission 320-385 nm) in 0.5 M urea at pH 7.4, 25 °C. (C) Natural logarithm of the observed folding/unfolding microscopic rate constants for DACM-M-TTR (blue ○) compared to data previously published for M-TTR (red ●) (Conti et al. 2014), plotted as a function of urea concentration (chevron plot), at pH 7.4, 25 °C. (D) Refolding time course of DACM-M-TTR (blue ○) monitored by DACM fluorescence (excitation 290 nm, emission > 385 nm) in 0.5 M urea at pH 7.4, 25 °C.

3.1.3.4 FRET efficiency of the amyloidogenic and aggregated states of M-TTR

The FRET analysis was also used to investigate the structure of M-TTR under conditions in which the protein converts into amyloid fibrils, i.e. at pH 4.4, 37 °C (Jiang et al. 2001b; Lai et al. 1996). In order to check that these conditions of pH and temperature also promoted aggregation of DACM-M-TTR and identify conditions suitable for slow aggregation (so that the initial monomeric DACM-M-TTR can be compared with the aggregated state), DACM-M-TTR aggregation was studied at a protein concentration of 15 μM, pH 4.4, 37 °C, under the effect of different ionic strengths, that is in the presence of 0, 30, 60, 90 and 137 mM NaCl. The time courses of turbidity at 450 nm show a gradual increase of the rate of turbidity development with the increase of ionic strength (Figure 3.10A). The sigmoidal pattern of the intermediate time courses indicates that formation of amyloid fibrils involves the typical three phases of the amyloid fibril formation process: an initial lag phase (nucleation), a subsequent growth phase (elongation) and a final saturation phase (plateau). At 30 mM NaCl the time length of the first phase was relatively large but aggregation could still be observed, so that I selected this condition of ionic strength to study the aggregation of the protein.

DLS measurements confirmed that DACM-M-TTR was monomeric immediately after incubation at pH 4.4 (Figure 3.10B). Indeed, the size distributions of M-TTR and DACM-M-TTR at pH 7.4, used here as references of monomeric conformations, had major peaks of hydrodynamic diameters at 4.20±0.11 and 5.03±0.10 nm, respectively, with the slightly higher increase of the latter due to the presence of DACM moiety (see above). The size distributions acquired immediately after incubation at pH 4.4 were found to have major peaks at 4.65±0.26 and 5.60±0.30 nm, respectively (Figure 3.10B). These were both slightly higher than those of the corresponding proteins at pH 7.4, most likely as a consequence of the partial unfolding of the proteins at pH 4.4 (Lai et al. 1996), but were still lower than those of partially unfolded dimers or higher order oligomers.

Hence, both M-TTR and DACM-M-TTR were incubated at 1, 3, 7, 14, 28 μM in 20 mM acetate buffer, 30 mM NaCl, pH 4.4, 37 °C, and fluorescence spectra were collected at different time points, to measure the FRET efficiency (*E*) values as aggregation proceeded (Figure 3.10C,D). The changes of the florescence intensity with time suggest a change in the structure of M-TTR and DACM-TTR as aggregation proceeds (Figures 3.10C,D). The FRET efficiency also increased with

the time of incubation (Figure 3.10E). Since M-TTR and DACM-M-TTR aggregate with different rates under the selected conditions, the FRET efficiency values are meaningful only immediately after incubation (time 0 s) and at the plateau of the aggregation process (time 3000 s) when both proteins are completely monomeric and aggregated, respectively. The FRET *E* value of the amyloidogenic state at 0 s was found to be 0.73±0.02, very similar to that measured for the folded proteins at pH 7.4, 25 °C, indicating an unchanged distance between Trp41 and Cys10 upon partial unfolding at pH 4.4, 37 °C (Figure 3.10F). By contrast, the FRET efficiency value at 3000 s was found to be 0.82±0.01, indicating a structural change upon aggregation at pH 4.4, 37 °C and suggesting that one or both tryptophan residues come into close proximity to Cys10 in the aggregated species, either within the same molecule or in adjacent molecules of M-TTR (Figure 3.10F).

3.1.4 Toxicity of M-TTR aggregates

The toxicity of the M-TTR aggregates at different time points and different salt conditions was assessed using human neuroblastoma SH-SY5Y cell cultures and evaluating cell viability using the MTT reduction inhibition assay. For this purpose, the various aggregates were transferred from the solutions in which they were formed into a different buffer condition and then added to the cell culture media before performing the MTT reduction assay. Twelve different types of samples were obtained by incubating individually M-TTR for 500, 1000, 1500 and 2000 s at 37 °C, pH 4.4 under the three different ionic strengths of 0, 30 and 137 mM NaCl, respectively, as shown in the time courses displayed in Figure 3.10A.

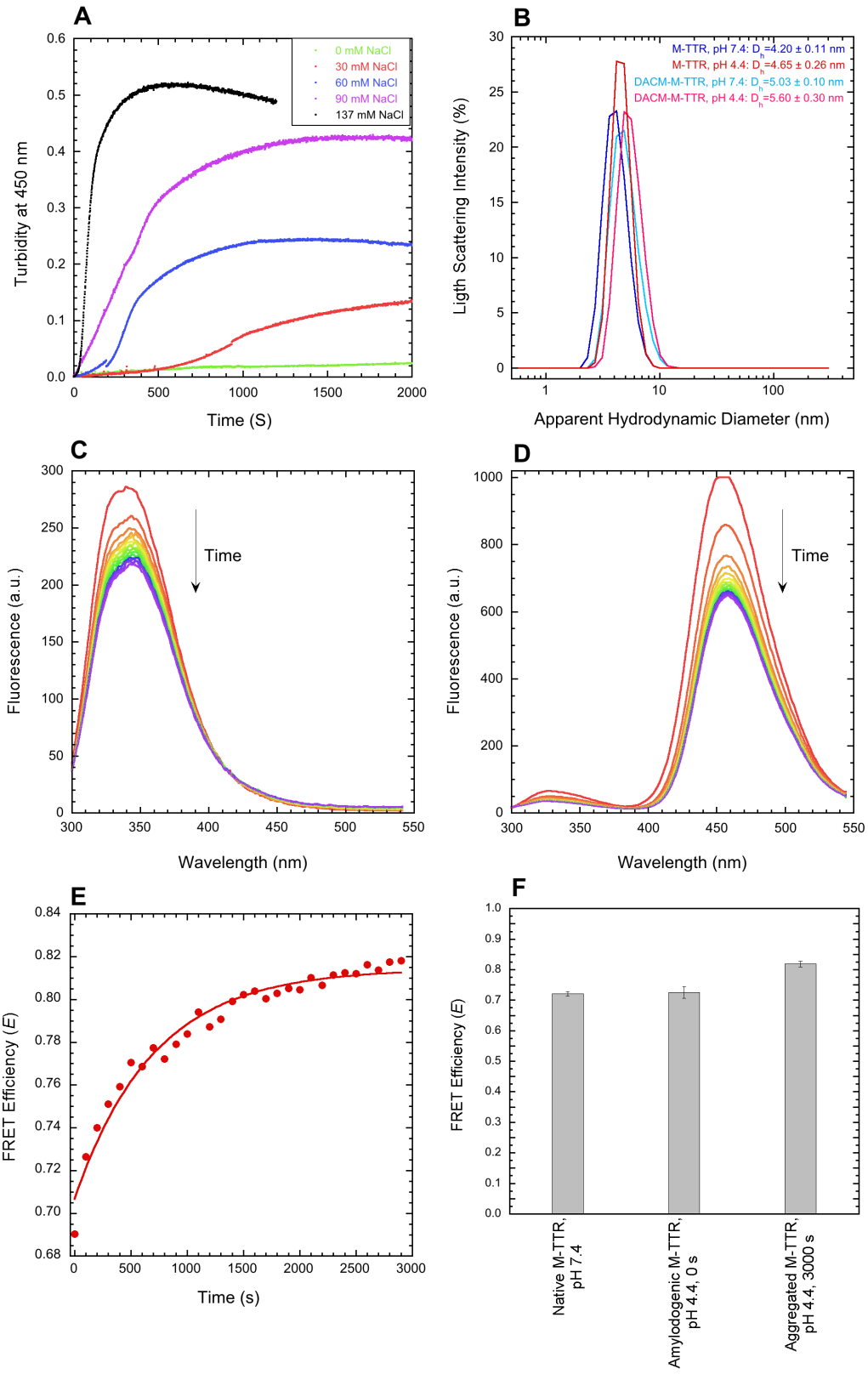

Figure 3.10. FRET of the amyloidogenic and aggregated states of M-TTR. (A) Effect of different NaCl concentrations on the kinetics of 15 µM DACM-M-TTR aggregation in 20 mM sodium phosphate buffer, pH 4.4, 37 °C, monitored with turbidimetry at 450 nm. (B) DLS size distributions of M-TTR and DACM-M-TTR at both pH 7.4 and 4.4. (c, d) Fluorescence intensity spectra at different time points for M-TTR (C) and DACM-M-TTR (D) in 20 mM sodium phosphate buffer, 30 mM NaCl, pH 4.4, 37 °C. (E) FRET efficiency (*E*) during aggregation. Conditions as in panels c,d. (F) FRET efficiency (*E*) for native M-TTR at pH 7.4, 25 °C (first bar), amyloidogenic monomeric M-TTR at pH 4.4, 37 °C, 0 s (second bar) and aggregated M-TTR at pH 4.4, 37 °C, 3000 s (third bar).

The samples of M-TTR obtained without NaCl caused a significant decrease in the viability of SH-SY5Y cells (Figure 3.11A). The aggregates formed by M-TTR in 30 mM and 137 mM NaCl, however, showed significant toxicity only at time points of 500 and 1000 s, which were observed to reduce slightly the cellular viability (Figure 3.11B,C). In control experiments, the native state of M-TTR was tested and found in no case to cause detectable cellular dysfunction (Figure 3.11).

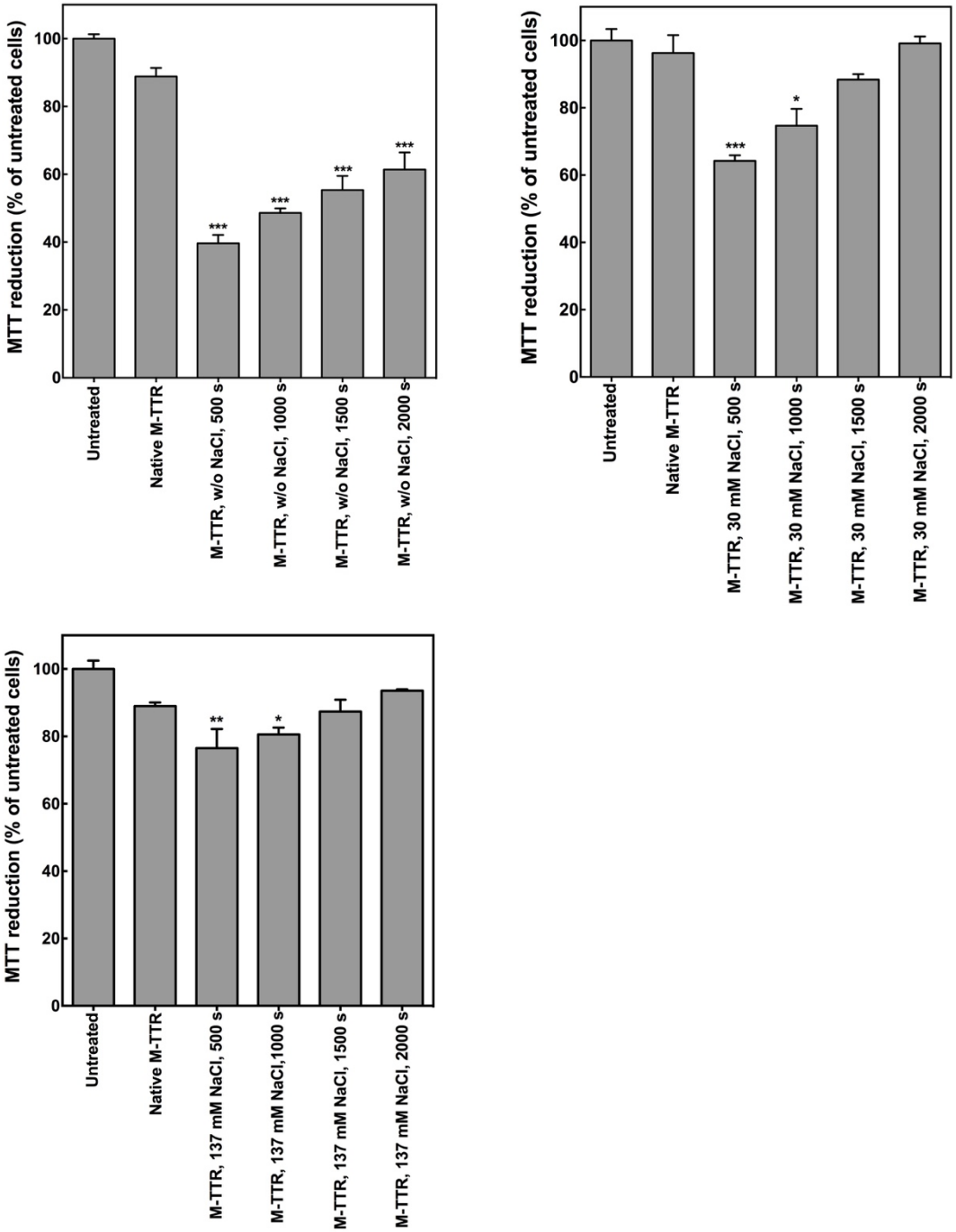

Figure 3.11. Toxicity of the M-TTR aggregates. 3-(4,5-dimethylthiazol-2- yl)-2,5-diphenyltetrazolium bromide (MTT) reduction assay using SH-SY5Y cells treated with different aggregated M-TTR samples. Error bars correspond to standard errors of the means of 3 independent experiments. Single, double, and triple asterisks refer to p < 0.05, <0.01, and <0.001, respectively, with respect to untreated cells.

3.1.5 Purification and analysis of W41F and W79F mutants of M-TTR

Although Trp79 is quenched and more distant than Trp41 to Cys10 in the folded state, doubts remain in partially or fully unfolded states and in aggregated states, where Trp79 may not be quenched and may be placed closer to Cys10 than Trp41. I therefore inserted single point mutations in the gene encoding M-TTR and I purified and labelled two single mutants of M-TTR, replacing either Trp41 or Trp79 by a phenylalanine residue (W79F and W41F) and repeated the FRET experiments to assess the involvement of individual inter-residue distances in the overall measured FRET (Figure 3.12).

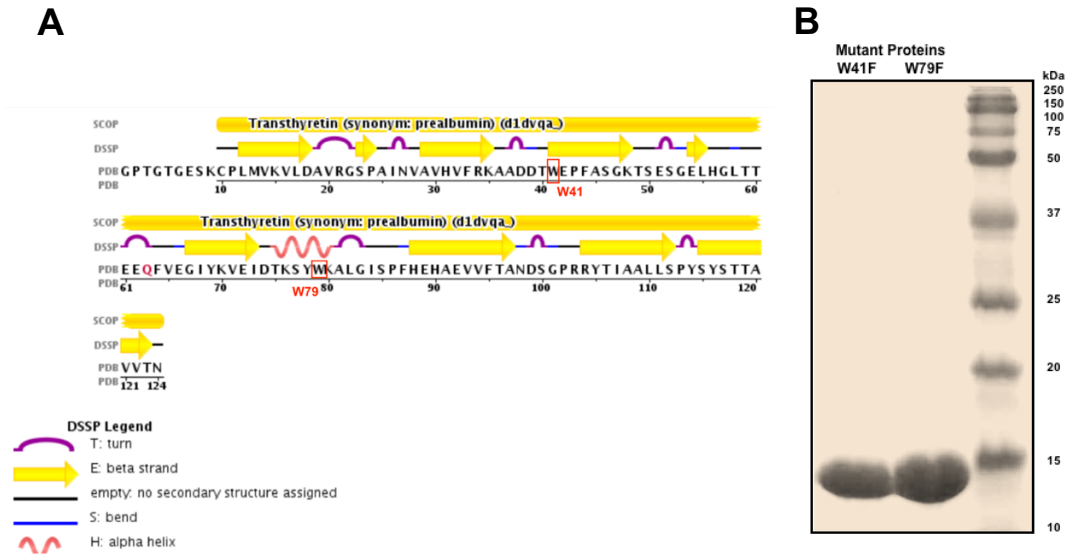

Figure 3.12. Gene sequence and purification of mutant proteins. (A) Gene sequence of the human TTR, mutant amino acids are indicated by red boxes. (B) SDS-PAGE of W41F and W79F M-TTR after purification. An aliquot of the W41F-M-TTR after purification (40 µg, left) and an aliquot of the W79F-M-TTR (40 µg, right) were loaded.

The W79F mutant has a far-UV circular dichroism (CD) spectrum very similar to that of non-mutated M-TTR in 20 mM phosphate buffer, pH 7.4, 25 °C, with a negative peak around 215 nm and a positive peak at 196 nm, typical of β-sheet structure (Figure 3.13A). By contrast, the W41F mutant is remarkably different, with mean residue ellipticity peaks characterized by a low intensity, that is reminiscent of protein aggregation (Figure 3.13A). The DLS analysis at pH 7.4, 25 °C confirmed that both W79F-M-TTR and DACM-W79F-M-TTR are monomeric, whereas both W41F-M-TTR and DACM-W41F-M-TTR are aggregated (Figure 3.13B). As a

further evidence that W41F M-TTR aggregates rapidly under native conditions, the time courses of turbidity at 15 µM protein concentration, 20 mM phosphate buffer, 0-137 mM NaCl, pH 7.4, 37 °C indicate that W41F M-TTR is already aggregated in all conditions under native conditions, including at 0 mM NaCl (Figure 3.13C). The FRET *E* value measured for 15 µM W41F-M-TTR at pH 7.4, 25 °C reports on the aggregated state and was found to be 0.81±0.01, close to the FRET *E* value of aggregated M-TTR, which shows that Trp79 gets closer to the DACM upon

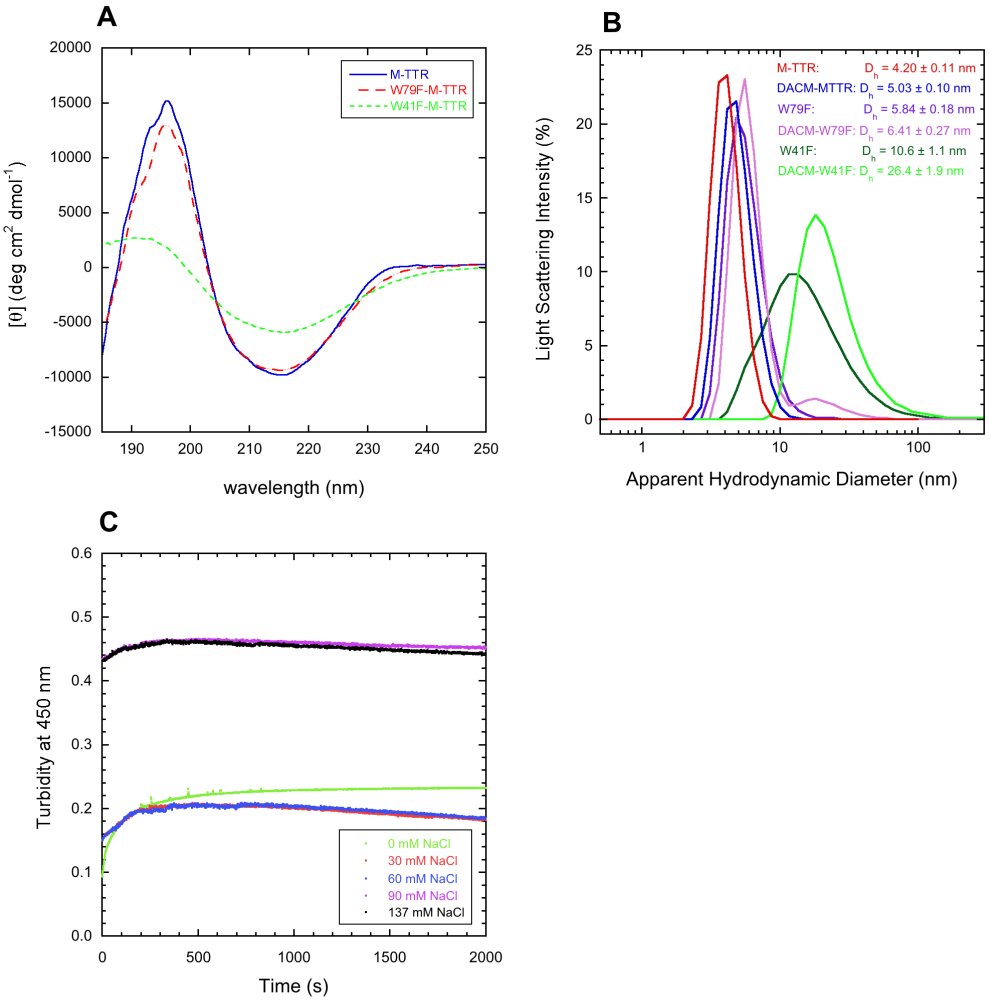

aggregation, relative to the native state.

Figure 3.13. Structural and aggregation properties of W41F and W79F M-TTR mutants. (A) Far-UV CD spectra of the non-mutated and mutant forms of M-TTR obtained in 20 mM phosphate buffer, pH 7.4, 25 °C. (B) Size distributions by DLS of unlabelled and labelled wild-type, W79F and W41F M-TTR at pH 7.4, 25 °C. (C) Aggregation time courses of W41F M-TTR at pH 7.4, 37 °C in the presence of 0-137 mM NaCl.

3.1.6 Comparison of the FRET efficiency values of mutant and non-mutated M-TTR

Since W79F M-TTR, unlike the W41F variant, appears to be soluble and monomeric at pH 7.4, 25 °C, I repeated the same experiments carried out with non-mutated M-TTR, as the mutant provides the opportunity to measure the distance between DACM and Trp41 in the absence of possible artefacts (Figure 3.14). The FRET *E* value of the folded state of W79F-M-TTR at pH 7.4, 25 °C was found to be 0.76±0.02 (Figure 3.14A), which is close to the value of non-mutated M-TTR (*E*=0.72±0.02). This indicates that the mutation does not alter significantly the inter-residue distance between Cys10 and Trp41 in native M-TTR and reinforces the view that the FRET *E* value determined for wild-type M-TTR mainly reports on Trp41 and its distance from DACM.

The analysis of the urea denaturation curves of the unlabelled and labelled W79F mutant, monitored with tryptophan fluorescence, yielded values of $\Delta G_{H_2O}^{U-F}$ of 13.0±1.4 and 8.6±0.9 kJ mol^{-1}, respectively, *m* values of 4.3±0.4 and 4.2±0.4 kJ mol^{-1} M^{-1}, respectively, C_m values of 3.0±0.1 and 2.0±0.2 M, respectively (Figure 3.14B). The $\Delta G_{H_2O}^{U-F}$ values of W79F-M-TTR and DACM-W79F-M-TTR are significantly lower than those of the corresponding wild-type proteins, indicating that the mutation lowers the conformational stability of the folded state. Moreover, the $\Delta G_{H_2O}^{U-F}$ value of DACM-W79F-M-TTR is significantly lower than that of W79F-M-TTR, indicating that the DACM-labelling lowers the conformational stability of the folded state, as observed for non-mutated M-TTR. The FRET *E* values measured after denaturation in 5 M and 6 M urea (*E* = 0.30±0.05 and *E* = 0.24±0.02, respectively) are lower than those in 0 M and 1 M urea (*E* = 0.70±0.04 and *E* = 0.68±0.03, respectively), indicating a higher distance between the DACM group and the Trp41 residue (Figure 3.14D). The FRET *E* value in 1.0 M urea is similar or just slightly lower than that determined in 0.0 M urea, confirming that the equilibrium molten globule state detectable at low urea concentrations has an unmodified distance between the DACM moiety and Trp41. The plot of DACM fluorescence *versus* urea concentration confirms that the distance between the DACM moiety and the Trp41 residue increases upon unfolding (Figure 3.14C).

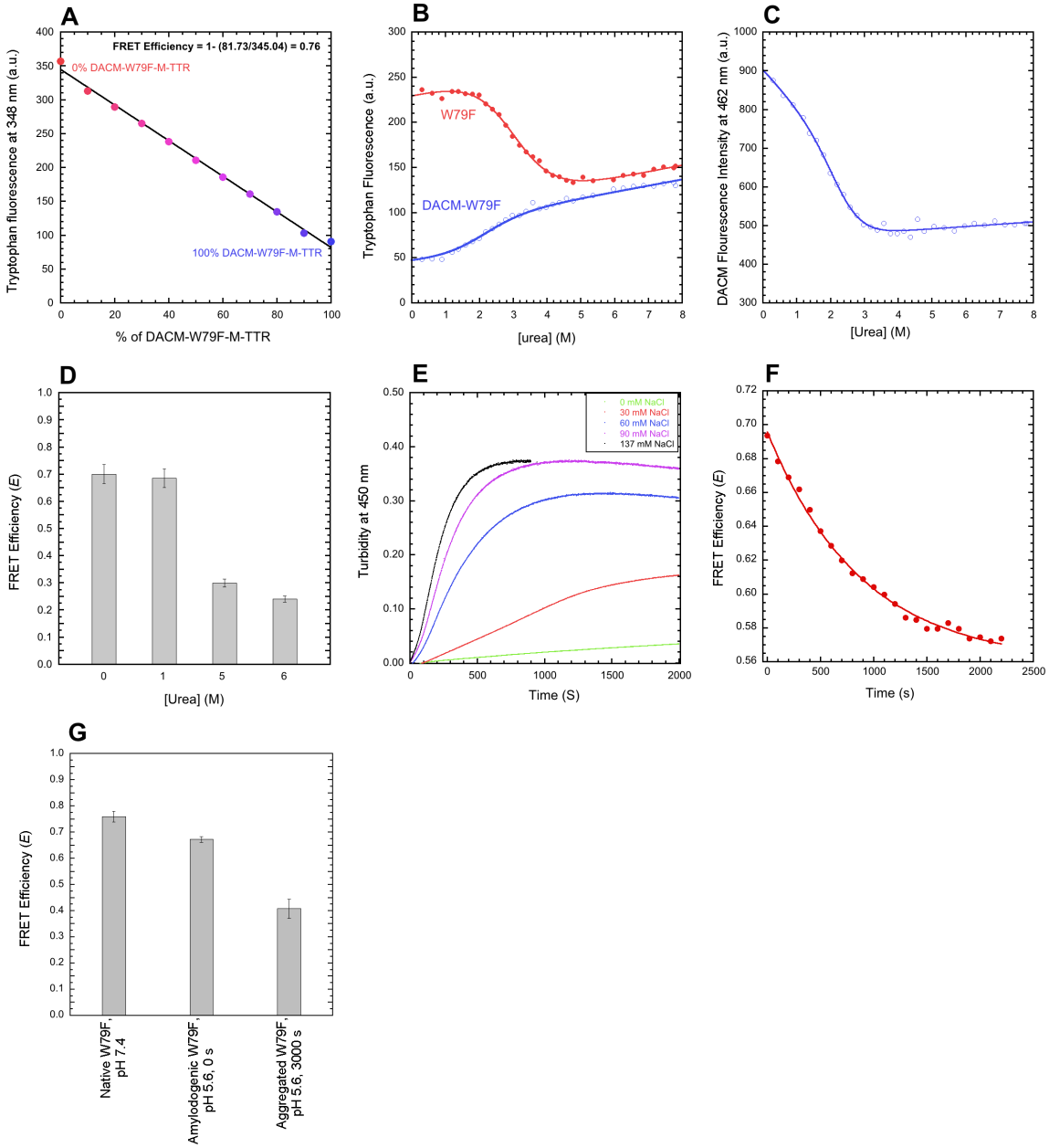

Figure 3.14. FRET of W79F-M-TTR under different conditions. (A) Tryptophan fluorescence emission at 342 nm *versus* the percentage of DACM-W79F-M-TTR, at pH 7.4, 25 °C. The straight line represents the best fit of the data points to a linear function. (B) Urea denaturation curves (spectroscopic signal *versus* urea concentration at equilibrium) using tryptophan fluorescence at 330 nm and 365 nm as a spectroscopic probe for W79F-M-TTR and DACM-W79F-M-TTR, respectively, pH 7.4, 25 °C (C) Urea denaturation curve of DACM-W79F-M-TTR, using DACM fluorescence at 462 nm as a spectroscopic probe, pH 7.4, 25 °C. (D) FRET efficiency (*E*) values at the indicated urea concentrations. (E) Effect of different NaCl concentrations on the kinetics of 15 µM DACM-W79F-M-TTR aggregation in 20 mM acetate buffer, pH 5.6, 37 °C, monitored with turbidimetry at 450 nm. (F) FRET efficiency (*E*) during aggregation. Conditions were 20 mM acetate buffer, 30 mM NaCl, pH 5.6, 37 °C. (G) FRET efficiency (*E*) for native W79F-M-TTR at pH 7.4 (first bar), amyloidogenic monomeric W79F-M-TTR at pH 5.6, 0 s (second bar) and aggregated W79F-M-TTR at pH 5.6, 3000 s (third bar).

Folding of W79F-M-TTR and DACM-W79F-M-TTR was monitored in real time using the stopped-flow apparatus, similarly to the non-mutated protein (Figure 3.15A-C). The spectroscopic signals analyzed by imposing an off-pathway model (Conti et al. 2014) were thus used to calculate transient and equilibrium FRET *E* values of the folded (F), unfolded (U), and partially folded (PF) states (Figure 3.15D).

Results revealed that the transiently populated partially folded state for W79F-M-TTR has a DACM fluorescence significantly higher than those of both the folded and unfolded states (Figure 3.15C). However, this effect is less dramatic than that observed for the non-mutated protein (Figure 3.15D). Kinetic data analysis and calculation of the FRET *E* values highlighted several interesting features (Figure 3.15A-D). Apparent refolding rates in 0.5 M urea were found equal to 16.3±0.2 and 172±20 s^{-1} for M-TTR and W79F M-TTR, respectively, suggesting a strongly destabilized partially folded state following the W79F mutation. However, when the DACM label is attached to M-TTR, refolding rates in 0.5 M urea were found to be 20.2±0.2 for both DACM-M-TTR and DACM-W79F-M-TTR, suggesting a higher energy barrier for refolding when the label is attached to the W79F mutant. The FRET *E* value (Figure 3.15D) of the W79F partially folded state in 0.5 M urea is slightly lower than that of M-TTR (0.68±0.02, as opposed to 0.72±0.02), an observation that, together with that obtained with the refolding rates, is reminiscent of a slightly less compact partially folded state in the mutant.

I then attempted to study the aggregation process of the labelled and unlabeled W79F mutant at pH 4.4, 37 °C, as I did for the non-mutated M-TTR. However, the aggregation process was too fast and DLS measurements showed that the protein was aggregated immediately after incubation under these conditions. I therefore performed a preliminary study with DLS to identify a pH value and ionic strength ideal for slow aggregation of the labelled and unlabeled W79F mutant at a concentration of 15 μM and I found that at pH 5.6, both W79F-M-TTR and DACM-W79F-M-TTR aggregated sufficiently slowly to allow the detection and analysis of both the monomeric amylodogenic state and the aggregated state (data not shown). I therefore acquired time courses of aggregation for 15 μM W79F-M-TTR and DACM-W79F-M-TTR in 20 mM acetate buffer, pH 5.6, 37 °C in the presence of 0, 30, 60, 90 and 137 mM NaCl, using turbidimetry at 450 nm as a probe for aggregation (Figure 3.14E). I selected a NaCl concentration of 30 mM for FRET measurements and performed the experiments as described above for the wild-type protein (Figure 3.14F) determining FRET *E* values of 0.67±0.01 and 0.41±0.04 for the amyloidogenic and aggregated states, respectively (Figure 3.14G).

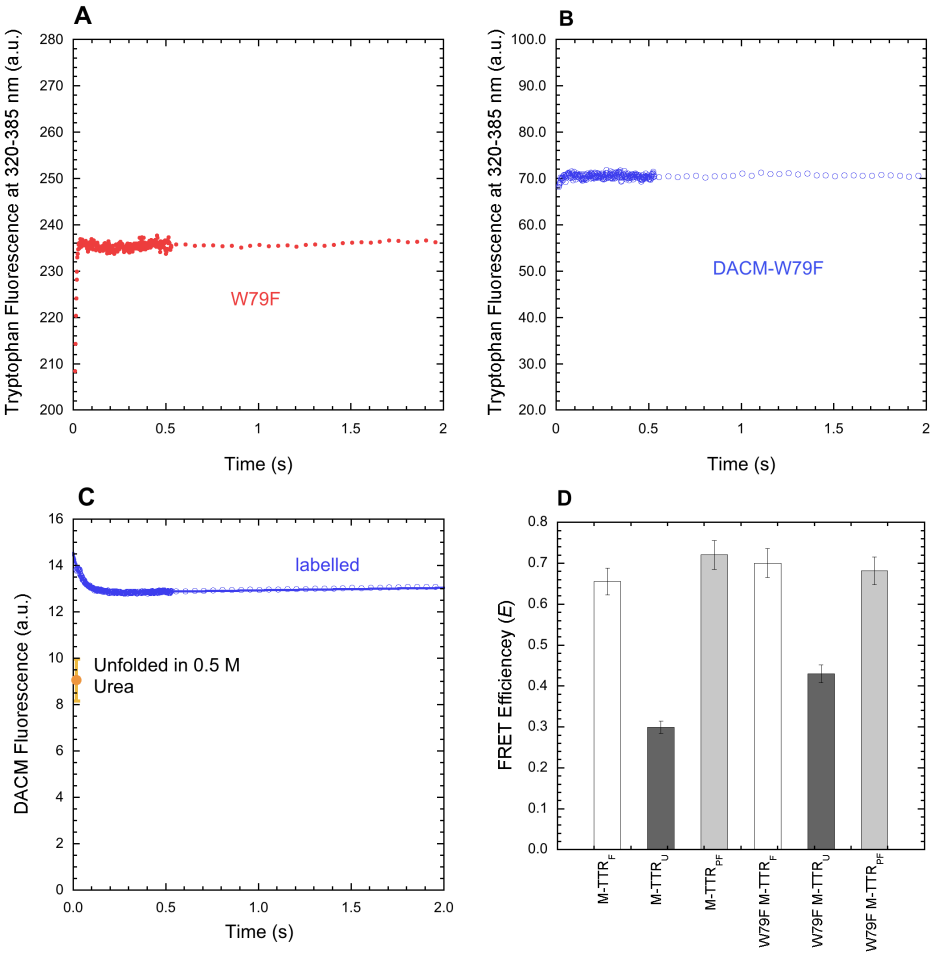

Figure 3.15. FRET of W79F-M-TTR during refolding. (A,B) Refolding time course of W79F-M-TTR (red ●) and DACM-W79F-M-TTR (blue ○) monitored by tryptophan fluorescence (excitation 290 nm, emission 320-385 nm) in 0.5 M urea at pH 7.4, 25 °C. (C) Refolding time course of DACM-W79F-M-TTR (blue ○) monitored by DACM fluorescence (excitation 290 nm, emission > 385 nm) in 0.5 M urea at pH 7.4, 25 °C. (D) Comparison between the FRET *E* values calculated, from the spectroscopic data, for the folded (F), unfolded (U) and partially folded (PF) states of M-TTR and W79F M-TTR in 0.5 M urea at pH 7.4, 25 °C.

Overall, the FRET *E* values measured for the native states at pH 7.4 and for the amyloidogenic states at mildly acidic pH for M-TTR and W79F-M-TTR are all similar, within experimental error, indicating that the distance between the DACM moiety attached to Cys10 and Trp41 does not change significantly in the transition from the native to the amylodogenic state. By contrast, the FRET *E* values measured for the aggregated states of M-TTR and W41F-M-TTR are similar (E=0.82±0.01, E=0.81±0.004, respectively), whereas that of W79F-M-TTR is substantially lower (E=0.53±0.04). This indicates that Trp79 is no longer quenched in the aggregated state and is closer than Trp41 to the DACM moiety of the same or adjacent protein molecule. Moreover, while Trp79 comes closer to DACM, Trp41 gets far away from DACM relative to the native state. Consequently, the FRET *E* value measured for non-mutated M-TTR in the aggregated state is dominated by the DACM-Trp79 distance.

3.2 Interaction of transthyretin with Aβ

3.2.1 The time course of $A\beta_{40}$ amyloid fibril formation monitored with ThT fluorescence

I first purified the $A\beta_{40}$ peptide. For purification of $A\beta_{40}$ several methods such as transformation, protein expression, fast protein liquid chromatography (FPLC) were used. As an evidence that $A\beta_{40}$ is monomeric, I assessed its size distribution by means of dynamic light scattering (DLS) at pH 7.4, 25 °C and compared it with those of M-TTR, W79F-M-TTR and wild-type tetrameric TTR (WT-TTR) (Figure 3.16). An apparent hydrodynamic diameter of 1.50±0.02 nm was observed for $A\beta_{40}$, which is consistent with that expected for unfolded peptide of this size (Granata et al. 2015). Overall, the DLS results indicate that M-TTR, W79F-M-TTR, WT-TTR and $A\beta_{40}$ are all monomeric.

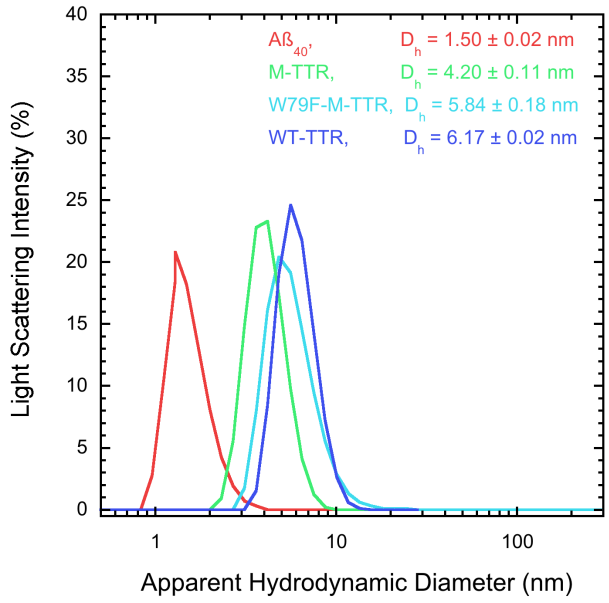

Figure 3.16. Size distribution of TTRs and $A\beta_{40}$. Size distributions of M-TTR, W79F-M-TTR, WT-TTR and $A\beta_{40}$ samples obtained with DLS at pH 7.4, 25 °C.

I then monitored aggregation of $A\beta_{40}$ at various concentrations in a buffer close to physiological and probing aggregation using ThT fluorescence at 480 nm (excitation 440 nm). In particular, $A\beta_{40}$ was incubated at concentrations of 5 μM, 10 μM, 15 μM and 20 μM in 20 mM phosphate buffer, 150 mM NaCl, 20 μM ThT, pH 7.4 at 37 °C. The ThT fluorescence of the resulting samples were measured at regular intervals of time and plotted as a function of time (Figure 3.17A). In all cases the

tome courses follow a sigmoidal curve with a lag phase where the ThT fluorescence is very low, an exponential phase where ThT fluorescence increases substantially with time and plateau where it remains constant. The length of the lag phase decreases with $A\beta_{40}$ concentration. Similarly, the steepness of the exponential phase increases with protein concentration, as well as the final ThT fluorescence measured at the plateau, which is, to a good approximation, proportional to peptide concentration (Figure 3.17A).

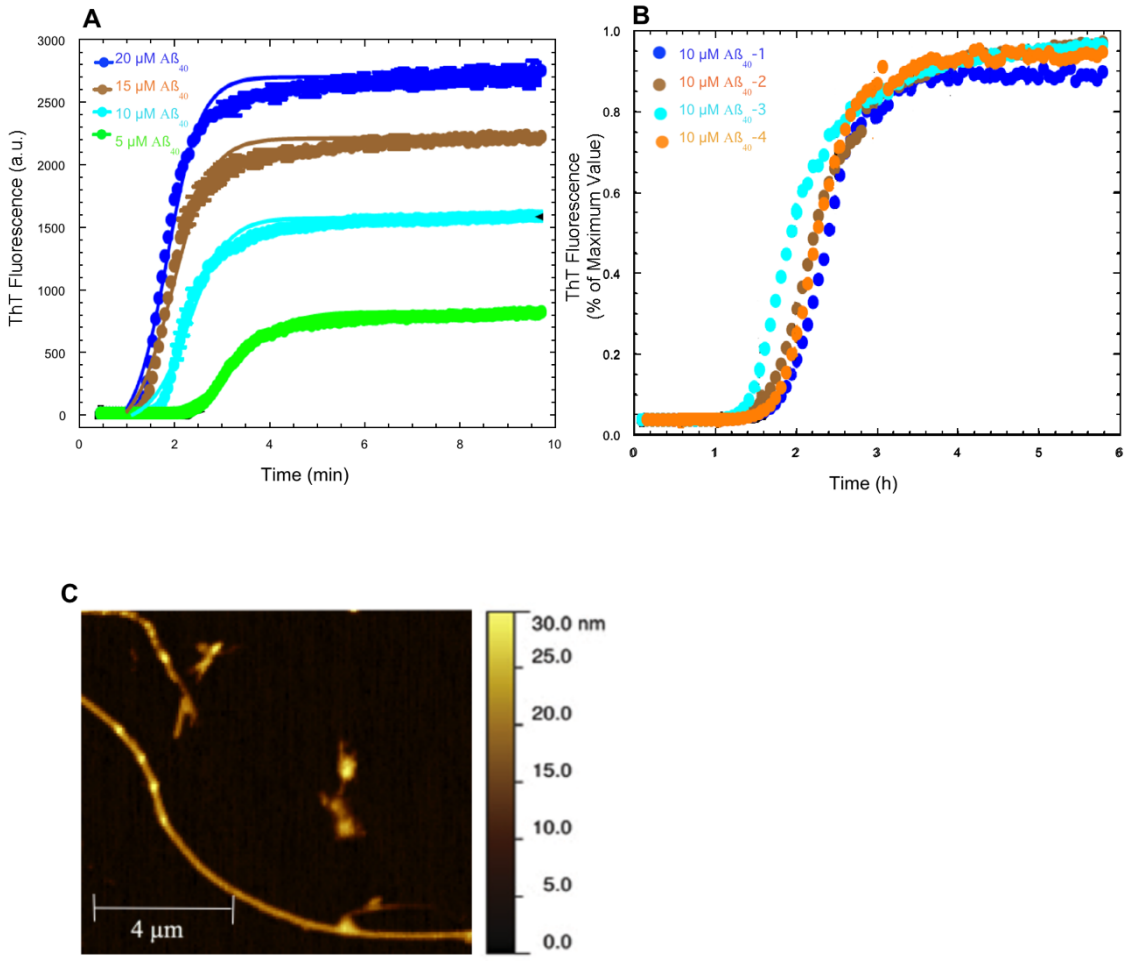

Figure 3.17. The time course of $A\beta_{40}$ amyloid fibril formation monitored with ThT fluorescence and AFM. (A) The ThT fluorescence of the resulting samples were measured at regular intervals of time and plotted as a function of time, $A\beta_{40}$ was incubated at concentrations of 5 μM, 10 μM, 15 μM and 20 μM in 20 mM phosphate buffer, 150 mM NaCl, 20 μM ThT, pH 7.4 at 37 °C. (B) An $A\beta_{40}$ concentration of 10 μM was selected and new time courses with this $A\beta_{40}$ concentration under the same experimental conditions were acquired to check whether or not they are reproducible. (C) The ThT-positive aggregated material present at the plateau of the sample aged for 10 hr at a peptide concentration of 10 μM was analysed using atomic force microscopy (AFM).

An $A\beta_{40}$ concentration of 10 μM was selected and new time courses with this $A\beta_{40}$ concentration under the same experimental conditions were acquired to check whether or not they are reproducible. The four time courses were largely superimposable, confirming that the aggregation kinetics are satisfactorily

reproducible under the tested conditions (Figure 3.17B). This condition was used to assess the effect of the various forms and concentrations of TTRs in inhibiting amyloid fibril formation by $A\beta_{40}$ (see below).

The ThT-positive aggregated material present at the plateau of the sample aged for 10 hr at a peptide concentration of 10 μM was analysed using atomic force microscopy (AFM), indicating the presence of amyloid-like fibrils (Figure 3.17C).

3.2.2 The time course of $A\beta_{40}$ amyloid fibril formation in the presence of TTRs

The time course of amyloid fibril formation by $A\beta_{40}$ at a peptide concentration of 10 μM was then studied in the presence of wt tetrameric TTR at 15 different concentrations ranging from 0.0001 μM to 10 μM (Figure 3.18A). In all these experiments the TTR concentration refers to that of the tetramer and not monomeric subunits of TTR. TTR concentrations up to 0.05 μM did not have any inhibitory effect and the time courses were largely superimposable to that recorded in the absence of TTR, with a lag phase of ca. 2 h. A TTR concentration of 0.08 μM slightly decelerated amyloid fibril formation by elongating the lag phase and retarding the occurrence of the exponential phase. This effect was more marked with a TTR concentration of 0.1 μM, with a lag phase as long as ca. 7 h. A TTR concentration of 0.2 μM retarded dramatically the occurrence of the exponential phase, which started only after ca. 15 h and was also slower. TTR concentrations of 0.3-10 μM abolished completely $A\beta_{40}$ aggregation within the investigated time frame.

This analysis was repeated in the presence of a double mutant of TTR carrying two single mutations (F87M/L110M) designed to destabilise the molecular interface between the subunits that compose the tetramer (Jiang et al. 2001b). This double mutant, generally referred to as M-TTR, was shown to be stable as a monomer at neutral pH (Jiang et al. 2001b). The time course of amyloid fibril formation by 10 μM $A\beta_{40}$ was studied in the presence of 15 different concentrations of M-TTR, ranging from 0.0001 μM to 10 μM (Figure 3.18B). In all these experiments the M-TTR concentration refers to that of the monomer of M-TTR. M-TTR concentrations up to 0.08 μM did not have any inhibitory effect with respect to that recorded in the absence of M-TTR, with a lag phase of ca. 2 h. A M-TTR concentration of 0.1 μM was the lowest able to decelerate amyloid fibril formation, again by elongating the lag phase and retarding the occurrence of the exponential phase. This effect was more

marked with M-TTR concentration of 0.2, 0.3, 0.5, 1.0 μM, with lag phases of ca. 2.5, 3.5, 5 and 9 h, respectively. M-TTR concentrations of 2, 5, and 10 μM abolished completely aggregation of $A\beta_{40}$ within the interval of time studied here. Interestingly, when the concentrations of both wt tetrameric TTR and M-TTR are quantified in terms of monomeric units, the two TTR species appear to have similar effects in inhibiting amyloid fibril formation by $A\beta_{40}$ (Figure 3.18A,B).

I also analysed the effect of a mutant of M-TTR carrying the W79F amino acid substitution (Figure 3.18C). This mutant (W79F-M-TTR) was shown to be destabilised by 7.4±0.1 kJ mol^{-1} relative to non mutated M-TTR , but was also found to possess a native-like fold and is very useful for the FRET studies as it has only one tryptophan residue at position 41. W79F M-TTR concentrations up to 0.08 μM did not have any inhibitory effect with respect to that recorded in the absence of M-TTR, with a lag phase of ca. 2 h. A W79F M-TTR concentration of 0.1 μM was the lowest one to decelerate amyloid fibril formation, again by elongating the lag phase and retarding the occurrence of the exponential phase. The lag phase was ca. 4.5 h and for this reason this mutant appears to be more effective than non-mutated M-TTR, which produced a lag phase of ca. 2.5 h at the same protein concentration. W79F M-TTR concentrations of 0.2, 0.3 and 0.5 μM produced lag phases of ca. 5, 7 and 9.5 h, respectively, again longer than those observed at corresponding concentrations of non-mutated M-TTR. Concentrations of 1, 2, 5, and 10 μM abolished completely aggregation of $A\beta_{40}$ in this interval of time. I have repeated the experiment with the same mass concentrations of M-TTR, W79F-M-TTR and WT-TTR to compare the kinetic profiles of the aggregation of a 10 μM solution of $A\beta_{40}$ in the absence and presence of M-TTR, W79F-M-TTR and WT-TTR, respectively (Figure 3.19).

When the three forms of TTR studied here were incubated under the same experimental conditions for 15 h, the ThT fluorescence was not found to increase, even using concentrations of TTR as high as 50 μM (Figure 3.18D). This indicates that TTR molecules do not contribute to the observed kinetic traces of $A\beta_{40}$ aggregation and simply have an inhibitory effect. The half-time analysis shows that no aggregation of $A\beta_{40}$ could be observed with more than 0.2 molar equivalent for

all proteins within 20 hours, i.e. the half-time was 10 times higher than the half-time observed with $A\beta_{40}$ alone in the absence of TTR molecules (Figure 3.18E).

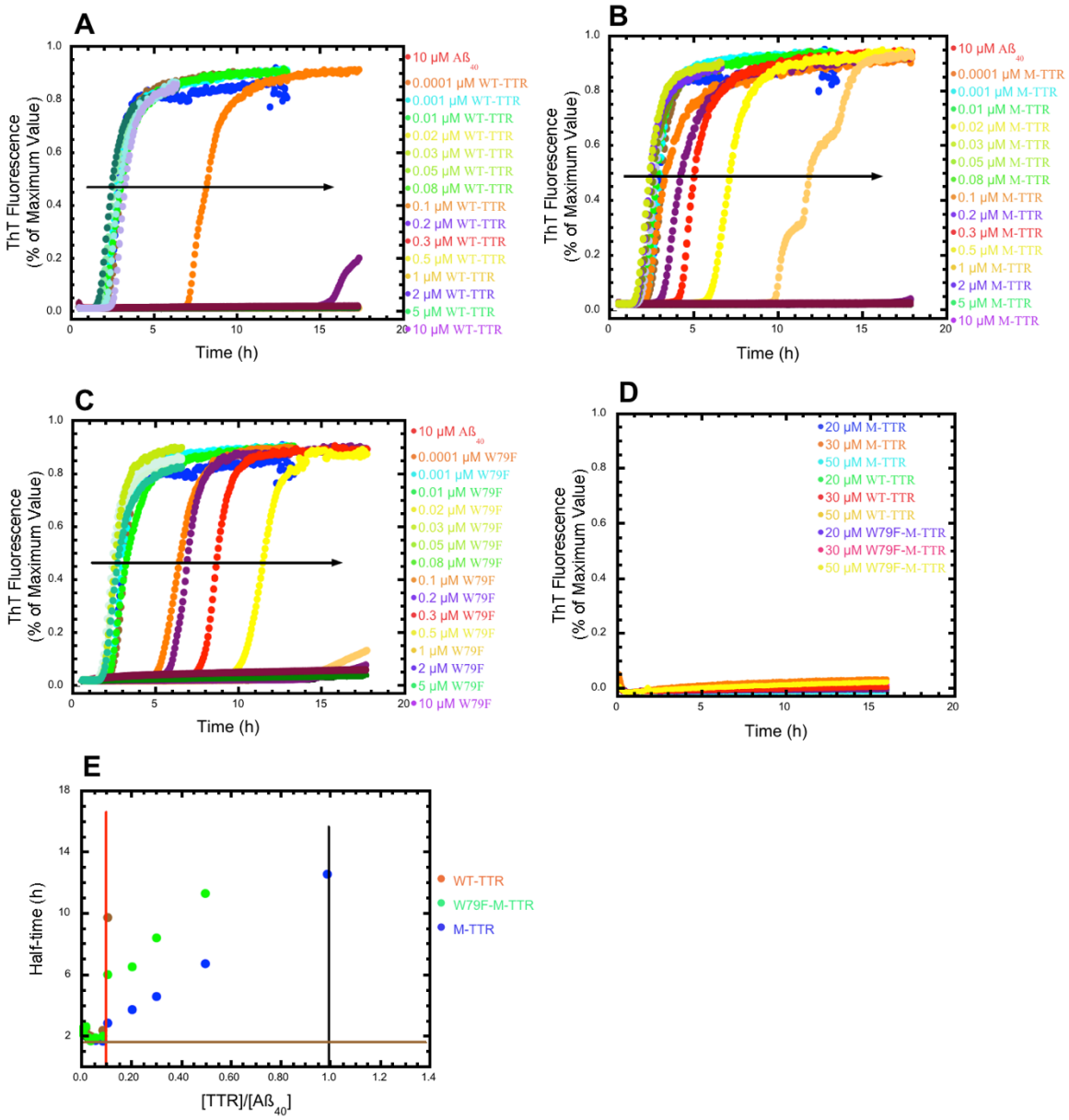

Figure 3.18. Time courses of $A\beta_{40}$ amyloid fibril formation in the presence of TTRs. (A) Time course of amyloid fibril formation by 10 μM $A\beta_{40}$ in the presence of WT-TTR at 15 different concentrations ranging from 0.0001 μM to 10 μM tetramer (concentrations refer to tetramers). (B) Time e course of amyloid fibril formation by 10 μM $A\beta_{40}$ studied in the presence of 15 different concentrations of M-TTR, ranging from 0.0001 μM to 10 μM monomer (concentrations refer to monomers). (C) Time course of amyloid fibril formation by 10 μM $A\beta_{40}$ studied in the presence of 15 different concentrations of W79F-M-TTR, ranging from 0.0001 μM to 10 μM monomer (concentrations refer to monomers). (D) The three forms of TTR studied here were incubated under the same experimental conditions for 15 h in the absence of $A\beta_{40}$. The ThT fluorescence was not found to increase, even using concentrations of TTR as high as 50 μM. (E) The half-time analysis shows that no aggregation of $A\beta_{40}$ could be observed with more than 0.2 molar equivalents for all proteins within 20 hours.

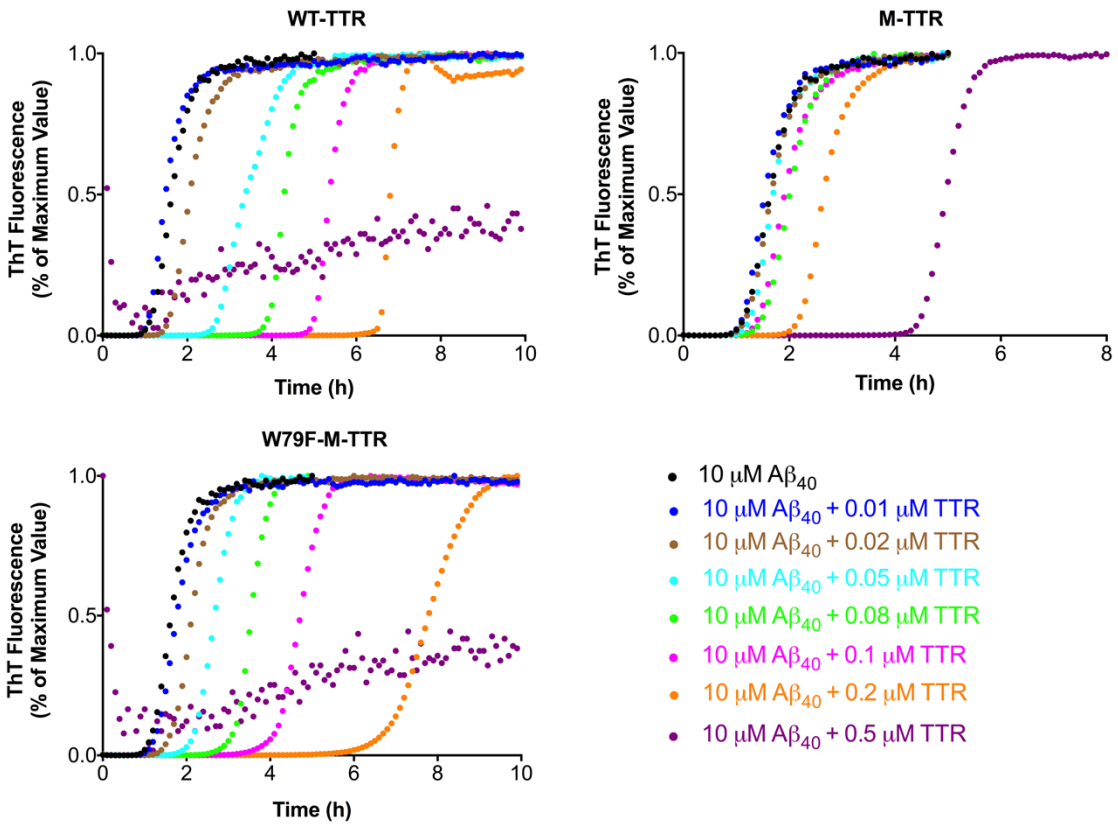

Figure 3.19. Time courses of $A\beta_{40}$ amyloid fibril formation in the presence of TTRs. (A) Kinetic profiles of the aggregation of a 10 μM solution of $A\beta_{40}$ in the absence and presence of different concentrations of M-TTR, shown in different colours. (B) Kinetic profiles of the aggregation of a 10 μM solution of $A\beta_{40}$ in the absence and presence of different concentrations of W79F-M-TTR, shown in different colours. (C) Kinetic profiles of 10 μM $A\beta_{40}$ aggregation in the absence and presence of substoichoimetric ratios of the WT-TTR that are shown in different colours. All concentrations refer to monomer.

The unseeded data has shown that the M-TTR, W79F-M-TTR and WT-TTR all delay the aggregation of $A\beta_{40}$, with the inhibition potency going from WT-TTR > W79F-M-TTR > M-TTR (Figures 3.18 and 3.19). This shows that the inhibition could either occur on the primary or secondary pathways, or both, of $A\beta_{40}$. We also measured the aggregation kinetics of a 10 μM $A\beta_{40}$ sample in the presence of $A\beta_{40}$ fibril seeds at a mass concentration equal to 5% or 35% of the initial $A\beta_{40}$ monomer (Figure 3.20). When the time courses of $A\beta_{40}$ aggregation was studied with preformed seeds, the aggregation of $A\beta_{40}$ was found to be accelerated, as the slow primary nucleation process is bypassed and thus only the secondary pathway is solely responsible for the creation of aggregates (Figure 3.20A). Increase of the seeds from 5% to 35% causes the process to be accelerated. All TTRs are able to delay the aggregation process of $A\beta_{40}$ in the presence of both 5% and 35% seeds, showing that their inhibition are on secondary pathways (Figure 3.20B,C). This manner of inhibition is also consistent with WT-TTR > W79F-M-TTR > M-TTR as we see in

the unseeded data. Thus, the seeded data suggest that TTRs can inhibit the secondary pathways of $A\beta_{40}$ aggregation. It is not known with the present data if the inhibitory action of all TTRs also occurs on primary nucleation or only on secondary nucleation. Further analysis is needed to address this issue.

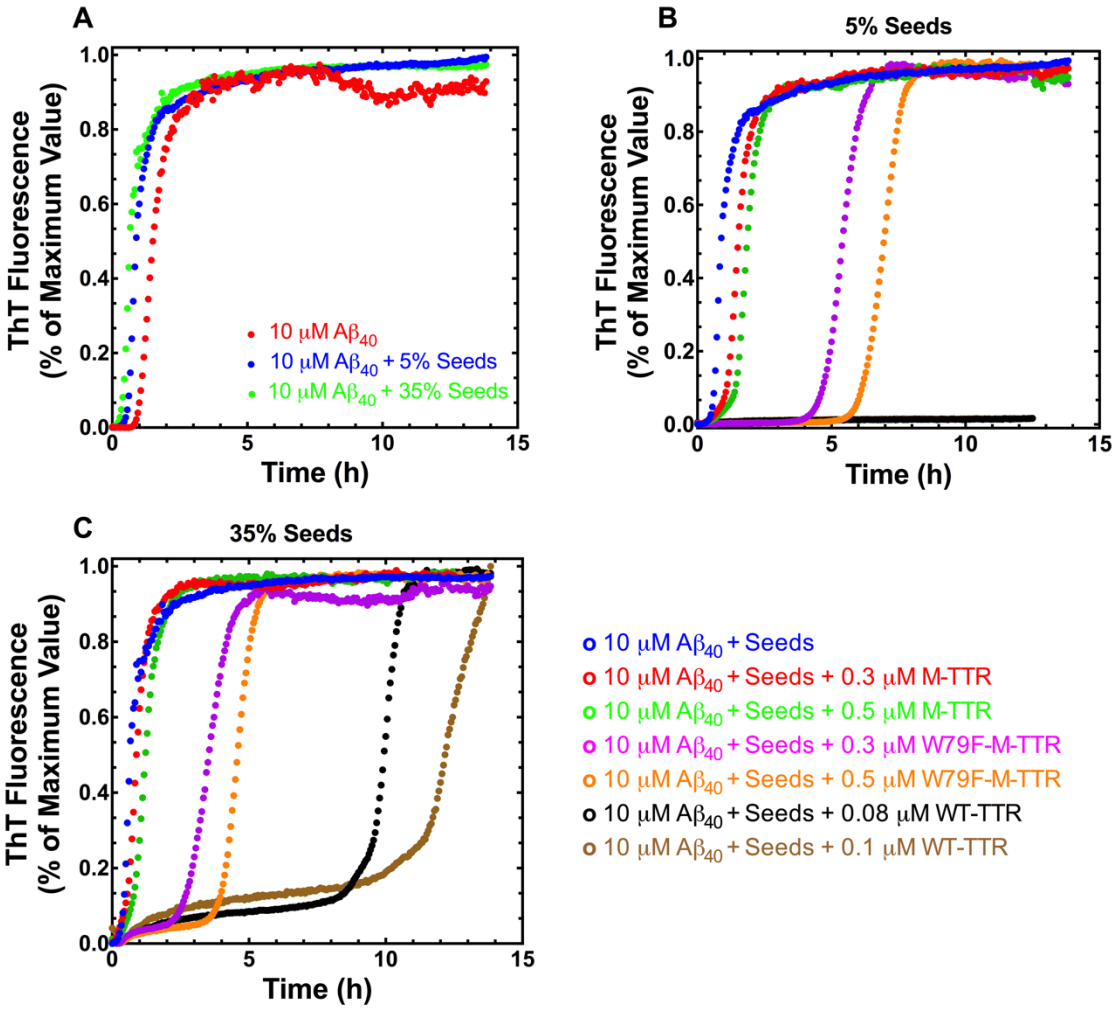

Figure 3.20. (A) Kinetic aggregation profiles of 10 μM $A\beta_{40}$ in the absence and presence of 5% and 35% of preformed seeds. (B) Kinetic profiles of the aggregation of a 10 μM $A\beta_{40}$ solution in the presence of 5% of preformed seeds, in the absence or presence of different concentrations of TTRs. (C) Kinetic profiles of the aggregation of a 10 μM $A\beta_{40}$ solution in the presence of 35% of preformed seeds, in the absence or presence of different concentrations of TTRs.

3.2.3 The $A\beta_{40}$/TTR interaction during amyloid formation by $A\beta_{40}$ monitored with intrinsic fluorescence and FRET

WT-TTR and M-TTR have two tryptophan residues per molecule at positions 41 and 79, whereas W79F M-TTR has only one tryptophan at position 41. By contrast, $A\beta_{40}$ does not have any tryptophan residues, making it possible to attribute the observed intrinsic fluorescence observed when both TTR and $A\beta_{40}$ are present in the sample

only to TTR. $A\beta_{40}$ was incubated at a concentration of 10 μM in 20 mM phosphate buffer, 150 mM NaCl, 20 μM ThT, pH 7.4 at 37 °C, under the same conditions described above. At regular time intervals aliquots were withdrawn and mixed with either WT-TTR, M-TTR or W79F-M-TTR. Final conditions were 9 μM $A\beta_{40}$, 3 μM TTR monomer (in one of its three forms) 150 mM NaCl, 18 μM ThT, pH 7.4, 37 °C. The tryptophan intrinsic fluorescence was then measured for each of the samples immediately after mixing and plotted *versus* time (Figure 3.21A). The tryptophan fluorescence of all three forms of TTR are similar at time 0, in the absence of $A\beta_{40}$, because all forms adopt a native state, have the same protein concentrations (3 μM monomer) and Trp79 is quenched in the native state (Lai et al. 1996), making the W79F mutant of M-TTR similar to the other two forms in terms of emitted fluorescence (Figure 3.21A). As aggregation of $A\beta_{40}$ proceeds, the tryptophan intrinsic fluorescence increases in all cases until an apparent equilibrium is reached. The fluorescence increase is rapid for WT-TTR and M-TTR and slower for W79F-M-TTR, with apparent rate constants of 0.122±0.058 min^{-1}, 0.105±0.057 min^{-1} and 0.026±0.008 min^{-1}, respectively.

In all three samples, such an increase of fluorescence occurs mainly within the lag phase of the process of amyloid fibril formation of $A\beta_{40}$, suggesting that the chemical environment around the Trp residues of TTR molecules changes before mature $A\beta_{40}$ fibrils are formed to any significant extent and when $A\beta_{40}$ oligomers are accumulating. Since M-TTR and W79F M-TTR do not bind monomeric $A\beta_{40}$, as reported previously using ITC and NMR measurements (Li et al. 2013), the observed changes can only be attributed to the binding to $A\beta_{40}$ in its oligomeric state. Although it was previously reported that WT-TTR binds $A\beta_{40}$ when the latter adopts both a monomeric and oligomeric state, the binding of monomeric $A\beta_{40}$ to native WT-TTR occurs within the T_4 hormone binding pocket with no substantial change of the structure around Trp41 (Li et al. 2013), allowing the change of intrinsic fluorescence occurring for WT-TTR to be attributed mainly to the binding of WT-TTR to $A\beta_{40}$ in its oligomer form.

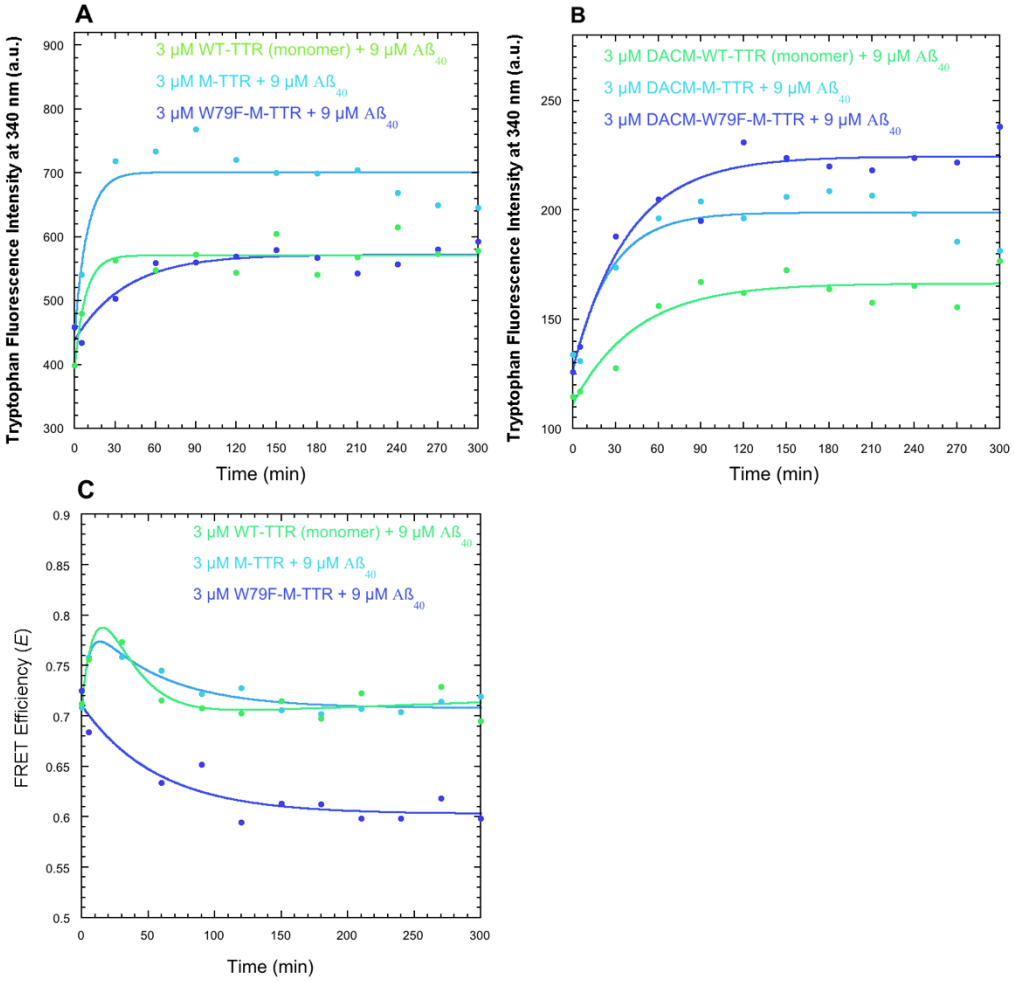

Figure 3.21. The $A\beta_{40}$/TTR interaction during amyloid formation by $A\beta_{40}$ monitored with intrinsic fluorescence and FRET. (A) The tryptophan intrinsic fluorescence was measured for each of the samples immediately after mixing an aliquot of $A\beta_{40}$ undergoing aggregation and an aliquot of TTR and plotted *versus* time for WT-TTR, M-TTR and W79F-M-TTR. (B) The analysis was repeated under identical experimental conditions using all three forms of TTR labelled with the DACM moiety covalently attached to Cys10: DACM-WT-TTR, DACM-M-TTR, DACM-W79F-M-TTR. (C) The time courses of FRET E values.

The analysis was repeated under identical experimental conditions using all three forms of TTR labelled with the DACM moiety covalently attached to Cys10: DACM-WT-TTR, DACM-M-TTR, DACM-W79F-M-TTR (Figure 3.21B). The initial fluorescence at time 0, in the absence of $A\beta_{40}$, is very low due to the energy transfer from Trp41 to the DACM moiety and is again similar for all three forms of TTR. The fluorescence then increases in all cases, but with apparent rate constants significantly different for DACM-WT-TTR and DACM-M-TTR with respect to the unlabelled forms, i.e. 0.022±0.008 min^{-1} and 0.038±0.014 min^{-1}, respectively. By contrast, the fluorescence increase for DACM-W79F-M-TTR occurs with a rate similar to that of unlabelled mutant, i.e. 0.026±0.006 min^{-1}.

By dividing the values reported in Figure 3.21B by those reported in Figure 3.21A for any given TTR form at any given time plots of FRET efficiency (*E*) versus

time can be reconstructed for three forms of TTR (Figure 3.21C). This analysis shows that the FRET *E* value of WT-TTR and M-TTR increases slightly, but significantly, within the first 30 min and then decreases on a slower time scale. By contrast, the FRET *E* value of W79F-M-TTR decreases with time on a slow time scale. The whole analysis was repeated again and I obtained time courses of FRET *E* values similar to those reported in Figure 3.21C, making these results reproducible and not casually associated with a high signal-to-noise ratio.

3.2.4 The $A\beta_{40}$/TTR interaction monitored with far-UV circular dichroism

In order to investigate whether or not the three forms of TTR used here are fully or partially unfolded following the interaction with $A\beta_{40}$ under our conditions of analysis, I acquired the far-UV circular dichroism (CD) spectra of the various proteins alone or after a 30 min incubation. I first acquired the far-UV CD spectra of the various proteins individually using a total protein concentration of 0.1 mg ml^{-1}, corresponding to 22 and 7 μM for $A\beta_{40}$ and TTR monomers, respectively (Figure 3.22A). All three forms of TTR have a spectrum typical of an all-β protein with a negative peak at ca. 216 nm and a positive peak at ca. 196 nm. By contrast, $A\beta_{40}$ has a far-UV CD spectrum typical of a largely unfolded protein with little residual secondary structure, as it shows a negative peak at ca. 200 nm and a shoulder at ca. 202-225 nm. I then acquired the far-UV CD spectra after incubating WT-TTR and $A\beta_{40}$ for 30 min at a total protein concentration of 0.1 mg ml^{-1} and using a 1:3 molar ratio of WT-TTR: $A\beta_{40}$ as described in the *Methods* section. The spectrum is largely superimposable to that obtained by averaging the spectra recorded with the two proteins individually (Figure 3.22B). Similar conclusions could be obtained when the analysis was repeated after incubating M-TTR and $A\beta_{40}$ for 30 min (Figure 3.22C) and after incubating W79F-M-TTR and $A\beta_{40}$ for 30 min (Figure 3.22D). Hence, this analysis indicates that the TTR/$A\beta_{40}$ interaction does not fully or partially unfold the secondary structure of the various TTR molecules studied here.

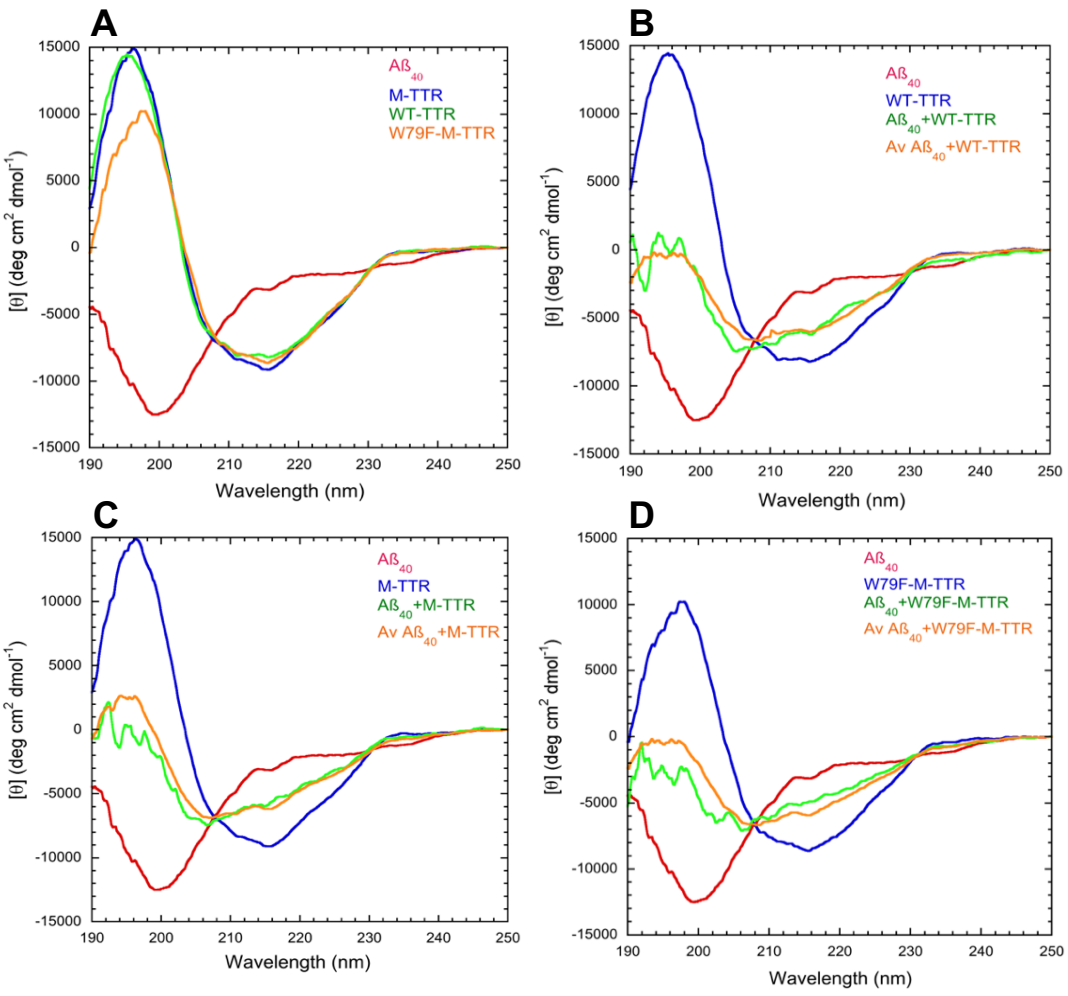

Figure 3.22. The $A\beta_{40}$/TTR interaction monitored with far-UV circular dichroism. (A) Far-UV CD spectra of the various proteins measured individually using a protein concentration of 0.1 mg ml^{-1}. (B) Far-UV CD spectra measured after incubating WT-TTR and $A\beta_{40}$ for 30 min at a total protein concentration of 0.1 mg ml^{-1} and using a 1:3 molar ratio of WT-TTR:$A\beta_{40}$ as described in the *Methods* section for WT-TTR. (C) Far-UV CD spectra measured after incubating M-TTR and $A\beta_{40}$ for 30 min at a total protein concentration of 0.1 mg ml^{-1} and using a 1:3 molar ratio of M-TTR:Aβ40. (D) Far-UV CD spectra measured after incubating W79F-M-TTR and $A\beta_{40}$ for 30 min at a total protein concentration of 0.1 mg ml^{-1} and using a 1:3 molar ratio of W79F-M-TTR:$A\beta_{40}$.

3.2.5 The interaction between toxic $A\beta_{42}$ oligomers and TTRs

It was previously shown that monomeric TTR interacts with pre-formed toxic oligomers of $A\beta_{40}$ and $A\beta_{42}$ and inhibit their toxicity (Cascella et al. 2013; Li et al. 2013). As a source of Aβ toxic oligomers I used the amyloid derived diffusible ligands (ADDLs) formed by $A\beta_{42}$ that were previously shown to be toxic to mice organotypic hippocampal slice cultures as detected measuring the uptake of fluorescence-labelled calcein, the uptake of ethidium homodimer, the inhibition of long term potentiation and the decrease of MTT reduction (Lambert et al. 1998). In addition, they were found to decrease the viability of rat hippocampal neurons by measuring the NMDA receptor-mediated calcium uptake and subsequent ROS levels

increase, by detecting abnormal synapse composition, shape, and density (Lacor et al. 2004) and by measuring the transport of mitochondria along axons (Wang et al. 2010).

M-TTR and DACM-M-TTR were incubated at a concentration of 4 μM in the absence and presence of preformed $A\beta_{42}$ ADDLs at a concentration of 12 μM (monomer equivalents) in PBS buffer, pH 7.4, 37 °C. The resulting fluorescence spectra were recorded after 0, 20, 40 and 60 min using an excitation wavelength of 280 nm (Figure 3.23A-D). The fluorescence spectra of both M-TTR and DACM-M-TTR in the absence of $A\beta_{42}$ ADDLs were found to be stable within the first hour of incubation (Figure 3.23A,B), indicating the stability of unlabeled and labeled proteins under these conditions. By contrast, the spectra recorded for both M-TTR and DACM-M-TTR in the presence of $A\beta_{42}$ ADDLs decreased in intensity with time (Figure 3.23C,D), indicating a progressive interaction with the ADDLs. As expected, $A\beta_{42}$ ADDLs in the absence of M-TTR did not show any significant fluorescence, indicating the absence of any significant contribution in the acquired fluorescence spectra (Figure 3.23E). The FRET *E* value of M-TTR was measured at all four time points, both in the absence and presence of $A\beta_{42}$ ADDLs (Figure 3.23F). In the former case, it was found to be stable with time and similar to that measured for M-TTR labeled with DACM at Cys10. In the latter case, by contrast, it was found to decrease progressively, indicating that a conformational change occcurs for M-TTR following the interaction with $A\beta_{42}$ ADDLs.

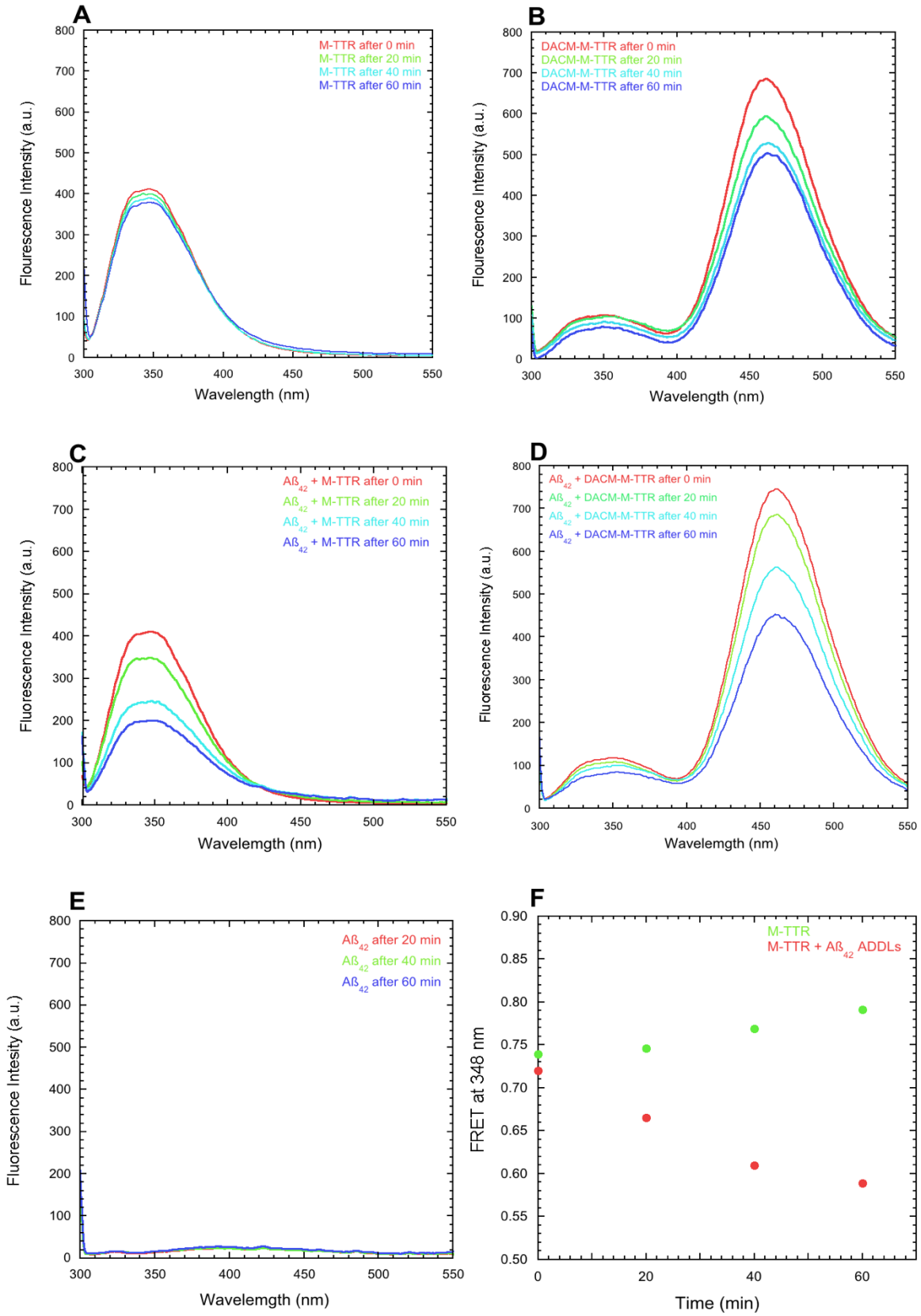

Figure 3.23. Interaction between toxic $A\beta_{42}$ oligomers (ADDLs) and M-TTR. (A-D) Fluorescence spectra recorded for both M-TTR (A,C) and DACM-M-TTR (B,D) in the absence (A,B) and presence (C,D) of $A\beta_{42}$ ADDLs. (E) Spectra recorded for $A\beta_{42}$ ADDLs in the absence of M-TTR. (F) FRET *E* of M-TTR measured at all four time points, both in the absence and presence of $A\beta_{42}$ ADDLs.

This analysis was repeated for the W79F mutant of M-TTR leading to very similar results (Figure 3.24). This confirms that a conformational change occurs also for W79F M-TTR following the interaction with $A\beta_{42}$ ADDLs and indicates an increased spatial distance between the DACM moiety attached to Cys10 and the two tryptophan residues, particularly Trp41.

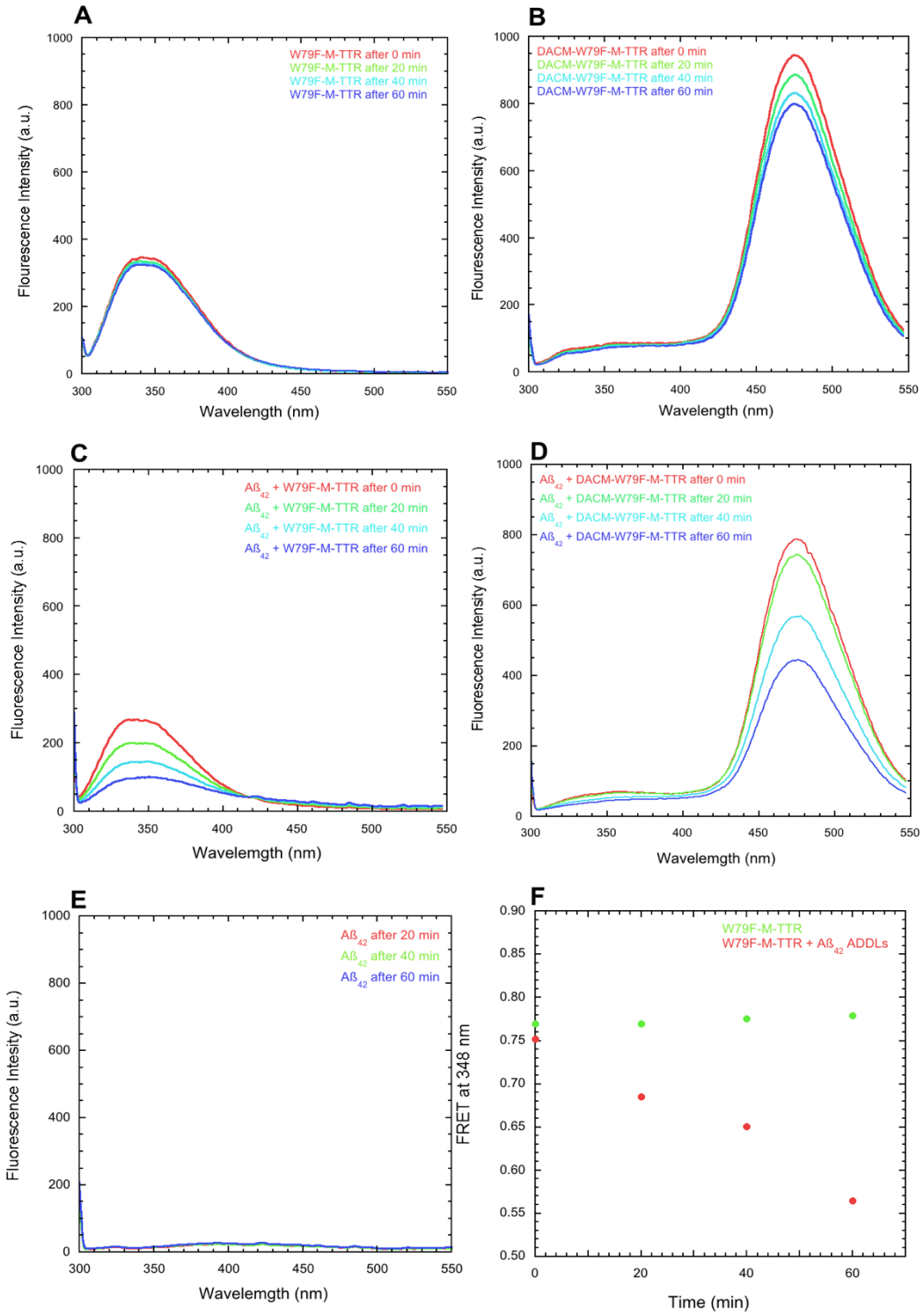

Figure 3.24. Interaction between toxic $A\beta_{42}$ oligomers (ADDLs) and W79F-M-TTR. (A-D) Fluorescence spectra recorded for both W79F-M-TTR (A,C) and DACM-W79F-M-TTR (B,D) in the absence (A,B) and presence (C,D) of $A\beta_{42}$ ADDLs. (E) Spectra recorded for $A\beta_{42}$ ADDLs in the absence of W79F-M-TTR. (F) FRET *E* of W79F-M-TTR measured at all four time points, both in the absence and presence of $A\beta_{42}$ ADDLs.

3.2.6 Study of the interaction between toxic $A\beta_{42}$ oligomers and TTRs with far-UV circular dichroism

To further investigate the interaction between ADDLs and TTRs, we used far-UV circular dichroism. It has previously been shown that $A\beta_{40}$ does not change the secondary structure of transthyretin during $A\beta_{40}$ aggregation (section 3.2.4). Here, I have further studied the interaction between preformed $A\beta_{42}$ ADDLs and both M-TTR and W79F-M-TTR in 20 mM sodium phosphate buffer, pH 7.4, 37 °C. I first obtained the far-UV CD spectra of the TTRs and $A\beta_{42}$ ADDLs individually using a total protein concentration of 0.1 mg ml^{-1}, corresponding to 22 and 7 μM for $A\beta_{42}$ and TTR monomers, respectively (Figure 3.25A,B). All fours spectra of M-TTR obtained at different time points of 0, 20, 40 and 60 min are typical of an all-β protein with a negative peak at ca. 210-216 nm and a positive peak at *ca*. 196 nm (Figure 3.25A). By contrast, $A\beta_{42}$ ADDLs have a far-UV CD spectrum typical of a largely unfolded protein with little residual secondary structure, as it shows small values of mean residue ellipticity down to 218 nm (Figure 3.25B). Because of the presence of DMSO in the solution, we cannot acquire the CD spectrum below 218 nm. I then acquired the far-UV CD spectra after incubating 0.1 mg/ml TTRs and 0.1 mg/ml $A\beta_{42}$ ADDLs for 0, 20, 40 and 60 min at a total protein concentration of 0.2 mg ml^{-1}, as described in the *Methods* section (Figure 3.25C). The spectra are largely superimposable to those obtained with M-TTR individually. Similar conclusions could be obtained when the analysis was repeated after incubating W79F-M-TTR and $A\beta_{42}$ ADDLs both individually and together for 0, 20, 40 and 60 min (Figure 3.26). Hence, this analysis indicates that the TTR/$A\beta_{42}$ ADDLS interaction does not fully or partially unfold the secondary structure of the various TTR molecules studied here.

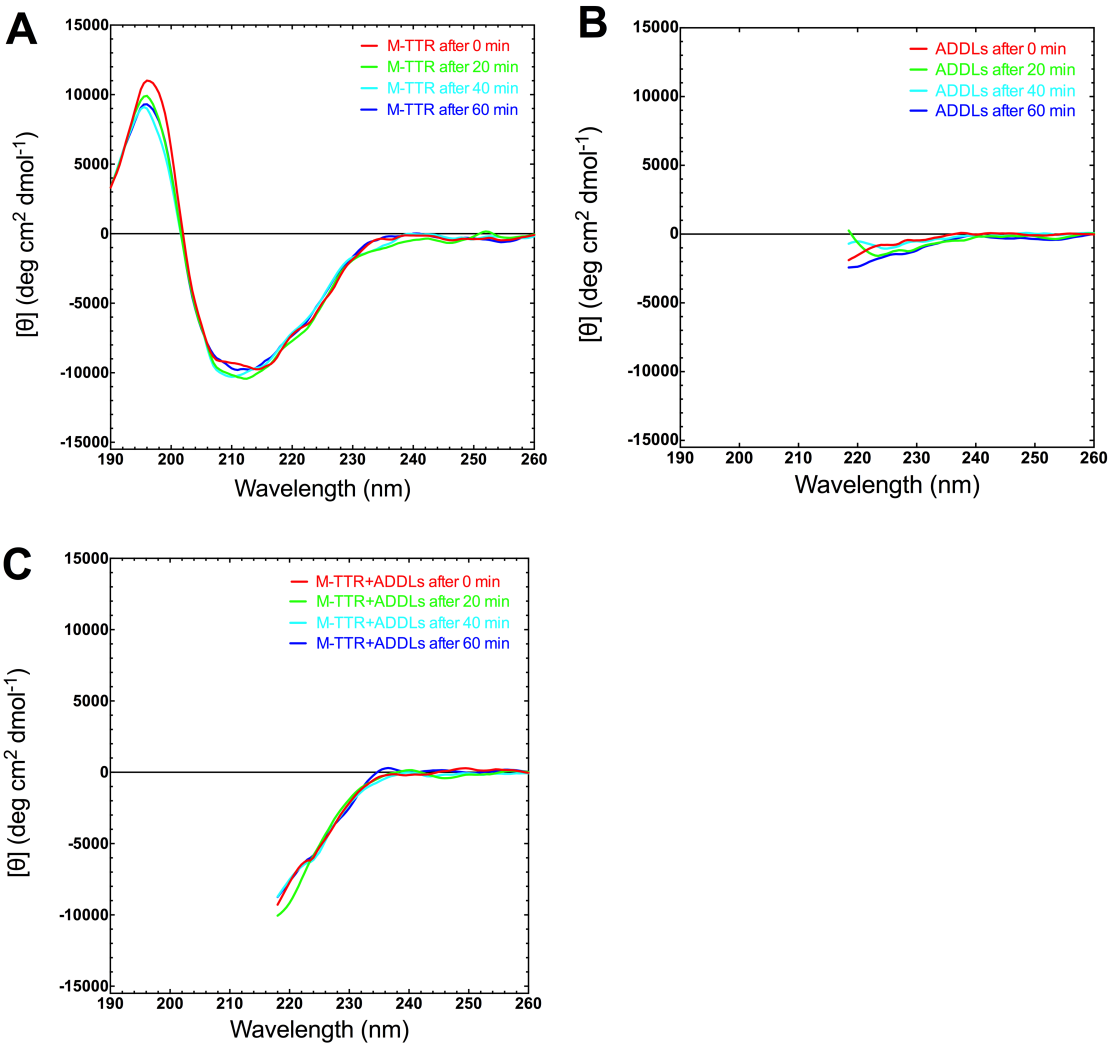

Figure 3.25. The $A\beta_{42}$ ADDLs/M-TTR interaction monitored with far-UV circular dichroism. (A) Far-UV CD spectra of M-TTR measured at 0, 20, 40 and 60 min using a protein concentration of 0.1 mg ml^{-1}. (B) Far-UV CD spectra measured for $A\beta_{42}$ ADDLs at 0, 20, 40 and 60 min using a protein concentration of 0.1 mg ml^{-1} (C) Far-UV CD spectra measured after incubating M-TTR and $A\beta_{42}$ ADDLs for 0, 20, 40 and 60 min using a total protein concentration of 0.2 mg ml^{-1} and using a 1:1 mass ratio of M-TTR: $A\beta_{42}$ ADDLs.

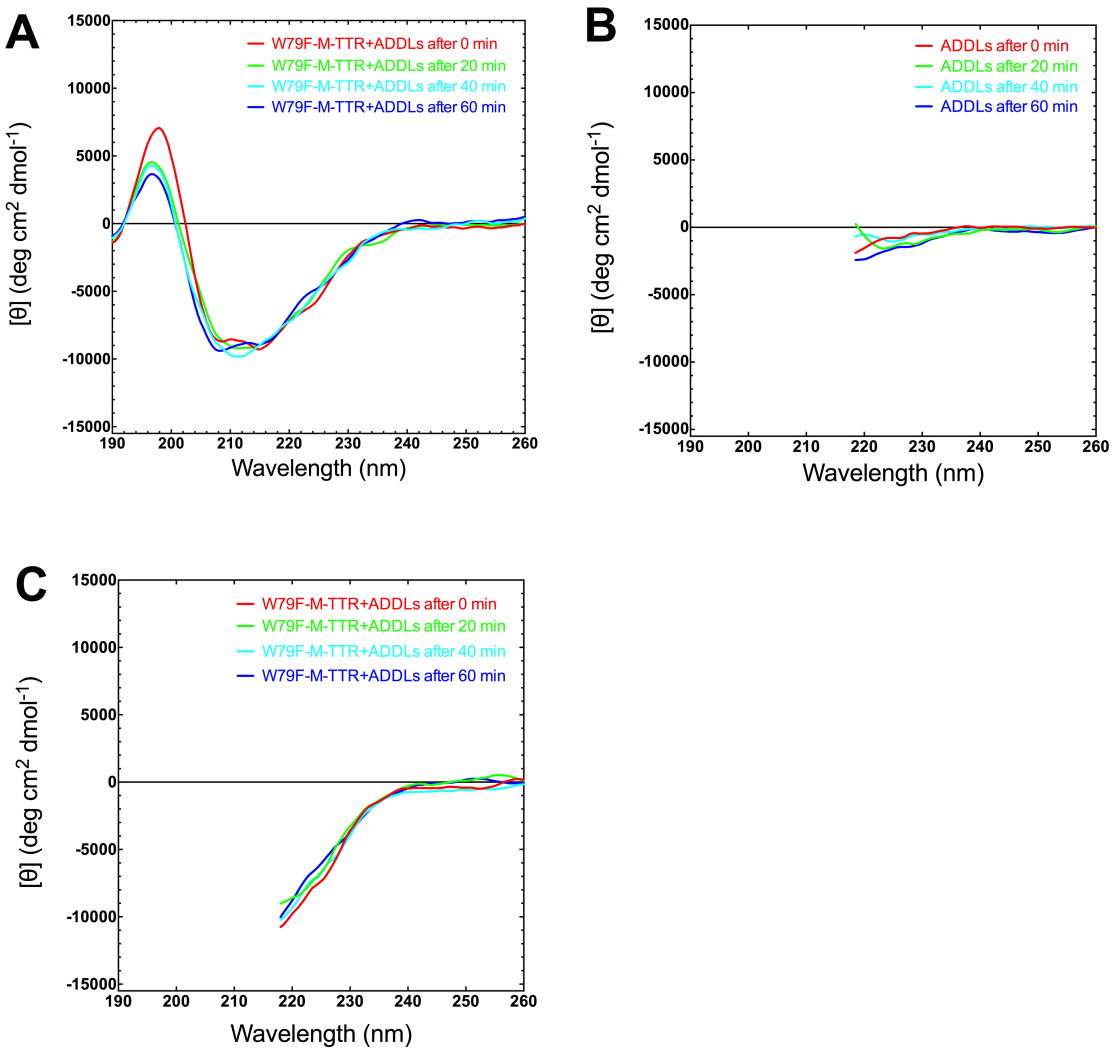

Figure 3.26. The $A\beta_{42}$ ADDLs/W79F-M-TTR interaction monitored with far-UV circular dichroism. (A) Far-UV CD spectra of W79F-M-TTR measured at 0, 20, 40 and 60 min using a protein concentration of 0.1 mg ml^{-1}. (B) Far-UV CD spectra measured for $A\beta_{42}$ ADDLs at 0, 20, 40 and 60 min using a protein concentration of 0.1 mg ml^{-1} (C) Far-UV CD spectra measured after incubating W79F-M-TTR and $A\beta_{42}$ ADDLs for 0, 20, 40 and 60 min using a total protein concentration of 0.2 mg ml^{-1} and using a 1:1 mass ratio of M-TTR: $A\beta_{42}$ ADDLs.

Chapter 4
Discussion

4.1 The various conformational states of monomeric transthyretin monitored with FRET

The production of a mutant of human wild-type TTR that is stable as a monomer, generally referred to as M-TTR (Jiang et al. 2001b), has greatly facilitated the study of the folding process of this protein, of the structural perturbations occurring in the conversion of the fully folded monomer to the amyloidogenic state at weakly acidic pH values, of the aggregation process from such a state and of the mechanism of action of TTR as a toxin detoxifier (Cappelli et al. 2016; Cascella et al. 2013; Conti et al. 2014; Hurshman et al. 2004; Jiang et al. 2001b; Lim et al. 2013). Following the observation that M-TTR contains only a solvent-exposed cysteine residue at position 10 that can be potentially labelled with a coumarin derivative able to act as an acceptor of the fluorescence of the naturally present tryptophan residues at positions 41 and 79, I generated a coumarin-labelled M-TTR molecule (DACM-M-TTR) to investigate the spatial distance between the coumarin moiety at position 10 and Trp41/Trp79, particularly Trp41, which is non-quenched and spatially closer to Cys10.

Six conformational states of M-TTR have been investigated, namely (i) the fully folded state at pH 7.4, (ii) the urea-unfolded state at pH 7.4, (iii) the molten globule state populated at equilibrium at low urea concentrations, pH 7.4, (iv) the partially folded state accumulating transiently during folding, pH 7.4 (v) the amyloidogenic state at pH 4.4 and (vi) the aggregated state at pH 4.4.

The first study performed at pH 7.4, 25 °C, no added denaturants, indicated that DACM-M-TTR is folded, monomeric in solution, singly and uniformly labelled, and maintains a structure superimposable to that of unlabeled M-TTR. The labelled protein is less stable than the unlabeled one, as indicated by the lower free energy change of unfolding ($\Delta G_{H_2O}^{U-F}$), but this is attributable to the high sensitivity of the $\Delta G_{H_2O}^{U-F}$ value to covalent modifications, as indicated by the many observations accumulated so far that most mutants of TTR are indeed less stable than the wild-type protein, regardless of the position and type of the mutation (Sekijima et al. 2005). A FRET efficiency (*E*) value of 0.72±0.02 was obtained for DACM-M-TTR at pH 7.4. Such a value is largely due to the energy transfer from Trp41 to DACM, both because the fluorescence of Trp79 is quenched (Lai et al. 1996) and because Trp79 is more distant than Trp41 from Cys10 (Jiang et al. 2001b; Peterson et al. 1998). The observation that the W79F mutant of DACM-M-TTR features a similar FRET *E*

value under the same conditions, supports this hypothesis. A FRET *E* value of 0.72±0.02 results into a spatial distance of 23.2±2.0 nm, between Trp41 and DACM.

The conversion of the non-mutated and W79F mutant forms of M-TTR from their folded state to the amyloidogenic state at pH 4.4 (or 5.6 in the case of the W79F-M-TTR) does not change significantly the FRET *E* value and the related distance between DACM and Trp41, indicating that β-strand C, where Trp41 is located, does not increase its distance from Cys10 and does not unfold upon such conversion. This observation is particularly important as previous structural investigations on WT-TTR, carried out with spectroscopic methods, limited proteolysis and hydrogen/deuterium exchange monitored with NMR, attributed such a structural conversion mainly to the unfolding of β-strands C/D and the interconnecting loop (Lai et al. 1996) or to the entire β-sheet CBEF (Liu et al. 2000). If this was the case, a decrease of the FRET *E* value should have been observed upon acidification, given the high sensitivity of FRET to even minor structural perturbations or increased dynamics. Our observation is indeed in agreement with more recent observations obtained with solution NMR that the whole CBEF β-sheet, including β-strand C, does not unfold, nor does it increase its structural dynamics, upon conversion of native M-TTR and WT-TTR into the amyloidogenic state at mildly acidic pH (Das et al. 2014; Lim et al. 2016a; Lim et al. 2013). A unifying picture of the amyloidogenic state of TTR at mildly low pH (pH 3.9-5.5) that is consistent with all recent data obtained so far with different techniques is that of a largely native-like state with the entire DAGH β-sheet, the D-E loop, the E-F α-helix and its associated residues from the A-B loop, exhibiting structural fluctuations, in the presence of a substantially folded and packed CBEF β-sheet.

The equilibrium molten globule state of M-TTR or W79F-M-TTR populated at low urea concentrations, pH 7.4, has a FRET *E* value similar to those of the folded and amyloidogenic states of the same proteins isoforms, suggesting that the Cys10-Trp41 distance is not significantly altered in such a conformational state. It is interesting to compare the structural information collected so far on such molten globule state of M-TTR (Conti et al. 2014) with that obtained for the amyloidogenic state of M-TTR and WT-TTR at pH 3.9-5.0 (Das et al. 2014; Jiang et al. 2001b; Lai et al. 1996; Lim et al. 2016a; Lim et al. 2013), to assess whether the two conformational states are essentially similar albeit populated under different conditions. The two conformational states share similar FRET *E* values and near-UV CD spectra, but different intrinsic fluorescence and far-UV CD spectra. The molten

globule state of M-TTR in 2.0 M urea, pH 7.4, has a far-UV CD spectrum different from that of the folded/amyloidogenic states (Lim et al. 2016a), which appear to be similar between them (Conti et al. 2014; Lai et al. 1996). Indeed, the molten globule state indicates a substantial unfolding of some portions of the protein (Conti et al. 2014). The molten globule state in 2.0 M urea, pH 7.4, unlike the amyloidogenic state at pH 4.4, has an intrinsic fluorescence spectrum similar to that of the folded state at pH 7.4 (Conti et al. 2014; Lai et al. 1996). Hence, it appears that the two conformational states are structurally distinct. It will be important to establish the amyloidogenic nature of the molten globule state, which may be as important as the amyloidogenic state populated at low pH.

As far as the off-pathway, partially folded state formed transiently during folding at pH 7.4 is concerned, it has a FRET *E* value significantly higher than that of the folded and amyloidogenic states, in both the non-mutated and W79F isoforms of the protein, suggesting that Trp41 is closer to Cys10 than it is in the folded/amyloidogenic states. This result reinforces the view that such a conformational state is an off-pathway species with some non-native contacts that need to be unfolded before folding can proceed (Conti et al. 2014). The kinetic and amyloidogenic conformational states share similar values of mean residue ellipticity, at least at 219 nm, and both induce an increase and blue-shift of the ANS dye (Conti et al. 2014; Jiang et al. 2001b; Lai et al. 1996). However, in addition to showing different FRET *E* values, they also differ for the intrinsic fluorescence spectra, exhibiting a fluorescence intensity higher and lower than the folded state at pH 7.4, respectively (Conti et al. 2014; Lai et al. 1996). Again, it appears that the two conformational states are structurally distinct.

The aggregated state of M-TTR at mildly low pH has a high FRET *E* value ($E = 0.82 \pm 0.01$). The W41F mutant has a similar value ($E = 0.81 \pm 0.04$), but that of the W79F mutant is remarkably lower ($E = 0.41 \pm 0.04$). This indicates that, following aggregation, Trp79 (the tryptophan residue monitorable in the W41F mutant) is released from its intrinsic natural quencher present in the folded/amyloidogenic state and moves closer to the DACM molecule, belonging either to the same or to an adjacent molecule. By contrast, Trp41 is more distant from DACM in the aggregated state. Three models of TTR amyloid fibrils have been proposed so far (Bateman et al. 2011; Lim et al. 2016b; Serag et al. 2002). Unfortunately, the level of structural detail of the three models is not sufficiently high to establish with acceptable accuracy the positions the two tryptophan residues and to use our FRET data to support either

model. However, our data indicate that Trp79 is within or close to the core of the TTR aggregate, whereas Trp41 is in a region that is not tightly packed in the aggregates. In addition, our FRET *E* values will hopefully be of use once our technical progress will allow to gain more structural insight into the TTR amyloid fibrils.

Another interesting observation emerging from these results is the high aggregation propensity exhibited by the W41F mutant, which was indeed found to be insoluble even under native conditions, limiting our FRET analysis to the aggregated state. Among the many mutants of TTR associated with TTR diseases, one has been reported to involve Trp41 (W41L) and to cause vitreous opacity with amyloid-material positive for TTR in the vitreous fluid of the index patient (Yazaki et al. 2002a; Yazaki et al. 2002b). W41F and W41L TTRs share similarly high aggregation propensities, observed *in vivo* and *in vitro*, respectively, suggesting that Trp41 is a very important amino acid residue for maintaining the stability and solubility of native TTR.

4.2 The conformational changes occurring on monomeric transthyretin when acting as a detoxifier

TTR inhibits Aβ toxicity in an *in vitro* cell culture, as shown in this study as well as in several other reports (Cascella et al. 2013; Li et al. 2013; Schwarzman et al. 1994). Many observations have suggested an interaction between the monomeric amyloidogenic precursor of TTR and the peptide Aβ associated with Alzheimer diseases (Schwarzman et al. 1994; Serot et al. 1997). However, the specificity of the interaction was questioned in the absence of detailed characterization of the binding (Li et al. 2013). I used the FRET technique to characterise the interaction between tetrameric and monomeric TTR (WT-TTR, M-TTR, W79F-M-TTR) and Aβ peptide in both the process of aggregation, that is the conversion of its monomeric state into well-defined amyloid fibrils, as well as on pre-formed toxic oligomers called amyloid-derived diffusible ligands (ADDLs). This study takes advantage of the absence of cysteine and tryptophan residues in Aβ, which will not interfere with the FRET measurements of TTRs.

The time course of amyloid fibril formation by 10 μM $A\beta_{40}$ was studied under conditions close to physiological and starting from a monomeric state of the $A\beta_{40}$

peptide, in the presence of wild-type tetrameric TTR (WT-TTR) at 15 different concentrations ranging from 0.0001 μM to 10 μM (from 0.0004 μM to 40 μM monomeric equivalents). This study showed inhibition of aggregation of $A\beta_{40}$ by transthyretin molecules. Concentrations of 0.3 μM or higher (corresponding to 1.2 μM or higher for the monomer) abolished completely aggregation of $A\beta_{40}$. This analysis was repeated in the presence of M-TTR. The time course of amyloid fibril formation by 10 μM $A\beta_{40}$ was studied in the presence of 15 different concentrations of M-TTR, ranging from 0.0001 μM to 10 μM. M-TTR. M-TTR concentrations of 2 μM or higher abolished completely aggregation of $A\beta_{40}$ within the interval of time studied here. Interestingly, when the concentrations of both WT-TTR and M-TTR are quantified in terms of monomeric units, the two TTR species appear to have similar effects in inhibiting amyloid fibril formation by $A\beta_{40}$. I also analysed the effect of W79F M-TTR on $A\beta_{40}$ amyloid fibril formation. Concentrations of 1 μM or higher abolished completely aggregation of $A\beta_{40}$ in this interval of time. When the three forms of TTR studied here were incubated under the same experimental conditions for 15 h but in the absence of $A\beta_{40}$, the ThT fluorescence was not found to increase, even using concentrations of TTR as high as 50 μM. This indicates that TTR molecules do not contribute to the observed kinetic traces of $A\beta_{40}$ aggregation and simply have an inhibitory effect. The half-time analysis shows that no aggregation of $A\beta_{40}$ could be observed with more than 0.2 molar equivalents for WT-TTR, M-TTR and W79F-M-TTR within 20 hours, i.e. the half-time was 10 times higher than the half-time observed with $A\beta_{40}$ alone in the absence of TTR molecules.

I also studied the conformational change of all three TTR variants following the interaction with $A\beta_{40}$ during aggregation at a molar ratio of 1:3 (TTR:$A\beta_{40}$). In particular, the FRET *E* of TTRs during aggregation of $A\beta_{40}$ was monitored and the results showed a change in FRET *E* of all TTR molecules as $A\beta_{40}$ aggregation proceeds, indicating a conformational conversion upon $A\beta_{40}$/TTR interaction. The changes of the FRET *E* values of all three TTR variants (WT-TTR, M-TTR and W79F-M-TTR) occur within the lag phase of the process of amyloid fibril formation of $A\beta_{40}$, indicating that the interaction between the two proteins occurs at the oligomeric state of $A\beta_{40}$, before the fibrils form.

Interestingly, for both WT-TTR and M-TTR a rapid increase of the FRET *E* value is followed by a slow decrease, both changes occurring within the lag phase of the sigmoidal curve of the $A\beta_{40}$ aggregation process. For W79F-M-TTR a rapid increase of the FRET *E* value is missing and only the slow decrease is apparent. This

suggests that the second slower decrease of the FRET *E* value is caused by an increase of the spatial distance between Trp41 and the DACM moiety attached to Cys10. The first rapid increase is most likely caused by a conformational change involving Trp79, which is present only in M-TTR and WT-TTR, but is more difficult to interpret in terms of changes of the spatial distance between Trp79 and the DACM molecule attached to Cys10: indeed, Trp79 is quenched in native M-TTR (Lai et al. 1996) and the rapid increase of intrinsic fluorescence detected in both M-TTR and WT-TTR following the interaction with $A\beta_{40}$, but not in the corresponding DACM-labelled counterparts, reveals that it becomes at least in part unquenched in the two unlabelled proteins. Thus, it is likely that the first rapid increase of the FRET value is caused by a conformational change occurring on Trp41, but the result is difficult to interpret in terms of change of spatial distance from Cys10.

The far-UV CD spectra of WT-TTR, M-TTR and W79F M-TTR in the absence and presence of $A\beta_{40}$ undergoing aggregation were compared after 30 min, showing that there are no changes in the secondary structure of TTRs after binding to $A\beta_{40}$ while it converts from monomers to oligomer. This indicates that the conformational changes occurring on the three TTR variants following the interaction with $A\beta_{40}$ oligomers are subtle, do not involve a substantial unfolding of the monomeric TTR molecule, but are monitorable with FRET, which is indeed very sensitive to small changes of the spatial distance between the FRET donor and acceptor pair, as the FRET *E* value depends on the sixth power of such a distance (Lakowicz 2006).

While it has been known for many years that Aβ monomers assemble into large neurotoxic amyloid fibrils (Lorenzo and Yankner 1994; Pike et al. 1993), recent studies show that non-fibrillar Aβ-derived toxins also exist. These toxic soluble species comprise Aβ-derived diffusible ligands (ADDLs) (Lambert et al. 1998; Longo et al. 2000). The ADDLs comprise small, soluble $A\beta_{1\text{-}42}$ oligomers which form below the critical concentrations needed to form protofibrils and fibrils. *In vitro*, TTR binds to all forms of soluble Aβ, monomer, oligomer and fibrils (Buxbaum et al. 2008; Du and Murphy 2010; Liu and Murphy 2006). TTR binds to Aβ better at 37 °C than 25 °C, binds to Aβ aggregates better than monomers (Buxbaum et al. 2008; Du and Murphy 2010; Liu and Murphy 2006), and to $A\beta_{1\text{-}42}$ better than $A\beta_{1\text{-}40}$ (Buxbaum et al. 2008; Liu and Murphy 2006; Schwarzman et al. 2004). The binding is highly dependent on the quaternary structure of TTR (Du and Murphy 2010). In this study, the conformational changes of binding of $A\beta_{42}$ ADDLs to TTRs was studied by the

FRET techniques. M-TTR and DACM-M-TTR were incubated at a concentration of 4 μM in the absence and presence of preformed $A\beta_{42}$ ADDLs at a concentration of 12 μM (monomer equivalents). The fluorescence spectra of both M-TTR and DACM-M-TTR in the absence of $A\beta_{42}$ ADDLs were found to be stable within the first hour of incubation, indicating the stability of unlabeled and labeled proteins under these conditions. Consequently, the FRET *E* value is also stable within this time frame. By contrast, the spectra recorded for both M-TTR and DACM-M-TTR in the presence of $A\beta_{42}$ ADDLs decreased in intensity with time, indicating a progressive interaction with the ADDLs. As expected, $A\beta_{42}$ ADDLs in the absence of M-TTR did not show any significant fluorescence, indicating its lack of contribution in the acquired fluorescence spectra. The FRET *E* value of M-TTR measured during incubation, in the presence of $A\beta_{42}$ ADDLs was found to decrease progressively, indicating that a conformational change occurs for M-TTR following the interaction with $A\beta_{42}$ ADDLs. This analysis was repeated for the W79F mutant of M-TTR leading to very similar results. This confirms that a conformational change occurs also for W79F M-TTR following the interaction with $A\beta_{42}$ ADDLs and indicates an increased spatial distance between the DACM moiety attached to Cys10 and the two tryptophan residues, particularly Trp41.

4.3 Conclusions

In conclusion, the FRET study described here provides insight into the structural changes occurring during the folding, unfolding and aggregation of TTR, as well as during its "chaperone" activity during Aβ fibril formation. The most important achievements of our results is the clarification of the degree of unfolding and dynamics of β-strand C in the formation of the amyloidogenic state and upon interaction with Aβ oligomers causing cell dysfunction and the establishment of the concept that both the molten globule state and kinetically trapped species accumulating during folding are structurally distinct from such a state, indicating that TTR is a highly plastic protein able to populate a number of structurally discrete conformational states.

5.3 Acknowledgements

This work was supported by the Iranian Ministry of Science, Research and Technology through the studentship granted to Seyyed Abolghasem Ghadami for this project and the University of Florence for Fondi di Ateneo.

References

Achen, M. G., W. Duan, T. M. Pettersson, P. J. Harms, S. J. Richardson, M. C. Lawrence, R. E. Wettenhall, A. R. Aldred and G. Schreiber. 1993. "Transthyretin gene expression in choroid plexus first evolved in reptiles." Am J Physiol 265(5 Pt 2):R982-989.

Adams, P. D., P. V. Afonine, G. Bunkoczi, V. B. Chen, I. W. Davis, N. Echols, J. J. Headd, L. W. Hung, G. J. Kapral, R. W. Grosse-Kunstleve, A. J. McCoy, N. W. Moriarty, R. Oeffner, R. J. Read, D. C. Richardson, J. S. Richardson, T. C. Terwilliger and P. H. Zwart. 2010. "PHENIX: a comprehensive Python-based system for macromolecular structure solution." Acta Crystallogr D Biol Crystallogr 66(Pt 2):213-221.

Adamski-Werner, S. L., S. K. Palaninathan, J. C. Sacchettini and J. W. Kelly. 2004. "Diflunisal analogues stabilize the native state of transthyretin. Potent inhibition of amyloidogenesis." J Med Chem 47(2):355-374.

Adly, M. A. 2010. "Analysis of the expression pattern of the carrier protein transthyretin and its receptor megalin in the human scalp skin and hair follicles: hair cycle-associated changes." Histochem Cell Biol 134(6):591-602.

Aksenova, M. V., M. Y. Aksenov, D. A. Butterfield and J. M. Carney. 1996. "alpha-1-antichymotrypsin interaction with A beta (1-40) inhibits fibril formation but does not affect the peptide toxicity." Neurosci Lett 211(1):45-48.

Aleshire, S. L., C. A. Bradley, L. D. Richardson and F. F. Parl. 1983. "Localization of human prealbumin in choroid plexus epithelium." J Histochem Cytochem 31(5):608-612.

Almeida, M. R. and M. J. Saraiva. 2012. "Clearance of extracellular misfolded proteins in systemic amyloidosis: experience with transthyretin." FEBS Lett 586(18):2891-2896.

Alzheimer, A. . 1907. "Über eine eigenartige Erkrankung der Hirnrinde." Allgemeine Z Psychiatrie Psychisch-Gerichtliche Med 64:146-148.

Bartalena, L. 1990. "Recent achievements in studies on thyroid hormone-binding proteins." Endocr Rev 11(1):47-64.

Bateman, D. A., R. Tycko and R. B. Wickner. 2011. "Experimentally derived structural constraints for amyloid fibrils of wild-type transthyretin." Biophys J 101(10):2485-2492.

Bellovino, D., T. Morimoto, F. Tosetti and S. Gaetani. 1996. "Retinol binding protein and transthyretin are secreted as a complex formed in the endoplasmic reticulum in HepG2 human hepatocarcinoma cells." Exp Cell Res 222(1):77-83.

Benson, M. D. 1989. "Familial amyloidotic polyneuropathy." Trends Neurosci 12(3):88-92.

Bergstrom, J., A. Gustavsson, U. Hellman, K. Sletten, C. L. Murphy, D. T. Weiss, A. Solomon, B. O. Olofsson and P. Westermark. 2005. "Amyloid deposits in transthyretin-derived amyloidosis: cleaved transthyretin is associated with distinct amyloid morphology." J Pathol 206(2):224-232.

Blake, C. C., M. J. Geisow, I. D. Swan, C. Rerat and B. Rerat. 1974. "Strjcture of human plasma prealbumin at 2-5 A resolution. A preliminary report on the polypeptide chain conformation, quaternary structure and thyroxine binding." J Mol Biol 88(1):1-12.

Blake, C. C., I. D. Swan, C. Rerat, J. Berthou, A. Laurent and B. Rerat. 1971. "An x-ray study of the subunit structure of prealbumin." J Mol Biol 61(1):217-224.

Bonifacio, M. J., Y. Sakaki and M. J. Saraiva. 1996. "'In vitro' amyloid fibril formation from transthyretin: the influence of ions and the amyloidogenicity of TTR variants." Biochim Biophys Acta 1316(1):35-42.

Borek, C., J. E. Smith, D. R. Soprano and D. S. Goodman. 1981. "Regulation of retinol-binding protein metabolism by glucocorticoid hormones in cultured H4II EC3 liver cells." Endocrinology 109(2):386-391.

Brouillette, J. and R. Quirion. 2008. "Transthyretin: a key gene involved in the maintenance of memory capacities during aging." Neurobiol Aging 29(11):1721-1732.

Butler, J. S., A. Chan, S. Costelha, S. Fishman, J. L. Willoughby, T. D. Borland, S. Milstein, D. J. Foster, P. Goncalves, Q. Chen, J. Qin, B. R. Bettencourt, D. W. Sah, R. Alvarez, K. G. Rajeev, M. Manoharan, K. Fitzgerald, R. E. Meyers, S. V. Nochur, M. J. Saraiva and T. S. Zimmermann. 2016. "Preclinical evaluation of RNAi as a treatment for transthyretin-mediated amyloidosis." Amyloid 23(2):109-118.

Buxbaum, J. N. and N. Reixach. 2009. "Transthyretin: the servant of many masters." Cell Mol Life Sci 66(19):3095-3101.

Buxbaum, J. N., Z. Ye, N. Reixach, L. Friske, C. Levy, P. Das, T. Golde, E. Masliah, A. R. Roberts and T. Bartfai. 2008. "Transthyretin protects Alzheimer's mice from the behavioral and biochemical effects of Abeta toxicity." Proc Natl Acad Sci U S A 105(7):2681-2686.

Caporaso, G. L., K. Takei, S. E. Gandy, M. Matteoli, O. Mundigl, P. Greengard and P. De Camilli. 1994. "Morphologic and biochemical analysis of the intracellular trafficking of the Alzheimer beta/A4 amyloid precursor protein." J Neurosci 14(5 Pt 2):3122-3138.

Cappelli, S., A. Penco, B. Mannini, R. Cascella, M. R. Wilson, H. Ecroyd, X. Li, J. N. Buxbaum, C. M. Dobson, C. Cecchi, A. Relini and F. Chiti. 2016. "Effect of molecular chaperones on aberrant protein oligomers in vitro: super-versus sub-stoichiometric chaperone concentrations." Biol Chem 397(5):401-415.

Carro, E., J. L. Trejo, T. Gomez-Isla, D. LeRoith and I. Torres-Aleman. 2002. "Serum insulin-like growth factor I regulates brain amyloid-beta levels." Nat Med 8(12):1390-1397.

Cascella, R., S. Conti, B. Mannini, X. Li, J. N. Buxbaum, B. Tiribilli, F. Chiti and C. Cecchi. 2013. "Transthyretin suppresses the toxicity of oligomers formed by misfolded proteins in vitro." Biochim Biophys Acta 1832(12):2302-2314.

Cavallaro, T., R. L. Martone, A. J. Dwork, E. A. Schon and J. Herbert. 1990. "The retinal pigment epithelium is the unique site of transthyretin synthesis in the rat eye." Invest Ophthalmol Vis Sci 31(3):497-501.

Chiang, H. C., K. Iijima, I. Hakker and Y. Zhong. 2009. "Distinctive roles of different beta-amyloid 42 aggregates in modulation of synaptic functions." FASEB J 23(6):1969-1977.

Choi, S. H., S. N. Leight, V. M. Lee, T. Li, P. C. Wong, J. A. Johnson, M. J. Saraiva and S. S. Sisodia. 2007. "Accelerated Abeta deposition in APPswe/PS1deltaE9 mice with hemizygous deletions of TTR (transthyretin)." J Neurosci 27(26):7006-7010.

Coelho, T. 2007. "On the experience of epilepsy." Neurology 68(20):1737-1738.

Cohen, A. S. and E. Calkins. 1959. "Electron microscopic observations on a fibrous component in amyloid of diverse origins." Nature 183(4669):1202-1203.

Collaborative Computational Project, Number. 1994. "The CCP4 suite: programs for protein crystallography." Acta Crystallogr D Biol Crystallogr 50(Pt 5):760-763.

Colon, W. and J. W. Kelly. 1992. "Partial denaturation of transthyretin is sufficient for amyloid fibril formation in vitro." Biochemistry 31(36):8654-8660.

Connors, L. H., A. Lim, T. Prokaeva, V. A. Roskens and C. E. Costello. 2003. "Tabulation of human transthyretin (TTR) variants, 2003." Amyloid 10(3):160-184.

Conti, S., X. Li, S. Gianni, S. A. Ghadami, J. Buxbaum, C. Cecchi, F. Chiti and F. Bemporad. 2014. "A complex equilibrium among partially unfolded conformations in monomeric transthyretin." Biochemistry 53(27):4381-4392.

Costa, P. P., B. Jacobsson, V. P. Collins and P. Biberfeld. 1986a. "Unmasking antigen determinants in amyloid." J Histochem Cytochem 34(12):1683-1685.

Costa, R., A. Goncalves, M. J. Saraiva and I. Cardoso. 2008. "Transthyretin binding to A-Beta peptide--impact on A-Beta fibrillogenesis and toxicity." FEBS Lett 582(6):936-942.

Costa, R. H., E. Lai and J. E. Darnell, Jr. 1986b. "Transcriptional control of the mouse prealbumin (transthyretin) gene: both promoter sequences and a distinct enhancer are cell specific." Mol Cell Biol 6(12):4697-4708.

Costa, R. H., T. A. Van Dyke, C. Yan, F. Kuo and J. E. Darnell, Jr. 1990. "Similarities in transthyretin gene expression and differences in transcription factors: liver and yolk sac compared to choroid plexus." Proc Natl Acad Sci U S A 87(17):6589-6593.

Damas, A. M. and M. J. Saraiva. 2000. "Review: TTR amyloidosis-structural features leading to protein aggregation and their implications on therapeutic strategies." J Struct Biol 130(2-3):290-299.

Das, J. K., S. S. Mall, A. Bej and S. Mukherjee. 2014. "Conformational flexibility tunes the propensity of transthyretin to form fibrils through non-native intermediate states." Angew Chem Int Ed Engl 53(47):12781-12784.

Dickson, P. W., A. R. Aldred, P. D. Marley, D. Bannister and G. Schreiber. 1986. "Rat choroid plexus specializes in the synthesis and the secretion of transthyretin (prealbumin). Regulation of transthyretin synthesis in choroid plexus is independent from that in liver." J Biol Chem 261(8):3475-3478.

Dickson, P. W., A. R. Aldred, P. D. Marley, G. F. Tu, G. J. Howlett and G. Schreiber. 1985. "High prealbumin and transferrin mRNA levels in the choroid plexus of rat brain." Biochem Biophys Res Commun 127(3):890-895.

Dickson, P. W., A. R. Aldred, J. G. Menting, P. D. Marley, W. H. Sawyer and G. Schreiber. 1987. "Thyroxine transport in choroid plexus." J Biol Chem 262(29):13907-13915.

Du, J., P. Y. Cho, D. T. Yang and R. M. Murphy. 2012. "Identification of beta-amyloid-binding sites on transthyretin." Protein Eng Des Sel 25(7):337-345.

Du, J. and R. M. Murphy. 2010. "Characterization of the interaction of beta-amyloid with transthyretin monomers and tetramers." Biochemistry 49(38):8276-8289.

Eanes, E. D. and G. G. Glenner. 1968. "X-ray diffraction studies on amyloid filaments." J Histochem Cytochem 16(11):673-677.

Elovaara, I., C. P. Maury and J. Palo. 1986. "Serum amyloid A protein, albumin and prealbumin in Alzheimer's disease and in demented patients with Down's syndrome." Acta Neurol Scand 74(3):245-250.

Emsley, P. and K. Cowtan. 2004. "Coot: model-building tools for molecular graphics." Acta Crystallogr D Biol Crystallogr 60(Pt 12 Pt 1):2126-2132.

Episkopou, V., S. Maeda, S. Nishiguchi, K. Shimada, G. A. Gaitanaris, M. E. Gottesman and E. J. Robertson. 1993. "Disruption of the transthyretin gene results in mice with depressed levels of plasma retinol and thyroid hormone." Proc Natl Acad Sci U S A 90(6):2375-2379.

Evans, P. 2006. "Scaling and assessment of data quality." Acta Crystallogr D Biol Crystallogr 62(Pt 1):72-82.

Felding, P. and G. Fex. 1982. "Cellular origin of prealbumin in the rat." Biochim Biophys Acta 716(3):446-449.

Ferguson, R. N., H. Edelhoch, H. A. Saroff, J. Robbins and H. J. Cahnmann. 1975. "Negative cooperativity in the binding of thyroxine to human serum prealbumin. Preparation of tritium-labeled 8-anilino-1-naphthalenesulfonic acid." Biochemistry 14(2):282-289.

Ferrone, F. 1999. "Analysis of protein aggregation kinetics." Methods Enzymol 309:256-274.

Fex, G. and G. Johannesson. 1988. "Retinol transfer across and between phospholipid bilayer membranes." Biochim Biophys Acta 944(2):249-255.

Fleming, C. E., F. M. Mar, F. Franquinho, M. J. Saraiva and M. M. Sousa. 2009. "Transthyretin internalization by sensory neurons is megalin mediated and necessary for its neuritogenic activity." J Neurosci 29(10):3220-3232.

Fleming, C. E., M. J. Saraiva and M. M. Sousa. 2007. "Transthyretin enhances nerve regeneration." J Neurochem 103(2):831-839.

Florence, B., B. Seibert and J. W. Nelson. 1942. "Electrophoretic study of the blood protein response in tuberculosis." J. Biol. Chem. 143:29-38. .

Foss, T. R., R. L. Wiseman and J. W. Kelly. 2005. "The pathway by which the tetrameric protein transthyretin dissociates." Biochemistry 44(47):15525-15533.

Fung, W. P., T. Thomas, P. W. Dickson, A. R. Aldred, J. Milland, M. Dziadek, B. Power, P. Hudson and G. Schreiber. 1988. "Structure and expression of the rat transthyretin (prealbumin) gene." J Biol Chem 263(1):480-488.

Garzuly, F., R. Vidal, T. Wisniewski, F. Brittig and H. Budka. 1996. "Familial meningocerebrovascular amyloidosis, Hungarian type, with mutant transthyretin (TTR Asp18Gly)." Neurology 47(6):1562-1567.

Gavrilesco, K., J. Courcon, P. Hillion, J. Uriel, J. Lewin and P. Grabar. 1955. "A study of normal human cerebrospinal fluid by the immuno-electrophoretic mentod." Nature 176(4490):976.

Gjoen, T., T. Bjerkelund, H. K. Blomhoff, K. R. Norum, T. Berg and R. Blomhoff. 1987. "Liver takes up retinol-binding protein from plasma." J Biol Chem 262(23):10926-10930.

Goate, A., M. C. Chartier-Harlin, M. Mullan, J. Brown, F. Crawford, L. Fidani, L. Giuffra, A. Haynes, N. Irving, L. James and et al. 1991. "Segregation of a missense mutation in the amyloid precursor protein gene with familial Alzheimer's disease." Nature 349(6311):704-706.

Goncalves, P., H. Martins, S. Costelha, L. F. Maia and M. J. Saraiva. 2016. "Efficiency of silencing RNA for removal of transthyretin V30M in a TTR leptomeningeal animal model." Amyloid 23(4):249-253.

Goodman, D. S. 1985. "Retinoids and retinoid-binding proteins." Harvey Lect 81:111-132.

Gouet, P., E. Courcelle, D. I. Stuart and F. Metoz. 1999. "ESPript: analysis of multiple sequence alignments in PostScript." Bioinformatics 15(4):305-308.

Granata, D., F. Baftizadeh, J. Habchi, C. Galvagnion, A. De Simone, C. Camilloni, A. Laio and M. Vendruscolo. 2015. "The inverted free energy landscape of an intrinsically disordered peptide by simulations and experiments." Scientific Reports 5.

Gustafsson, S., E. Ihse, M. Y. Henein, P. Westermark, P. Lindqvist and O. B. Suhr. 2012. "Amyloid fibril composition as a predictor of development of cardiomyopathy after liver transplantation for hereditary transthyretin amyloidosis." Transplantation 93(10):1017-1023.

Hagen, G. A. and W. J. Elliott. 1973. "Transport of thyroid hormones in serum and cerebrospinal fluid." J Clin Endocrinol Metab 37(3):415-422.

Hammarstrom, P., X. Jiang, A. R. Hurshman, E. T. Powers and J. W. Kelly. 2002. "Sequence-dependent denaturation energetics: A major determinant in amyloid disease diversity." Proc Natl Acad Sci U S A 99 Suppl 4:16427-16432.

Hammarstrom, P., F. Schneider and J. W. Kelly. 2001. "Trans-suppression of misfolding in an amyloid disease." Science 293(5539):2459-2462.

Hammarstrom, P., R. L. Wiseman, E. T. Powers and J. W. Kelly. 2003. "Prevention of transthyretin amyloid disease by changing protein misfolding energetics." Science 299(5607):713-716.

Hardy, J. A. and G. A. Higgins. 1992. "Alzheimer's disease: the amyloid cascade hypothesis." Science 256(5054):184-185.

Harms, P. J., G. F. Tu, S. J. Richardson, A. R. Aldred, A. Jaworowski and G. Schreiber. 1991. "Transthyretin (prealbumin) gene expression in choroid plexus is strongly conserved during evolution of vertebrates." Comp Biochem Physiol B 99(1):239-249.

Haupt, H. and K. Heide. 1966. "[Crystallization of prealbumin from human serum]." Experientia 22(7):449-451.

Herbert, J., J. N. Wilcox, K. T. Pham, R. T. Fremeau, Jr., M. Zeviani, A. Dwork, D. R. Soprano, A. Makover, D. S. Goodman, E. A. Zimmerman and et al. 1986. "Transthyretin: a choroid plexus-specific transport protein in human brain. The 1986 S. Weir Mitchell award." Neurology 36(7):900-911.

Hornak, V., R. Abel, A. Okur, B. Strockbine, A. Roitberg and C. Simmerling. 2006. "Comparison of multiple Amber force fields and development of improved protein backbone parameters." Proteins 65(3):712-725.

Hornberg, A., T. Eneqvist, A. Olofsson, E. Lundgren and A. E. Sauer-Eriksson. 2000. "A comparative analysis of 23 structures of the amyloidogenic protein transthyretin." J Mol Biol 302(3):649-669.

Hou, X., M. I. Aguilar and D. H. Small. 2007. "Transthyretin and familial amyloidotic polyneuropathy. Recent progress in understanding the molecular mechanism of neurodegeneration." FEBS J 274(7):1637-1650.

Hulbert, A. J. 2000. "Thyroid hormones and their effects: a new perspective." Biol Rev Camb Philos Soc 75(4):519-631.

Hurshman, A. R., J. T. White, E. T. Powers and J. W. Kelly. 2004. "Transthyretin aggregation under partially denaturing conditions is a downhill polymerization." Biochemistry 43(23):7365-7381.

Hurshman Babbes, A. R., E. T. Powers and J. W. Kelly. 2008. "Quantification of the thermodynamically linked quaternary and tertiary structural stabilities of transthyretin and its disease-associated variants: the relationship between stability and amyloidosis." Biochemistry 47(26):6969-6984.

Ihse, E., C. Rapezzi, G. Merlini, M. D. Benson, Y. Ando, O. B. Suhr, S. Ikeda, F. Lavatelli, L. Obici, C. C. Quarta, O. Leone, H. Jono, M. Ueda, M. Lorenzini, J. Liepnieks, T. Ohshima, M. Tasaki, T. Yamashita and P. Westermark. 2013. "Amyloid fibrils containing fragmented ATTR may be the standard fibril composition in ATTR amyloidosis." Amyloid-Journal of Protein Folding Disorders 20(3):142-150.

Ingbar, S. H. 1963. "Observations concerning the binding of thyroid hormones by human serum prealbumin." J Clin Invest 42:143-160.

Ingenbleek, Y. and M. De Visscher. 1979. "Hormonal and nutritional status: critical conditions for endemic goiter epidemiology?" Metabolism 28(1):9-19.

Jacobsson, B. 1989. "Localization of transthyretin-mRNA and of immunoreactive transthyretin in the human fetus." Virchows Arch A Pathol Anat Histopathol 415(3):259-263.

Jacobsson, B., V. P. Collins, L. Grimelius, T. Pettersson, B. Sandstedt and A. Carlstrom. 1989. "Transthyretin immunoreactivity in human and porcine liver, choroid plexus, and pancreatic islets." J Histochem Cytochem 37(1):31-37.

Jaroniec, C. P., C. E. MacPhee, N. S. Astrof, C. M. Dobson and R. G. Griffin. 2002. "Molecular conformation of a peptide fragment of transthyretin in an amyloid fibril." Proc Natl Acad Sci U S A 99(26):16748-16753.

Jarrett, J. T. and P. T. Lansbury, Jr. 1993. "Seeding "one-dimensional crystallization" of amyloid: a pathogenic mechanism in Alzheimer's disease and scrapie?" Cell 73(6):1055-1058.

Jiang, C., H. Lu, K. A. Vincent, S. Shankara, A. J. Belanger, S. H. Cheng, G. Y. Akita, R. A. Kelly, M. A. Goldberg and R. J. Gregory. 2002. "Gene expression profiles in human cardiac cells subjected to hypoxia or expressing a hybrid form of HIF-1 alpha." Physiol Genomics 8(1):23-32.

Jiang, X., J. N. Buxbaum and J. W. Kelly. 2001a. "The V122I cardiomyopathy variant of transthyretin increases the velocity of rate-limiting tetramer dissociation, resulting in accelerated amyloidosis." Proc Natl Acad Sci U S A 98(26):14943-14948.

Jiang, X., C. S. Smith, H. M. Petrassi, P. Hammarstrom, J. T. White, J. C. Sacchettini and J. W. Kelly. 2001b. "An engineered transthyretin monomer that is nonamyloidogenic, unless it is partially denatured." Biochemistry 40(38):11442-11452.

Jinno, Y., T. Matsumoto, T. Kamel, T. Kondoh, S. Maeda, S. Araki, K. Shimada and N. Niikawa. 1986. "Localization of the human prealbumin gene to 18p11.1-q12.3 by gene dose effect study of Southern blot hybridization." Jinrui Idengaku Zasshi 31(3):243-248.

Johnson, S M , R L Wiseman, N Reixach, J Paulsson, S Choi, E T Powers, J N Buxbaum and J W Kelly. 2010. Protein Misfolding Diseases: Current and Emerging Principles. Hoboken, New Jersey: John Wiley & Sons, Ltd.

Johnson, S. M., S. Connelly, C. Fearns, E. T. Powers and J. W. Kelly. 2012. "The transthyretin amyloidoses: from delineating the molecular mechanism of aggregation linked to pathology to a regulatory-agency-approved drug." J Mol Biol 421(2-3):185-203.

Johnson, S. M., S. Connelly, I. A. Wilson and J. W. Kelly. 2009. "Toward optimization of the second aryl substructure common to transthyretin amyloidogenesis inhibitors using biochemical and structural studies." J Med Chem 52(4):1115-1125.

Jungermann, K. and N. Katz. 1989. "Functional specialization of different hepatocyte populations." Physiol Rev 69(3):708-764.

Kabat, E. A., D. H. Moore and H. Landow. 1942. "An Electrophoretic Study of the Protein Components in Cerebrospinal Fluid and Their Relationship to the Serum Proteins." J Clin Invest 21(5):571-577.

Kabat, H. and M. Levine. 1942. "Capillary Emboli as a Lethal Factor in Burns." Science 96(2499):476-477.

Kanai, M., A. Raz and D. S. Goodman. 1968. "Retinol-binding protein: the transport protein for vitamin A in human plasma." J Clin Invest 47(9):2025-2044.

Kang, J., H. G. Lemaire, A. Unterbeck, J. M. Salbaum, C. L. Masters, K. H. Grzeschik, G. Multhaup, K. Beyreuther and B. Muller-Hill. 1987. "The precursor of Alzheimer's disease amyloid A4 protein resembles a cell-surface receptor." Nature 325(6106):733-736.

Kelly, J. W. 1998. "The alternative conformations of amyloidogenic proteins and their multi-step assembly pathways." Curr Opin Struct Biol 8(1):101-106.

Kelly, J. W., W. Colon, Z. H. Lai, H. A. Lashuel, J. McCulloch, S. L. McCutchen, G. J. Miroy and S. A. Peterson. 1997. "Transthyretin quaternary and tertiary structural changes facilitate misassembly into amyloid." Advances in Protein Chemistry, Vol 50 50:161-181.

Klabunde, T., H. M. Petrassi, V. B. Oza, P. Raman, J. W. Kelly and J. C. Sacchettini. 2000. "Rational design of potent human transthyretin amyloid disease inhibitors." Nat Struct Biol 7(4):312-321.

Kohda, K., S. Jinde, K. Iwamoto, M. Bundo, N. Kato and T. Kato. 2006. "Maternal separation stress drastically decreases expression of transthyretin in the brains of adult rat offspring." Int J Neuropsychopharmacol 9(2):201-208.

Kohno, K., J. A. Palha, K. Miyakawa, M. J. Saraiva, S. Ito, T. Mabuchi, W. S. Blaner, H. Iijima, S. Tsukahara, V. Episkopou, M. E. Gottesman, K. Shimada, K. Takahashi, K. Yamamura and S. Maeda. 1997. "Analysis of amyloid deposition in a transgenic mouse model of homozygous familial amyloidotic polyneuropathy." Am J Pathol 150(4):1497-1508.

Kopelman, M., U. Cogan, S. Mokady and M. Shinitzky. 1976. "The interaction between retinol-binding proteins and prealbumins studied by fluorescence polarization." Biochim Biophys Acta 439(2):449-460.

Korenberg, J. R., S. M. Pulst, R. L. Neve and R. West. 1989. "The Alzheimer amyloid precursor protein maps to human chromosome 21 bands q21.105-q21.05." Genomics 5(1):124-127.

Lacor, P. N., M. C. Buniel, L. Chang, S. J. Fernandez, Y. Gong, K. L. Viola, M. P. Lambert, P. T. Velasco, E. H. Bigio, C. E. Finch, G. A. Krafft and W. L. Klein. 2004. "Synaptic targeting by Alzheimer's-related amyloid beta oligomers." J Neurosci 24(45):10191-10200.

LaFerla, F. M., K. N. Green and S. Oddo. 2007. "Intracellular amyloid-beta in Alzheimer's disease." Nat Rev Neurosci 8(7):499-509.

Lai, Z., W. Colon and J. W. Kelly. 1996. "The acid-mediated denaturation pathway of transthyretin yields a conformational intermediate that can self-assemble into amyloid." Biochemistry 35(20):6470-6482.

Lakowicz, Joseph R. 2006. Principles of fluorescence spectroscopy. 3rd Edition. New York: Springer.

Lambert, M. P., A. K. Barlow, B. A. Chromy, C. Edwards, R. Freed, M. Liosatos, T. E. Morgan, I. Rozovsky, B. Trommer, K. L. Viola, P. Wals, C. Zhang, C. E. Finch, G. A. Krafft and W. L. Klein. 1998. "Diffusible, nonfibrillar ligands derived from Abeta1-42 are potent central nervous system neurotoxins." Proc Natl Acad Sci U S A 95(11):6448-6453.

Lashuel, H. A., C. Wurth, L. Woo and J. W. Kelly. 1999. "The most pathogenic transthyretin variant, L55P, forms amyloid fibrils under acidic conditions and protofilaments under physiological conditions." Biochemistry 38(41):13560-13573.

Lazarov, O., J. Robinson, Y. P. Tang, I. S. Hairston, Z. Korade-Mirnics, V. M. Lee, L. B. Hersh, R. M. Sapolsky, K. Mirnics and S. S. Sisodia. 2005. "Environmental enrichment reduces Abeta levels and amyloid deposition in transgenic mice." Cell 120(5):701-713.

Lee, J., Y. Hwang, W. Kang, S. J. Seong, M. S. Lim, H. W. Lee, D. S. Yim, D. R. Sohn, S. Han and Y. R. Yoon. 2012. "Population pharmacokinetic/pharmacodynamic modeling of clopidogrel in Korean healthy volunteers and stroke patients." J Clin Pharmacol 52(7):985-995.

Leslie, A.G.W. 1992. "Joint CCP4 and ESF-EACMB Newsletter on Protein Crystallography " (SERC Daresbury Laboratory, Warrington).

Li, X., E. Masliah, N. Reixach and J. N. Buxbaum. 2011. "Neuronal production of transthyretin in human and murine Alzheimer's disease: is it protective?" J Neurosci 31(35):12483-12490.

Li, X., X. Zhang, A. R. Ladiwala, D. Du, J. K. Yadav, P. M. Tessier, P. E. Wright, J. W. Kelly and J. N. Buxbaum. 2013. "Mechanisms of transthyretin inhibition of beta-amyloid aggregation in vitro." J Neurosci 33(50):19423-19433.

Lie, J. T. and P. I. Hammond. 1988. "Pathology of the senescent heart: anatomic observations on 237 autopsy studies of patients 90 to 105 years old." Mayo Clin Proc 63(6):552-564.

Lim, K. H., A. K. Dasari, I. Hung, Z. Gan, J. W. Kelly and D. E. Wemmer. 2016a. "Structural Changes Associated with Transthyretin Misfolding and Amyloid Formation Revealed by Solution and Solid-State NMR." Biochemistry 55(13):1941-1944.

Lim, K. H., A. K. Dasari, I. Hung, Z. Gan, J. W. Kelly, P. E. Wright and D. E. Wemmer. 2016b. "Solid-State NMR Studies Reveal Native-like beta-Sheet Structures in Transthyretin Amyloid." Biochemistry 55(37):5272-5278.

Lim, K. H., H. J. Dyson, J. W. Kelly and P. E. Wright. 2013. "Localized Structural Fluctuations Promote Amyloidogenic Conformations in Transthyretin." Journal of Molecular Biology 425(6):977-988.

Link, C. D. 1995. "Expression of human beta-amyloid peptide in transgenic Caenorhabditis elegans." Proc Natl Acad Sci U S A 92(20):9368-9372.

Liu, J., J. Lan, P. Zhao, F. Zheng, J. Song, P. Zhang and X. Sun. 2014. "Evidence of the presence of amyloid substance in the blood of familial amyloidotic polyneuropathy patients with ATTR Val30Met mutation." Int J Clin Exp Pathol 7(11):7795-7800.

Liu, K., H. S. Cho, D. W. Hoyt, T. N. Nguyen, P. Olds, J. W. Kelly and D. E. Wemmer. 2000. "Deuterium-proton exchange on the native wild-type transthyretin tetramer identifies the stable core of the individual subunits and indicates mobility at the subunit interface." J Mol Biol 303(4):555-565.

Liu, L. and R. M. Murphy. 2006. "Kinetics of inhibition of beta-amyloid aggregation by transthyretin." Biochemistry 45(51):15702-15709.

Liz, M. A., C. J. Faro, M. J. Saraiva and M. M. Sousa. 2004. "Transthyretin, a new cryptic protease." J Biol Chem 279(20):21431-21438.

Liz, M. A., C. E. Fleming, A. F. Nunes, M. R. Almeida, F. M. Mar, Y. Choe, C. S. Craik, J. C. Powers, M. Bogyo and M. M. Sousa. 2009. "Substrate specificity of transthyretin: identification of natural substrates in the nervous system." Biochem J 419(2):467-474.

Liz, M. A., C. M. Gomes, M. J. Saraiva and M. M. Sousa. 2007. "ApoA-I cleaved by transthyretin has reduced ability to promote cholesterol efflux and increased amyloidogenicity." J Lipid Res 48(11):2385-2395.

Long, F., A. A. Vagin, P. Young and G. N. Murshudov. 2008. "BALBES: a molecular-replacement pipeline." Acta Crystallogr D Biol Crystallogr 64(Pt 1):125-132.

Longo, V. D., K. L. Viola, W. L. Klein and C. E. Finch. 2000. "Reversible inactivation of superoxide-sensitive aconitase in Abeta1-42-treated neuronal cell lines." J Neurochem 75(5):1977-1985.

Lorenzo, A. and B. A. Yankner. 1994. "Beta-amyloid neurotoxicity requires fibril formation and is inhibited by congo red." Proc Natl Acad Sci U S A 91(25):12243-12247.

Loun, B. and D. S. Hage. 1992. "Characterization of thyroxine-albumin binding using high-performance affinity chromatography. I. Interactions at the warfarin and indole sites of albumin." J Chromatogr 579(2):225-235.

Maccioni, R. B., J. P. Munoz and L. Barbeito. 2001. "The molecular bases of Alzheimer's disease and other neurodegenerative disorders." Arch Med Res 32(5):367-381.

Mangione, P. P., R. Porcari, J. D. Gillmore, P. Pucci, M. Monti, M. Porcari, S. Giorgetti, L. Marchese, S. Raimondi, L. C. Serpell, W. Chen, A. Relini, J. Marcoux, I. R. Clatworthy, G. W. Taylor, G. A. Tennent, C. V. Robinson, P. N. Hawkins, M. Stoppini, S. P. Wood, M. B. Pepys and V. Bellotti. 2014. "Proteolytic cleavage of Ser52Pro variant transthyretin triggers its amyloid fibrillogenesis." Proc Natl Acad Sci U S A 111(4):1539-1544.

Marcoux, J., P. P. Mangione, R. Porcari, M. T. Degiacomi, G. Verona, G. W. Taylor, S. Giorgetti, S. Raimondi, S. Sanglier-Cianferani, J. L. Benesch, C. Cecconi, M. M. Naqvi, J. D. Gillmore, P. N. Hawkins, M. Stoppini, C. V. Robinson, M. B. Pepys and V. Bellotti. 2015. "A novel mechano-enzymatic cleavage mechanism underlies transthyretin amyloidogenesis." EMBO Mol Med 7(10):1337-1349.

Mazur-Kolecka, B., J. Frackowiak, R. T. Carroll and H. M. Wisniewski. 1997. "Accumulation of Alzheimer amyloid-beta peptide in cultured myocytes is enhanced by serum and reduced by cerebrospinal fluid." J Neuropathol Exp Neurol 56(3):263-272.

McCammon, M. G., D. J. Scott, C. A. Keetch, L. H. Greene, H. E. Purkey, H. M. Petrassi, J. W. Kelly and C. V. Robinson. 2002. "Screening transthyretin amyloid fibril inhibitors: characterization of novel multiprotein, multiligand complexes by mass spectrometry." Structure 10(6):851-863.

Mccutchen, S. L., W. Colon and J. W. Kelly. 1993. "Transthyretin Mutation Leu-55-Pro Significantly Alters Tetramer Stability and Increases Amyloidogenicity." Biochemistry 32(45):12119-12127.

McNicholas, S., E. Potterton, K. S. Wilson and M. E. Noble. 2011. "Presenting your structures: the CCP4mg molecular-graphics software." Acta Crystallogr D Biol Crystallogr 67(Pt 4):386-394.

Mendel, C. M., R. R. Cavalieri, L. A. Gavin, T. Pettersson and M. Inoue. 1989. "Thyroxine transport and distribution in Nagase analbuminemic rats." J Clin Invest 83(1):143-148.

Merched, A., J. M. Serot, S. Visvikis, D. Aguillon, G. Faure and G. Siest. 1998. "Apolipoprotein E, transthyretin and actin in the CSF of Alzheimer's patients: relation with the senile plaques and cytoskeleton biochemistry." FEBS Lett 425(2):225-228.

Miroy, G. J., Z. Lai, H. A. Lashuel, S. A. Peterson, C. Strang and J. W. Kelly. 1996. "Inhibiting transthyretin amyloid fibril formation via protein stabilization." Proc Natl Acad Sci U S A 93(26):15051-15056.

Mita, S., S. Maeda, K. Shimada and S. Araki. 1984. "Cloning and sequence analysis of cDNA for human prealbumin." Biochem Biophys Res Commun 124(2):558-564.

Monaco, H. L., M. Rizzi and A. Coda. 1995. "Structure of a complex of two plasma proteins: transthyretin and retinol-binding protein." Science 268(5213):1039-1041.

Murakami, T., Y. Ohsawa, L. Zhenghua, K. Yamamura and Y. Sunada. 2010. "The transthyretin gene is expressed in Schwann cells of peripheral nerves." Brain Res 1348:222-225.

Murakami, T., Y. Yasuda, S. Mita, S. Maeda, K. Shimada, T. Fujimoto and S. Araki. 1987. "Prealbumin gene expression during mouse development studied by in situ hybridization." Cell Differ 22(1):1-9.

Murshudov, G. N., A. A. Vagin and E. J. Dodson. 1997. "Refinement of macromolecular structures by the maximum-likelihood method." Acta Crystallogr D Biol Crystallogr 53(Pt 3):240-255.

Nagata, Y., F. Tashiro, S. Yi, T. Murakami, S. Maeda, K. Takahashi, K. Shimada, H. Okamura and K. Yamamura. 1995. "A 6-kb upstream region of the human transthyretin gene can direct developmental, tissue-specific, and quantitatively normal expression in transgenic mouse." J Biochem 117(1):169-175.

Nazarov, P. V., R. B. Koehorst, W. L. Vos, V. V. Apanasovich and M. A. Hemminga. 2006. "FRET study of membrane proteins: simulation-based fitting for analysis of membrane protein embedment and association." Biophys J 91(2):454-466.

Nunes, A. F., M. J. Saraiva and M. M. Sousa. 2006. "Transthyretin knockouts are a new mouse model for increased neuropeptide Y." FASEB J 20(1):166-168.

O'Brien, C. R. and W. T. Wong. 2001. "Intermittent vomiting and weight loss in an old dog." Aust Vet J 79(4):251, 260-251.

Oliveira, S. M., C. A. Ribeiro, I. Cardoso and M. J. Saraiva. 2011. "Gender-dependent transthyretin modulation of brain amyloid-beta levels: evidence from a mouse model of Alzheimer's disease." J Alzheimers Dis 27(2):429-439.

Oppenheimer, J. H. 1968. "Role of plasma proteins in the binding, distribution and metabolism of the thyroid hormones." N Engl J Med 278(21):1153-1162.

Palha, J. A. 2002. "Transthyretin as a thyroid hormone carrier: function revisited." Clin Chem Lab Med 40(12):1292-1300.

Palha, J. A., M. T. Hays, G. Morreale de Escobar, V. Episkopou, M. E. Gottesman and M. J. Saraiva. 1997. "Transthyretin is not essential for thyroxine to reach the brain and other tissues in transthyretin-null mice." Am J Physiol 272(3 Pt 1):E485-493.

Palha, J. A., J. Nissanov, R. Fernandes, J. C. Sousa, L. Bertrand, M. B. Dratman, G. Morreale de Escobar, M. Gottesman and M. J. Saraiva. 2002. "Thyroid hormone distribution in the mouse brain: the role of transthyretin." Neuroscience 113(4):837-847.

Pensalfini, A., M. Zampagni, G. Liguri, M. Becatti, E. Evangelisti, C. Fiorillo, S. Bagnoli, E. Cellini, B. Nacmias, S. Sorbi and C. Cecchi. 2011. "Membrane cholesterol enrichment prevents Abeta-induced oxidative stress in Alzheimer's fibroblasts." Neurobiol Aging 32(2):210-222.

Peterson, S. A., T. Klabunde, H. A. Lashuel, H. Purkey, J. C. Sacchettini and J. W. Kelly. 1998. "Inhibiting transthyretin conformational changes that lead to amyloid fibril formation." Proc Natl Acad Sci U S A 95(22):12956-12960.

Pike, C. J., D. Burdick, A. J. Walencewicz, C. G. Glabe and C. W. Cotman. 1993. "Neurodegeneration induced by beta-amyloid peptides in vitro: the role of peptide assembly state." J Neurosci 13(4):1676-1687.

Pires, R. H., A. Karsai, M. J. Saraiva, A. M. Damas and M. S. Kellermayer. 2012. "Distinct annular oligomers captured along the assembly and disassembly pathways of transthyretin amyloid protofibrils." PLoS One 7(9):e44992.

Power, D. M., N. P. Elias, S. J. Richardson, J. Mendes, C. M. Soares and C. R. Santos. 2000. "Evolution of the thyroid hormone-binding protein, transthyretin." Gen Comp Endocrinol 119(3):241-255.

Powers, E. T. and D. L. Powers. 2006. "The kinetics of nucleated polymerizations at high concentrations: amyloid fibril formation near and above the "supercritical concentration"." Biophys J 91(1):122-132.

Pras, M., M. Schubert, D. Zucker-Franklin, A. Rimon and E. C. Franklin. 1968. "The characterization of soluble amyloid prepared in water." J Clin Invest 47(4):924-933.

Puskas, L. G., K. Kitajka, C. Nyakas, G. Barcelo-Coblijn and T. Farkas. 2003. "Short-term administration of omega 3 fatty acids from fish oil results in increased transthyretin transcription in old rat hippocampus." Proc Natl Acad Sci U S A 100(4):1580-1585.

Quintas, A., M. J. Saraiva and R. M. Brito. 1997. "The amyloidogenic potential of transthyretin variants correlates with their tendency to aggregate in solution." FEBS Lett 418(3):297-300.

Quintela, T., C. H. Alves, I. Goncalves, G. Baltazar, M. J. Saraiva and C. R. Santos. 2008. "5Alpha-dihydrotestosterone up-regulates transthyretin levels in mice and rat choroid plexus via an androgen receptor independent pathway." Brain Res 1229:18-26.

Quintela, T., I. Goncalves, G. Baltazar, C. H. Alves, M. J. Saraiva and C. R. Santos. 2009. "17beta-estradiol induces transthyretin expression in murine choroid plexus via an oestrogen receptor dependent pathway." Cell Mol Neurobiol 29(4):475-483.

Quintela, T., I. Goncalves, A. Martinho, C. H. Alves, M. J. Saraiva, P. Rocha and C. R. Santos. 2011. "Progesterone enhances transthyretin expression in the rat choroid plexus in vitro and in vivo via progesterone receptor." J Mol Neurosci 44(3):152-158.

Raz, A. and D. S. Goodman. 1969. "The interaction of thyroxine with human plasma prealbumin and with the prealbumin-retinol-binding protein complex." J Biol Chem 244(12):3230-3237.

Raz, A., T. Shiratori and D. S. Goodman. 1970. "Studies on the protein-protein and protein-ligand interactions involved in retinol transport in plasma." J Biol Chem 245(8):1903-1912.

Refai, E., N. Dekki, S. N. Yang, G. Imreh, O. Cabrera, L. Yu, G. Yang, S. Norgren, S. M. Rossner, L. Inverardi, C. Ricordi, G. Olivecrona, M. Andersson, H. Jornvall, P. O. Berggren and L. Juntti-Berggren. 2005. "Transthyretin constitutes a functional component in pancreatic beta-cell stimulus-secretion coupling." Proc Natl Acad Sci U S A 102(47):17020-17025.

Reixach, N., S. Deechongkit, X. Jiang, J. W. Kelly and J. N. Buxbaum. 2004. "Tissue damage in the amyloidoses: Transthyretin monomers and nonnative oligomers are the major cytotoxic species in tissue culture." Proc Natl Acad Sci U S A 101(9):2817-2822.

Reixach, N., T. R. Foss, E. Santelli, J. Pascual, J. W. Kelly and J. N. Buxbaum. 2008. "Human-murine transthyretin heterotetramers are kinetically stable and non-amyloidogenic. A lesson in the generation of transgenic models of diseases involving oligomeric proteins." J Biol Chem 283(4):2098-2107.

Ribeiro, C. A., M. J. Saraiva and I. Cardoso. 2012. "Stability of the transthyretin molecule as a key factor in the interaction with a-beta peptide--relevance in Alzheimer's disease." PLoS One 7(9):e45368.

Richardson, S. J., A. J. Bradley, W. Duan, R. E. Wettenhall, P. J. Harms, J. J. Babon, B. R. Southwell, S. Nicol, S. C. Donnellan and G. Schreiber. 1994. "Evolution of marsupial and other vertebrate thyroxine-binding plasma proteins." Am J Physiol 266(4 Pt 2):R1359-1370.

Robbins, J. and J. E. Rall. 1960. "Proteins associated with the thyroid hormones." Physiol Rev 40:415-489.

Rydh, A., O. Suhr, S. O. Hietala, K. R. Ahlstrom, M. B. Pepys and P. N. Hawkins. 1998. "Serum amyloid P component scintigraphy in familial amyloid polyneuropathy: regression of visceral amyloid following liver transplantation." Eur J Nucl Med 25(7):709-713.

Sakaki, T., A. Soga, Y. Yabusaki and H. Ohkawa. 1984. "Characterization of three forms of cytochrome P-450 isolated from liver microsomes of rats treated with 3-methylcholanthrene." J Biochem 96(1):117-126.

Sakaki, Y. and H. Sasaki. 1985. "[DNA diagnosis of familial amyloidotic polyneuropathy]." Rinsho Byori 33 Spec No 65:134-139.

Sandbrink, R., T. Hartmann, C. L. Masters and K. Beyreuther. 1996. "Genes contributing to Alzheimer's disease." Mol Psychiatry 1(1):27-40.

Santoro, M. M. and D. W. Bolen. 1988. "Unfolding free energy changes determined by the linear extrapolation method. 1. Unfolding of phenylmethanesulfonyl alpha-chymotrypsin using different denaturants." Biochemistry 27(21):8063-8068.

Santos, C. R. and D. M. Power. 1999. "Identification of transthyretin in fish (Sparus aurata): cDNA cloning and characterisation." Endocrinology 140(5):2430-2433.

Santos, D. B., K. C. Peres, R. P. Ribeiro, D. Colle, A. A. dos Santos, E. L. Moreira, D. O. Souza, C. P. Figueiredo and M. Farina. 2012. "Probucol, a lipid-lowering drug, prevents cognitive and hippocampal synaptic impairments induced by amyloid beta peptide in mice." Exp Neurol 233(2):767-775.

Saraiva, M. J. 2001. "Transthyretin mutations in hyperthyroxinemia and amyloid diseases." Hum Mutat 17(6):493-503.

Saraiva, M. J., P. P. Costa and D. S. Goodman. 1988. "Transthyretin (prealbumin) in familial amyloidotic polyneuropathy: genetic and functional aspects." Adv Neurol 48:189-200.

Sasaki, H., N. Yoshioka, Y. Takagi and Y. Sakaki. 1985. "Structure of the chromosomal gene for human serum prealbumin." Gene 37(1-3):191-197.

Schreiber, G., A. R. Aldred, A. Jaworowski, C. Nilsson, M. G. Achen and M. B. Segal. 1990. "Thyroxine transport from blood to brain via transthyretin synthesis in choroid plexus." Am J Physiol 258(2 Pt 2):R338-345.

Schwarzman, A. L., L. Gregori, M. P. Vitek, S. Lyubski, W. J. Strittmatter, J. J. Enghilde, R. Bhasin, J. Silverman, K. H. Weisgraber, P. K. Coyle and et al. 1994. "Transthyretin sequesters amyloid beta protein and prevents amyloid formation." Proc Natl Acad Sci U S A 91(18):8368-8372.

Schwarzman, A. L., M. Tsiper, H. Wente, A. Wang, M. P. Vitek, V. Vasiliev and D. Goldgaber. 2004. "Amyloidogenic and anti-amyloidogenic properties of recombinant transthyretin variants." Amyloid 11(1):1-9.

Sekijima, Y., R. L. Wiseman, J. Matteson, P. Hammarstrom, S. R. Miller, A. R. Sawkar, W. E. Balch and J. W. Kelly. 2005. "The biological and chemical basis for tissue-selective amyloid disease." Cell 121(1):73-85.

Selkoe, D. J., M. B. Podlisny, C. L. Joachim, E. A. Vickers, G. Lee, L. C. Fritz and T. Oltersdorf. 1988. "Beta-amyloid precursor protein of Alzheimer disease occurs as 110- to 135-kilodalton membrane-associated proteins in neural and nonneural tissues." Proc Natl Acad Sci U S A 85(19):7341-7345.

Serag, A. A., C. Altenbach, M. Gingery, W. L. Hubbell and T. O. Yeates. 2002. "Arrangement of subunits and ordering of beta-strands in an amyloid sheet." Nat Struct Biol 9(10):734-739.

Serot, J. M., D. Christmann, T. Dubost and M. Couturier. 1997. "Cerebrospinal fluid transthyretin: aging and late onset Alzheimer's disease." J Neurol Neurosurg Psychiatry 63(4):506-508.

Shnyrov, V. L., E. Villar, G. G. Zhadan, J. M. Sanchez-Ruiz, A. Quintas, M. J. Saraiva and R. M. Brito. 2000. "Comparative calorimetric study of non-amyloidogenic and amyloidogenic variants of the homotetrameric protein transthyretin." Biophys Chem 88(1-3):61-67.

Sivaprasadarao, A. and J. B. Findlay. 1994. "Structure-function studies on human retinol-binding protein using site-directed mutagenesis." Biochem J 300 (Pt 2):437-442.

Smith, T. J., F. B. Davis, M. R. Deziel, P. J. Davis, D. B. Ramsden and M. Schoenl. 1994. "Retinoic acid inhibition of thyroxine binding to human transthyretin." Biochim Biophys Acta 1199(1):76-80.

Sola, C., G. Mengod, A. Probst and J. M. Palacios. 1993. "Differential regional and cellular distribution of beta-amyloid precursor protein messenger RNAs containing and lacking the Kunitz protease inhibitor domain in the brain of human, rat and mouse." Neuroscience 53(1):267-295.

Soprano, D. R., J. Herbert, K. J. Soprano, E. A. Schon and D. S. Goodman. 1985. "Demonstration of transthyretin mRNA in the brain and other extrahepatic tissues in the rat." J Biol Chem 260(21):11793-11798.

Soprano, D. R., K. J. Soprano and D. S. Goodman. 1986. "Retinol-binding protein and transthyretin mRNA levels in visceral yolk sac and liver during fetal development in the rat." Proc Natl Acad Sci U S A 83(19):7330-7334.

Soprano, D. R., K. J. Soprano, M. L. Wyatt and D. S. Goodman. 1988. "Induction of the expression of retinol-binding protein and transthyretin in F9 embryonal carcinoma cells differentiated to embryoid bodies." J Biol Chem 263(34):17897-17900.

Sousa, J. C., G. M. de Escobar, P. Oliveira, M. J. Saraiva and J. A. Palha. 2005. "Transthyretin is not necessary for thyroid hormone metabolism in conditions of increased hormone demand." J Endocrinol 187(2):257-266.

Sousa, M. M., S. Du Yan, R. Fernandes, A. Guimaraes, D. Stern and M. J. Saraiva. 2001. "Familial amyloid polyneuropathy: receptor for advanced glycation end products-dependent triggering of neuronal inflammatory and apoptotic pathways." J Neurosci 21(19):7576-7586.

Sousa, M. M., R. Fernandes, J. A. Palha, A. Taboada, P. Vieira and M. J. Saraiva. 2002. "Evidence for early cytotoxic aggregates in transgenic mice for human transthyretin Leu55Pro." Am J Pathol 161(5):1935-1948.

Sparkes, R. S., H. Sasaki, T. Mohandas, K. Yoshioka, I. Klisak, Y. Sakaki, C. Heinzmann and M. I. Simon. 1987. "Assignment of the prealbumin (PALB) gene (familial amyloidotic polyneuropathy) to human chromosome region 18q11.2-q12.1." Hum Genet 75(2):151-154.

Stein, T. D. and J. A. Johnson. 2002. "Lack of neurodegeneration in transgenic mice overexpressing mutant amyloid precursor protein is associated with increased levels of transthyretin and the activation of cell survival pathways." J Neurosci 22(17):7380-7388.

Steinrauf, L. K., Y. J. Cao, J. Hamilton, J. Murrell, J. J. Liepnieks and M. D. Benson. 1991. "Preparation and crystallization of human transthyretin (prealbumin) variants." Biochem Biophys Res Commun 179(2):804-809.

Strittmatter, W. J., K. H. Weisgraber, D. Y. Huang, L. M. Dong, G. S. Salvesen, M. Pericak-Vance, D. Schmechel, A. M. Saunders, D. Goldgaber and A. D. Roses. 1993. "Binding of human apolipoprotein E to synthetic amyloid beta peptide: isoform-specific effects and implications for late-onset Alzheimer disease." Proc Natl Acad Sci U S A 90(17):8098-8102.

Tagoe, C. E., N. Reixach, L. Friske, D. Mustra, D. French, G. Gallo and J. N. Buxbaum. 2007. "In vivo stabilization of mutant human transthyretin in transgenic mice." Amyloid 14(3):227-236.

Tanskanen, M., T. Peuralinna, T. Polvikoski, I. L. Notkola, R. Sulkava, J. Hardy, A. Singleton, S. Kiuru-Enari, A. Paetau, P. J. Tienari and L. Myllykangas. 2008. "Senile systemic amyloidosis affects 25% of the very aged and associates with genetic variation in alpha2-macroglobulin and tau: a population-based autopsy study." Ann Med 40(3):232-239.

Teixeira, C. A., R. Almeida Mdo and M. J. Saraiva. 2016. "Impairment of autophagy by TTR V30M aggregates: in vivo reversal by TUDCA and curcumin." Clin Sci (Lond) 130(18):1665-1675.

Teng, M. H., J. Y. Yin, R. Vidal, J. Ghiso, A. Kumar, R. Rabenou, A. Shah, D. R. Jacobson, C. Tagoe, G. Gallo and J. Buxbaum. 2001. "Amyloid and nonfibrillar deposits in mice transgenic for wild-type human transthyretin: a possible model for senile systemic amyloidosis." Lab Invest 81(3):385-396.

Terry, C. J., A. M. Damas, P. Oliveira, M. J. Saraiva, I. L. Alves, P. P. Costa, P. M. Matias, Y. Sakaki and C. C. Blake. 1993. "Structure of Met30 variant of transthyretin and its amyloidogenic implications." EMBO J 12(2):735-741.

Thompson, J. L., M. M. Manore and J. R. Thomas. 1996. "Effects of diet and diet-plus-exercise programs on resting metabolic rate: a meta-analysis." Int J Sport Nutr 6(1):41-61.

Thylen, C., J. Wahlqvist, E. Haettner, O. Sandgren, G. Holmgren and E. Lundgren. 1993. "Modifications of Transthyretin in Amyloid Fibrils - Analysis of Amyloid from Homozygous and Heterozygous Individuals with the Met30 Mutation." Embo Journal 12(2):743-748.

Tsuzuki, K., R. Fukatsu, H. Yamaguchi, M. Tateno, K. Imai, N. Fujii and T. Yamauchi. 2000. "Transthyretin binds amyloid beta peptides, Abeta1-42 and Abeta1-40 to form complex in the autopsied human kidney - possible role of transthyretin for abeta sequestration." Neurosci Lett 281(2-3):171-174.

Tsuzuki, T., S. Mita, S. Maeda, S. Araki and K. Shimada. 1985. "Structure of the human prealbumin gene." J Biol Chem 260(22):12224-12227.

Vagin, A. and A. Teplyakov. 1997. "MOLREP: an automated program for molecular replacement." Journal of Applied Crystallography 30:1022-1025.

Vahlquist, A., L. Rask, P. A. Peterson and T. Berg. 1975. "The concentrations of retinol-binding protein, prealbumin, and transferrin in the sera of newly delivered mothers and children of various ages." Scand J Clin Lab Invest 35(6):569-575.

Vatassery, G. T., H. T. Quach, W. E. Smith, B. A. Benson and J. H. Eckfeldt. 1991. "A sensitive assay of transthyretin (prealbumin) in human cerebrospinal fluid in nanogram amounts by ELISA." Clin Chim Acta 197(1):19-25.

Vigo-Pelfrey, C., D. Lee, P. Keim, I. Lieberburg and D. B. Schenk. 1993. "Characterization of beta-amyloid peptide from human cerebrospinal fluid." J Neurochem 61(5):1965-1968.

Visser, N. V., A. H. Westphal, A. van Hoek, C. P. van Mierlo, A. J. Visser and H. van Amerongen. 2008. "Tryptophan-tryptophan energy migration as a tool to follow apoflavodoxin folding." Biophys J 95(5):2462-2469.

Wakasugi, S., S. Maeda, K. Shimada, H. Nakashima and S. Migita. 1985. "Structural comparisons between mouse and human prealbumin." J Biochem 98(6):1707-1714.

Wallace, M. R., F. E. Dwulet, P. M. Conneally and M. D. Benson. 1986. "Biochemical and molecular genetic characterization of a new variant prealbumin associated with hereditary amyloidosis." J Clin Invest 78(1):6-12.

Wallace, M. R., S. L. Naylor, B. Kluve-Beckerman, G. L. Long, L. McDonald, T. B. Shows and M. D. Benson. 1985. "Localization of the human prealbumin gene to chromosome 18." Biochem Biophys Res Commun 129(3):753-758.

Walsh, D. M., E. Thulin, A. M. Minogue, N. Gustavsson, E. Pang, D. B. Teplow and S. Linse. 2009. "A facile method for expression and purification of the Alzheimer's disease-associated amyloid beta-peptide." FEBS J 276(5):1266-1281.

Wang, J. F., R. Lu and Y. Z. Wang. 2010. "Regulation of beta cleavage of amyloid precursor protein." Neurosci Bull 26(5):417-427.

Wang, J., R. M. Wolf, J. W. Caldwell, P. A. Kollman and D. A. Case. 2004. "Development and testing of a general amber force field." J Comput Chem 25(9):1157-1174.

Watanabe, H., K. Misu, M. Hirayama, N. Hattori, T. Yoshihara, M. Doyu and G. Sobue. 2001. "Low cardiac 123I-MIBG uptake in late-onset familial amyloid polyneuropathy type I (TTR Met30)." J Neurol 248(7):627-629.

Wati, H., T. Kawarabayashi, E. Matsubara, A. Kasai, T. Hirasawa, T. Kubota, Y. Harigaya, M. Shoji and S. Maeda. 2009. "Transthyretin accelerates vascular Abeta deposition in a mouse model of Alzheimer's disease." Brain Pathol 19(1):48-57.

Weisner, B. and H. J. Roethig. 1983. "The concentration of prealbumin in cerebrospinal fluid (CSF), indicator of CSF circulation disorders." Eur Neurol 22(2):96-105.

Westermark, P., M. D. Benson, J. N. Buxbaum, A. S. Cohen, B. Frangione, S. Ikeda, C. L. Masters, G. Merlini, M. J. Saraiva and J. D. Sipe. 2007. "A primer of amyloid nomenclature." Amyloid 14(3):179-183.

Westermark, P., K. Sletten and K. H. Johnson. 1996. "Ageing and amyloid fibrillogenesis: lessons from apolipoprotein AI, transthyretin and islet amyloid polypeptide." Ciba Found Symp 199:205-218; discussion 218-222.

Wojtczak, A., V. Cody, J. R. Luft and W. Pangborn. 1996. "Structures of human transthyretin complexed with thyroxine at 2.0 A resolution and 3',5'-dinitro-N-acetyl-L-thyronine at 2.2 A resolution." Acta Crystallogr D Biol Crystallogr 52(Pt 4):758-765.

Yamamura, K., S. Wakasugi, S. Maeda, T. Inomoto, T. Iwanaga, M. Uehira, K. Araki, J. Miyazaki and K. Shimada. 1987. "Tissue-specific and developmental expression of human transthyretin gene in transgenic mice." Dev Genet 8(4):195-205.

Yamauchi, K., J. Nakajima, H. Hayashi and A. Hara. 1999. "Purification and characterization of thyroid-hormone-binding protein from masu salmon serum. A homolog of higher-vertebrate transthyretin." Eur J Biochem 265(3):944-949.

Yan, C., R. H. Costa, J. E. Darnell, Jr., J. D. Chen and T. A. Van Dyke. 1990. "Distinct positive and negative elements control the limited hepatocyte and choroid plexus expression of transthyretin in transgenic mice." EMBO J 9(3):869-878.

Yazaki, M., L. H. Connors, R. C. Eagle, Jr., S. R. Leff, M. Skinner and M. D. Benson. 2002a. "Transthyretin amyloidosis associated with a novel variant (Trp41Leu) presenting with vitreous opacities." Amyloid 9(4):263-267.

Yazaki, M., J. Varga, P. J. Dyck and M. D. Benson. 2002b. "A new transthyretin variant Leu55Gln in a patient with systemic amyloidosis." Amyloid 9(4):268-271.

Zlokovic, B. V. 2004. "Clearing amyloid through the blood-brain barrier." J Neurochem 89(4):807-811.

Acknowledgements

Firstly, I would like to express my sincere gratitude to my Professor Fabrizio Chiti for the continuous support of my PhD study and related research, for his patience, motivation, and immense knowledge. His guidance helped me in all the time of research and writing of this thesis. Without his guidance and persistent help this dissertation would not have been possible. I am also extremely thankful to Francesco Bemporad for sharing expertise, and sincere and valuable guidance and encouragement extended to me.

My sincere thanks also go to Prof. Christopher M. Dobson, Prof. Michele Vendruscolo and Prof. Tuomas P. J. Knowles who provided me an opportunity to join their team in Cambridge, and who gave access to the laboratory and research facilities, and Johnny Habchi, Benedetta Mannini and Sean Chia, who helped me for the experiments and research in Cambridge. Without they precious support it would not be possible to conduct this research. I would like to thank Stefano Ricagno, Benedetta Maria Sala, and Guido Tiana in Milan university for welcoming in their lab and helping me for the experiments.

I would like to thank my co-workers in the lab: Claudia, Roberta, Zohra, Mirella, Giulia, Filippo, Lucrezia, Demet, Simone, Edoardo, Sara, Eleonora, Ludovica, Caterina, Federica, Chiara, Niccolo', Matteo, Laxman. I also like to take this opportunity to express gratitude to all of the Department faculty members for their help and support.

Last but not the least, I would like to thank my family: my parents and my brothers and sisters for supporting me spiritually throughout writing this thesis and my life in general.

I also place on record, my sense of gratitude to one and all, who directly or indirectly, have lent their helping hand in this venture.